Lehrstuhl für Medizintechnik
Technische Universität München

Microcellular Injection Moulding for an Oesophageal Implant

Hongbin Wu

Vollständiger Abdruck der von der Fakultät für Maschinenwesen der Technischen Universität München zur Erlangung des akademischen Grades eines

Doktor-Ingenieurs

genehmigten Dissertation.

Vorsitzender: Univ.-Prof. Dr.-Ing. Michael F. Zäh

Prüfer der Dissertation:
1. Univ.-Prof. Dr. med., Dr.-Ing. habil. Erich Wintermantel
2. Univ.-Prof. Dr.-Ing. Horst Baier

Die Dissertation wurde am 10.08.2009 bei der Technischen Universität München eingereicht und durch die Fakultät für Maschinenwesen am 02.11.2009 angenommen

Dedication

This dissertation is dedicated to my immediate family, my wife Jingjing Cong, my parents Lide Wu and Ailing Li. None of this would have been possible without their love and patience. They have been a constant source of love, concern, support and strength all these years. I would like to express my heart-felt gratitude to them.

Abstract

This study introduces a method for producing a ring shaped polymer implant, which is to be placed around the sphincter of the oesophagus in order to reduce the amount of gastric juices reflux in the oesophagus. This idea of having a polymeric sleeve around the oesophagus has previously been applied by other authors, however not successfully due to migration of the implant along the oesophagus. The implant in this study consists of a porous inner side, in which tissue can grow in and by this prevent migration of the implant.

An industrial microcellular injection molding process, named MuCell®, was used to produce implants with a porous structure. As raw material a thermoplastic polyurethane was selected. Two molds were designed for the process study and for producing the implants. The process parameters affecting the pore structure, pore distribution and pore size, were analyzed in detail to ensure a suitable pore morphology for cell ingrowth. Key processing parameters for the pore size, morphology and porosity were identified. The MuCell® process was utilized successfully in this study to produce a medical implant for treating reflux diseases with an optimal pore structure for cell ingrowth.

Biocompatibility tests have proven that the implants need to be treated by surface treatments in order to improve their biocompatibility. Two surface treatment methods, plasma activation and TiO_2-coating, were performed to enhance cell adhesion and proliferation on the implant surface. After surface treatments biocompatibility of implants was seen to be increased. *In vitro* tests showed that the plasma activation and TiO_2-coating had similar effects, but *in vivo* tests revealed the plasma activation as being more effective. Cell and tissue ingrowth into the porous structure of the implants were observed. The implants following the named treatments were classified as biocompatible, thus suitable for surgical implantation.

Zusammenfassung

In dieser Arbeit wurde ein neues Implantat für die Behandlung der Reflux-Krankheit entwickelt. Eine Methode, die als MuCell® bekannt ist, wurde in dieser Arbeit verwendet, um ein poröses Implantat herzustellen. Das Implantat sollte um die Speiseröhre der Patienten, die an der gastroäsophagealen Reflux-Krankheit leiden, durch einen minimal-invasiven Eingriff gelegt werden, um damit passiv den Speiseröhren-Schließmuskel zu unterstützen. Im Vorversuch anderer Autoren wurde ein ähnliches Implantat um die Speiseröhre implantiert, jedoch ohne ausreichende Fixation durch Einwachsen von Gewebe. Es ist Ziel dieser Arbeit, eine optimale Porenstruktur zu erzeugen, die ein Einwachsen von Gewebe erlaubt und eine dauerhafte Fixierung ermöglicht.

Es ist gelungen, die gewünschte poröse Struktur und Prototypen des Implantates durch ein mikrozelluläres Spritzgießverfahren herzustellen. Thermoplastische Polyurethane wurden als Rohstoff verwendet. Die Porenmorphologie sowie Porengröße und Porosität des Implantates als Funktion der Veränderung der Prozess-Parameter wurden in dieser Arbeit ausführlich untersucht. Einige Kernparameter, die als die wichtigsten im Schaumspritzgießverfahren hinsichtlich des Einflusses auf die Porenmorphologie waren, wurden festgelegt. Das MuCell®-Verfahren wurde in dieser Studie erfolgreich für ein medizinisches Implantat zur Behandlung der Reflux-Krankheit eingesetzt.

Durch Versuche zur Biokompatibilität wurde bewiesen, dass, um die Biokompatibilität des Implantates zu verbessern, die Implantate mit Oberflächenbehandlungsmethoden behandelt werden müssen. Zwei Methoden, Plasmaaktivierung und TiO_2-Beschichtung, wurden zur Verbesserung der Zell-Adhäsion und -Proliferation auf der Oberfläche des Implantates angewendet. Nach der Oberflächenbehandlung war die Biokompatibilität der Implantate deutlich erhöht. Plasmaaktivierung und TiO_2-Beschichtung zeigten im *in-vitro* Test eine vergleichbare Wirkung. Jedoch zeigte sich im *in-vivo*-Test, dass die Plasmaaktivierung eine deutlichere Verbesserung der Biokompatibilität bewirkt. Zell- und Gewebeeinwachsverhalten in die poröse Struktur des Implantats wurden beobachtet und die Implantate wurden als biokompatibel nach der Herstellung und Behandlung klassifiziert. Mit dem vorliegenden Verhalten wurde ein chirurgisch einsetzbares neues Implantat erfolgreich entwickelt.

Acknowledgement

The research work has been carried out during the period of 2006-2009 at the Department and Chair for Medical Engineering, TU München, Garching b. München, Germany. The writing of this dissertation has been one of the most significant academic challenges I have ever had to face. Without the support, patience and guidance of the following people, this study would not have been completed.

First of all I would like to express my sincere gratitude to my supervisor Prof. Dr. med. Dr.-ing. habil Erich Wintermantel for giving me the opportunity to work in this Department, for this interesting theme. His wisdom, knowledge and commitment to the highest standards inspired and motivated me.

My first and second referee, Prof. Dr.-Ing. Michael F. Zäh and Prof. Dr.-Ing. Horst Baier, deserve my most sincere thanks for all the support, productive inputs during the entire project and especially for contributing their expertise to this work.

I would also like to thank my project partner Mr. Henning Schlicht from Medi-Globe GmbH. He has proven great help in mold construction and mechanics during the entire period of the project. The clinical partner, Mr. Armin Schneider from the MITI group, Klinikum rechts der Isar, deserves severe gratitude for the performing *in vivo* tests of the implants.

Dr. Havard J. Haugen deserves my thanks for his insightful comments and constructive criticisms at different stages of my research. As former staff of this Department he is deeply involved in this project through out the whole period. His help in micro-CT measurements let this dissertation become more valuable.

My thanks go out to all fellows and staff members of the Department. Particularly, I would like to acknowledge Dr. Markus Eblenkamp, Dr. Hector Perea, Mr. Erhard Krampe for their valuable discussions that helped me understand my research area better. I am indebted to my assistant, Mrs. Ilse Schunn, for her excellent work in chemical and biological experiments. I am also thankful to Mr. Uli Ebner and his staff members in Mechanical System and Technical Lab for their maintaining all the machines so efficiently.

Furthermore, I would like to thank Mrs. Susanne Schnell from IMETUM (Central Institute of Medical Engineering) for her kind instructions in the materials lab.

Also, I would like to acknowledge all students, without whom this dissertation would have been impossible. Their motivation and hard working mentality gave me great inspiration. Their names: Mr. Lei Song, Mr. Shen Qu, Ms. Lena Haas.

All of the above and many others have contributed substantially in one way or another to this thesis. I express my deepest gratitude and appreciation to all of them.

Table of contents

1 Introduction

1.1 Gastro-oesophageal reflux disease (GORD)

Gastro Oesophageal Reflux Disease (GORD) is a very common disease in Western Europe and North America and plays a very important role in the development of esophageal adenocarcinoma [108]. The definition of GORD is a longtime exposure of the oesophagus to gastric components such as acid, pepsin and bile [18]. Some studies have shown that there was an increasing incidence of adenocarcinomae of the esophageals and gastric cardia in the past two decades [154,207]. Furthermore oesophageal carcinoma is one of the eight most common cancers worldwide and growing rapidly in western Europe and North America [22,44,110].

Over 40 % of the general population in America had at least weekly occurrences of heartburn or regurgitation (symptoms of GORD) [52]. Drugs prescribed predominantly for GORD cost the UK National Health Service a projected pound sterling 625 million in 2004, 7 % of the primary care prescribing budget. The total cost to Swedish society of GORD in 1997 was $424 million dollars, or $63 per adult [2,122]. In USA the annual direct cost for managing the disease is estimated to be more than $9 billion dollars [169]. The people who have GORD have a high possibility to get the cancer and because of the long-term treatment with drugs the quality of life for these people has been decreased [88]. In summary there is a considerable need for good therapeutic treatment with high economic impact.

1.1.1 Description of GORD

The Fig. 1.1 shows a physiological diagram of the stomach. The oesophagus, diaphragma, lower oesophageal sphincter, stomach and duodenum compose the whole stomach system.

The lower oesophageal sphincter (LOS) is a specialized segment of the circular muscle layer of the distal oesophagus and accounts for approximately 90 % of the basal pressure at the oesophago-gastric junction [18]. The LOS functions as an anti-reflux barrier to protect the oesophagus from the caustic gastric content [4,18].

The food passes through the oesophagus and into the stomach under the function of a wavelike muscle contraction of the oesophageal wall. After the passage of the food, the LOS can contract itself to prevent the reflux of gastric fluids. Besides the LOS, there are also other additional barriers that contribute to the anti-reflux function. For example, the oesophagus has a secondary peristalsis that is called as oesophageal clearance which may aid to push reflux back into the stomach. Another mechanism is one of the components of the oesophagus is a cell membrane, which can restrict the diffusion rate of hydrogen into the epithelium, therefore

preventing the damage due to the acid; the oesophagus can also produce bicarbonate which neutralizes the acid of the gastric fluids [216].

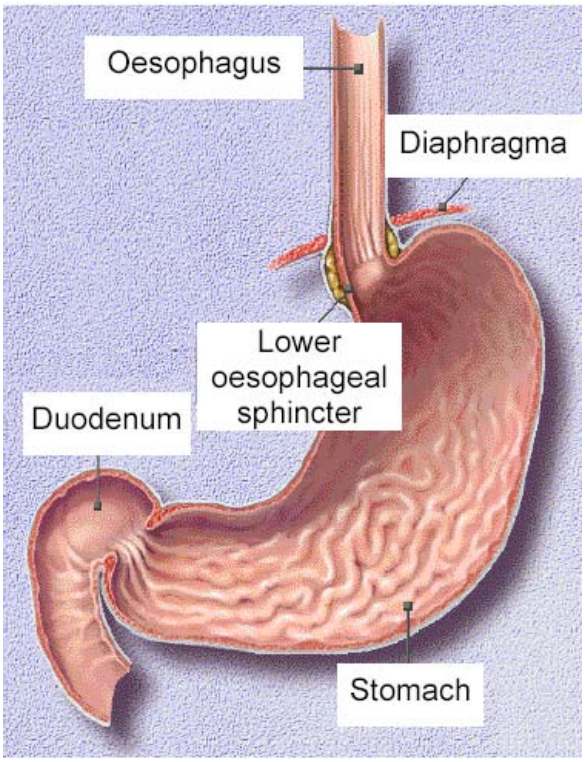

Fig. 1.1: Anatomical overview of the stomach (figure according to [77])

The definition of GORD is a longtime exposure of the oesophagus to gastric components such as acid, pepsin and bile [18]. How long the contact between gastric acid and oesophagus will be, is a decisive influence for the degree of GORD disease [15], because gastric acid is an erosion fact. Sometimes GORD leads to a disorder of the contractions of the oesophagus wall, even preventing self-cleaning of the stomach.

1.1.2 Causes and symptoms of GORD

There are many reasons that can lead to GORD, e.g. transient los relaxations (TLOSR), decreased LOS resting tone, impaired oesohageal clearance, delayed gastric emptying decreased salivation impaired tissue resistance [163,191]. Among the mentioned reasons it was commonly believed that a defective LOS pressure was the main mechanism underlying reflux in GORD patients. When the LOS completely or partially looses its function to close itself, the acid can reflux back in to the oesophagus [18]. It was not until 1982 that Dodds *et al.* showed that the majority (65 %) of GORD patients have reflux episodes during a TLOSR [46].

Another important factor leading to incompetence of the antireflux barrier is the presence of a hiatal hernia [92,183]. The hiatal hernia may promote reflux via several mechanisms [129]. Acid may be trapped in the hiatal sac ready to reflux when the LOS pressure is low. In addition, in the presence of a larger hiatal hernia, the two components of the sphincter complex, namely the LOS and crural diaphragm are disrupted leading to a significant change in pressure profile and reduced basal pressures [93,180].

There is some evidence for lifestyle factors being associated with the underlying causes of GORD. Obesity can disrupt the LOS, maybe due to the increased intra-abdominal pressure. Smoking, alcohol, coffee, and chocolate also have pharmacological effects that reduce the tone of the LOS's tone. Fatty foods delay gastric emptying, which could also predispose to the disease [42,55,58,131]. The group that has the biggest possibility to obtain GORD is male Caucasians. Thereby over 40 percent of the general population in America and Western Europe have at least weekly occurrences of heartburn or regurgitation, on the contrary under 7 % of the general population in Far East show the GORD frequently [52,73,94,122]. Some differences between oriental and Caucasians were considered as the possible reasons for a low frequency of GORD in the east. For example, gastric acid output is known to be lower among Chinese subjects compared with Caucasian individuals, the oriental has also a lower body mass index [94].

GORD leads to typical symptoms in summary named heartburn, in more severe cases it leads to oesophagitis, Barrett's oesophagus and even to carcinoma [18,55]. Heartburn is caused by the return flow of gastric components and was regarded as the main symptom of the GORD, though the other disease e.g. achalasia can also cause the heartburn [6]. If the heartburn occurs daily on a relative empty stomach, it is very possible that GORD is behind this symptom [101,121]. As mentioned above, because of low frequency of GORD in the east there is no word named as "heartburn" in Mandarin Chinese or Malay. Besides heartburn there are other symptoms of GORD e.g. regurgitation, dysfunctional swallowing and chest pains. Symptoms such as dysphagia (difficulty in swallowing), odynophagia (pain while swallowing), globus (lump in the throat), sore throat, laryngitis, water brash and cough are other possible symptoms of the disease, but their diagnostic use is uncertain [131].

Most of patients ignore the feeling of heartburn or the other symptoms of GORD at the early stage, because the feeling is not intensive. But since GORD is a gradual development process, it is a little late for treatment, when patients have a severe pain form of GORD and seek help from a doctor. For example (Fig. 1.2), dysphagia is found only in the late stage of reduced elasticity of the oesophagus. But in the early stage the oesophagus loses only part of the elasticity and the food can always pass through. In the late stage dysphagia occurs by reason of the loss of most of the elasticity of the oesophagus [31,83,131].

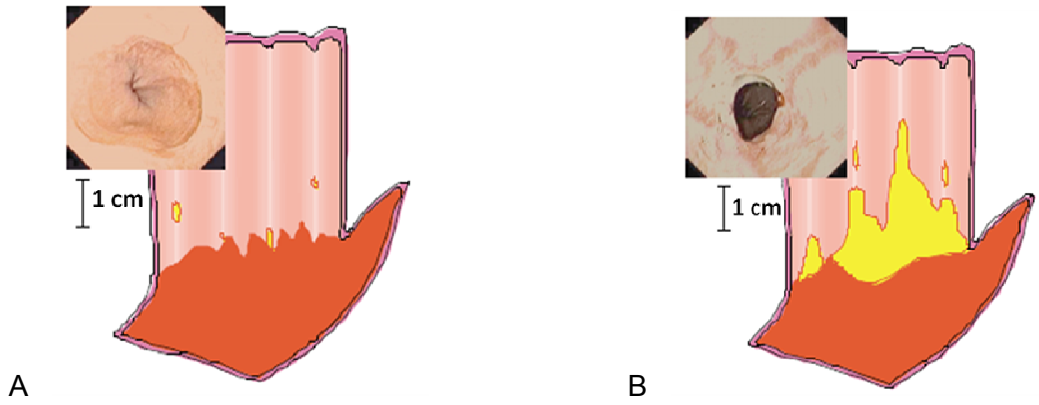

Fig. 1.2: Different stages of GORD
A) In the early stage the oesophagus has loosened part of its elasticity, but the food can still pass through. B) In the later stage, due to the loss of elasticity of the oesophagus, dysphagia occurs due to the resulting stiffness of the oesophagus [131].

Some studies show that symptoms of GORD often precede the development of esophageal adenocarcinoma [31,108], so that the heartburn and the other symptoms must be given proper attention. Therefore adequate treatment must be undertaken, most preferably, at earlier stages of the illness.

1.1.3 Treatment for GORD

At present there are normally 4 level treatment methods, general treatment, pharmacological therapy, endoscopic therapy and surgery therapy, which one will be chosen as standard therapy for the patients depends on the diagnosis of the disease and patients themselves.

1.1.3.1 General Treatment

Lifestyle advice is advocated as first-line treatment for the disease at early stage. Lifestyle factors, that are, clothing, body position, avoiding certain food, are only weakly associated with reflux symptoms, so it is unlikely that such treatment can cure the GORD of late stage. Nevertheless, advice such as stop smoking, reduce alcohol intake, weight loss, avoid fatty food, is likely to have wider benefits, even if the effect on reflux symptoms is small.

Studies show that lifestyle changes contribute to the healing of GORD [64,111,130,159], but most patients will not be satisfied with these first-line and need further treatment, which are on the following introduced**.**

1.1.3.2 Pharmacological therapy

Acid suppression is one of the most important methods of medical treatment in long-term treatment of the disease. Some studies indicate that H_2 receptor antagonists (H_2RA) were effective in the treatment of oesophagitis compared with placebo [29,51,158]. The other

studies show that Proton Pump Inhibitors (PPIs) were more effective than placebos in the treatment of GORD and also better than H_2RA therapy at 4-8 weeks [9,10,23,43,54].

There is, unfortunately, little literature available regarding how the acid suppression therapy affected the life quality of the patients. One study indicated that PPI therapy could improve the life quality, for example, reduced sleep disturbance, increased work productivity compared with placebo [200].

One problem of PPI therapy is that GORD usually relapses once drug therapy is stopped or disturbed, with about 80 % having oesophagitis relapse after 6-12 months [48]. A study [48] followed 1583 patients after curing of oesophagitis and compared the efficacy of PPIs with H_2RA over 24-52 weeks. The overall relapse of oesophagitis was 22 % in the PPI group compared with 58 % in the H_2RA group. This study [48] indicates also that, compared half-dose PPIs with H_2RA therapy in 1156 patients, 40 % of the PPI group had a relapse of oesophagitis after 24-52 weeks, whereas the H_2RA group had a relapse of 66 %.

Despite these findings, the pharmacological treatment is very successful and is always recommended as the first-line therapy for the treatment of GORD due to its high capability of healing reflux disease. But because of the relapse a long-term drug therapy is needed for the patients with GORD and the cost of the therapy will be high. If some patients can not suffer from taking medicament every day or the effect of the pharmacological treatment is not significant, other treatments need to be used.

1.1.3.3 Endoscopic therapy

Acid suppression does not aim at the main abnormality, the abnormal relaxation of the LOS (lower oesophageal sphincter) in reflux disease, which has led to great interest in new endoscopic therapies for the treatment of the disease. Three directions have been developed with endoscopic therapies for the treatment of the reflux disease:

- Endoscopic suturing devices for the lower oesophageal sphincter
- The endoscopic application of radio-frequency to the lower oesophagus
- The injection of bulking agents into the muscle layer of the distal oesophagus

Endoscopic suturing

Endoscopic suturing was initially introduced by Dr. Paul Swain from the Royal London Hospital, England, where the endoscopic sewing machine was invented [57,90]. The first method which was approved by Food and Drug Administration (FDA) is developed by Bard (EndoCinch™, Bard, Billerica, MA), named also as Bard® method, and protected under the U.S. patent number 5887594. The Function principle is described in Fig. 1.3.

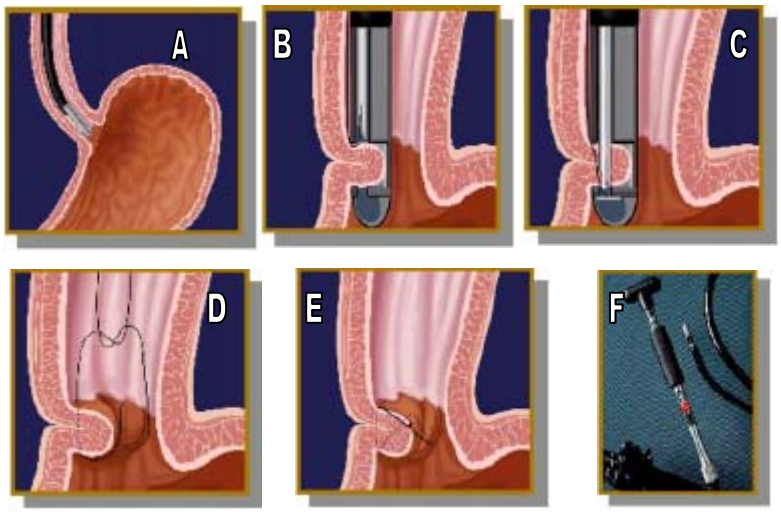

Fig. 1.3: Technical Step of the Bard method
A) Introducing the system through an overtube B) Muscosal tissue suction C) Needle penetration and suture tag development D) Suture of two gastric folds E) Securing knots and cutting sutures F) Bard method endoscoping suturing system (figure according to [57])

After placing the overtube in the oesophagus, the suturing system is passed below the Z-line, the gastric tissue is sucked into the stitching chamber of the instrument, and a stitch is applied. The whole equipment is then drawn back and reloaded with a second suture. After rotating the suturing system another stitch is placed near to the first one and two stitches are anchored with a clip device to create a plication. Two or more plications can be placed in each patient and therefore, the lower oesophageal sphincter is strengthened and gastric reflux is prevented. Disadvantages of this method are either the technical difficulty which has been mainly reported at the beginning of experience, or about the fact that endoscopic sewing is not uniformly reproducible [25]. The clinical results of this method were proved very successful. After following over 100 patients for 4 years a significant improvement of heartburn, together with an increase of length and basal pressure of lower oesophageal sphincter was reported [188]. Other studies described also the improvement of the GORD [19,119]. Of course several adverse events have been reported, such as pharyngitis, thoracic and abdominal pain, vomiting, muscosal laceration, self-limiting haemorrhage from the oesophagus and perforation, besides, the procedure of this treatment is also complicated [195].

At present another suturing device, also named NDO surgical endoscopic plicator, is an investigational device and is not commercialized. The first generation of this device has been approved by FDA, but the apparatus will not be released before the appearance of next generation.

Besides the EndoCinch^{TM} and NDO there are several similar suturing systems which were invented but not commercialized due to the adverse result of test on animals or lacking of clinical applications. The names are Wilson-Cook suturing system, Boston scientific suturing system, Medigus device and His-Wiz device [16,123,164,186]. Overall these suturing devices need to be compared with the EndoCinch^{TM} sewing system which is broadly used, and then, after enough clinical studies and commercial evaluation, these devices may be applied.

Radiofrequency delivery

The radiofrequency delivery has been used as an effective treatment of several diseases such as benign prostatic hyperplasia, sleep-disordered breathing, joint laxity, tumours, and cardiac dysrythmias [125,127,177,184,197]. The mechanism of Radiofrequency delivery is related either to wound contraction/remodelling or to nerve pathway ablation, depending on the specific disease pathophysiology. Recently, temperature controlled radiofrequency energy delivery has been reported to reduce the frequency of transient lower oesophageal sphincter relaxations by almost 50 % in animals as well as in humans [72,86]. The most common procedure is named Stretta System, which is produced by Curon Medical (Curon Medical, Inc., Sunnyvale, California) and also commercially available. The feasibility and clinical application has been reported in the last year by several centres, mainly in the USA [85,100,190,194].

The Stretta System consists of a disposable, flexible catheter, with needle electrodes. The catheter, which is positioned down to gastro-oesophaeal junction, has an inflatable balloon. After the locating of catheter, the balloon is inflated and four needles are deployed into the oesophageal wall. This device delivers a computer-based, temperature-controlled radiofrequency energy leading to thermal ablation and injury to the cardia. Fig. 1.4 shows the design of Stretta System and procedure. A thickening of the gastro-oesophageal musculature was observed after the procedure [38,100]. This method seems to be easy to learn and apply, shows also very little dependence on the operator, compared with the sewing procedures. The FDA (Food and Drug Administration) has approved this device after the safety and feasibility studies. Because of a manufacturing defect of the Stretta System some catheters were recalled at early stage of the application [165].

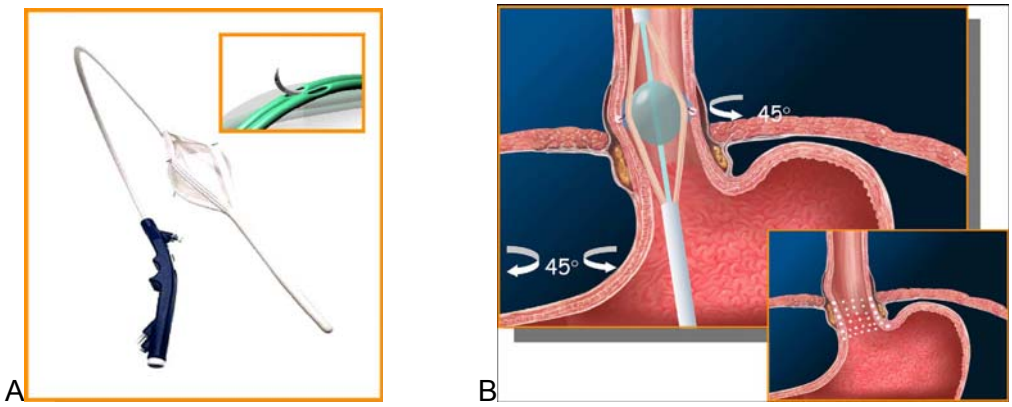

Fig. 1.4: The Stretta System and function mechanism
A) catheter with balloon and needle electrode B) RF delivery to the lower oesophagus. (figure according to according to [38,100])

The most clinical results were reported to be positive. An improvement of symptoms and quality of life was showed, together with a remarkable reduction (87 %) of PPI intake, at 6 months [193]. A long-term study (12, 24, 36, 48 months) has also shown that the Stretta System is a safe, effective, and durable treatment for the GORD. Either the symptoms and quality of life, or the decrease of dose of PPI was significantly to see [124,157]. Of cause the adverse events were also reported. Some patients have fever, chest pain, transient dysphagia and mucosal injury with erosions or even perforation during the procedure. From the adverse-events database of FDA, 10 from 453 patients (2 %) had complications such as perforations, bleedings, mucosal injuries, in the first 6 months; but this early significant adverse-event rate has decreased after 18 months from 2 % to 0,6 % [61].

Overall these studies provide evidence that the Stretta procedure has a safe, positive, long-term effect on reflux disease and is an effective treatment for the GORD.

Endoscopic Bulking Devices

A number of companies are developing endoluminal methods that attempt to add bulk to the LOS zone. The idea that bulking the LOS produces a barrier to gastroesophageal reflux is relatively old. In 1979, the FDA approved an external bulking device for reflux called the Angelchik prosthesis which was filled whit silicone and wrapped around the oesophagus by open surgery at the gastroesophageal junction and tied in place. Because of the complications and dysphagia this technique has been virtually abandoned [67,181].

There are several approaches at present. One of them was patented (US6098629) by Endonetics, under the trade name Gate Keeper^{TM} which was announced to have received FDA approval for clinical trials. This system is an endoscopically controlled overtube device which delivers dehydrated hydrogel implants into the submucosa of the cardia. After the

implantation the preformed hydrogel prosthesis swells to its maximum volume in 24 h [145,195].

A study reported that the prosthesis remained intact one and six months after treatment in 80.4 % and 70.4 % of the patients, acid reflux decreased significantly, the average LOS pressure increased significantly [63]. A long-term follow up study (24 months) showed likewise the improvement of the symptoms and reduction of PPI use [65]. Two serious side effects were reported, pharyngeal perforation and continuous nausea, requiring the removal of the prosthesis [53].

There are two other similar prostheses which are important for the endoscopic bulking device. One of them is Enteryx® (Enteric Medical Technology, Foster City, CA), which used a biocompatible polymer (8 w/v ethylene-vinylalcohol polymer) with a radiopaque contrast agent (30 w/v tantalum powder) dissolved in an organic liquid carrier as injection material. This device has just been approved by the FDA, which means, the clinic feasibility and safety of this method were proved and the result was satisfied. Several studies showed that this method was a safe and effective, and durable enduluminal therapy for the majority of treated patients. At 12 months, 84 % of patients used PPIs 54 % lower than before, at the same time, symptoms score, quality of life scores and oesophageal acid exposure were all significantly improved. The most common adverse event was transient retrosternal chest pain, injected material loss was also observed and re-injection was required in not too low a percentage (20 %) [30,87,140].

The other one is using polymethyl methacrylate (PMMA) as injection material like Gate Keeper™ [59]. In the short term a significant improvement of the symptoms was observed but a long-term study was not found.

Although in the initial phase of clinical application, all these bulking techniques appear easy to perform, but none of them was proved to be totally satisfied. The long-term result was always required by the clinic, reversibility should be desirable, especially in case of dysphagia.

1.1.3.4 Surgical therapy

Surgical therapy is besides above mentioned main treatments for GORD also an important treatment type. Since the other treatments such as pharmacological and endoscopic therapy are life-long therapies and consequently expensive, surgical therapy shows its cost advantage compared to the others. At the same time not every patient would like to depend on medication [7,196]; thus the surgical therapy is a good choice.

Surgery for GORD has been in a state of evolution over the last 70 years. The aim of surgery is to strengthen the lower oesophageal sphincter by wrapping the fundus of the stomach around it and consequently preventing the reflux. The most important antireflux surgeries are:

- Nissen fundoplication, including the modification form M. Rossetti [161]
- Belsey's wrap [14]
- Hill's gastropexy [80]

These surgeries are similar and the only difference is, where and how deeply the lower oesophageal sphincter is involved by the fundus of the stomach (Nissen 360°, Belsey's warp 240°, Hill' gastropexy 180°). Fig. 1.5 shows the procedure of Nissen fundoplication.

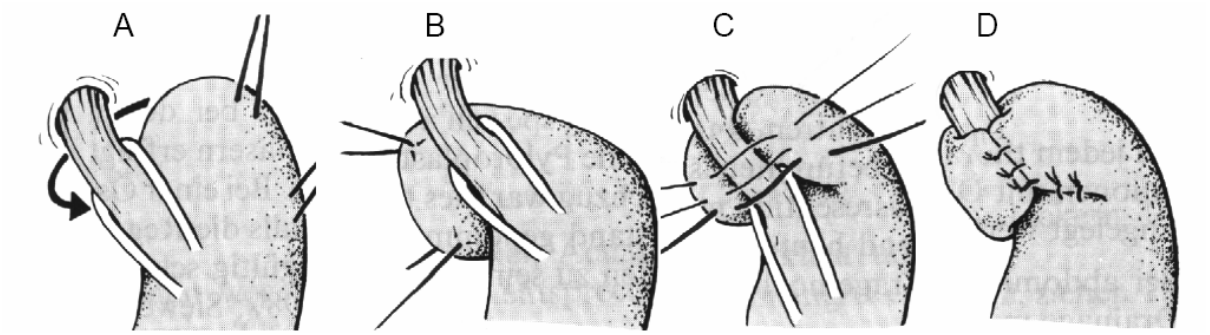

Fig. 1.5: Surgical sequence for Nissen fundoplication
A-C) the upper part of the stomach is wrapped around the lower sectionof the oesophagus. D) the LOS is transformed into a valve. (figure according to [141])

The Nissen fundoplication has been widely modified after it was invented, e.g. M. Rossetti modification in 1964, P. Donahue modification in 1985 [47], T. DeMeester Modification in 1986 [40]. A large experience with Nissen fundoplication was accordingly gained. It was report by Polk and Zeppa that 96 % of 994 patients who had surgical treatment reported a symptomatic improvement during a short follow-up period of 2.5 years [153]. Dr. T. DeMeester has shown that in his group 91 % of patients remained symptom-free in a 10 years follow-period. Another important finding was, the incidence of persistent dysphagia was decreased from 21 % to 3 % [41]. The latest report indicated that 187 from 226 (83 %) patients were highly satisfied with the clinical outcomes during a 10 years follow-up period [98].

Even if the surgical treatment is an effective method, the postoperative complications have been reported. The most common symptom is dysphagia by the patients who has previously no dysphagia [151]. Other commonly reported symptoms are early satiety, abdominal bloating, diarrhea, and recurrent reflux symptoms.

1.1.4 Conclusion of current treatment methods

Several guidelines have been published on the management of the disease [62,135,203]. The consensus at present is that PPIs are the most effective therapy and should be used as the first therapy of control of GORD, after the clinical diagnosis has been made (based on the basis of symptoms). If symptoms continue despite PPI use, endoscopy should be considered. The aim of long-term treatment is to step down management to the lowest level of medical therapy that controls symptoms, or consider surgery. Patients with a relapse should be restarted on therapy at the level that previously controlled their symptoms. Fundoplication surgery requires an experienced surgeon and should only be recommended for selected cases, for example, patients who have PPI intolerance or do not wish to take the medication long term.

None of the treatment methods is 100 % satisfying for most patients. On the other hand the GORD market is increasing quickly. That means, a relative safe, efficient and inexpensive method needs to be developed. At present there are many researchers who are attempting to find a solution. Which one could win the market is not yet clear. In this thesis a new implant for treating GORD is developed.

1.2 A new implant for treating GORD

The idea is to place a ring shape implant (Fig. 1.6) around the LOS. The implant has a porous inner side, which is supposed to enable tissue from LOS to grow into the implant and thus prevent the migration of the implant along LOS. Since the complete or partial loss of function of LOS is the main cause of the GORD, the implant is designed to aid and support the lacking pressure from the sphincter.

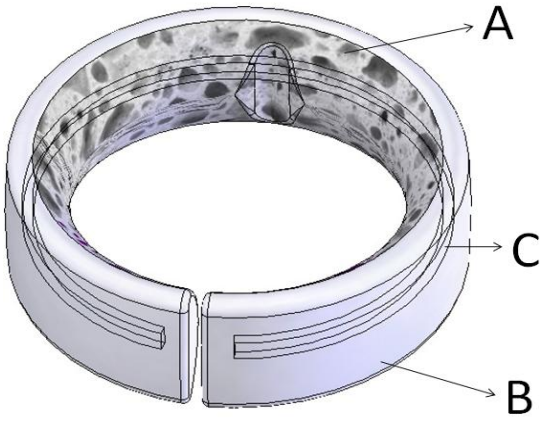

Fig. 1.6: Model of the implant with an inner porous and an outer non-porous surface
The goal is that cells will grow into the porous structure (A), thus preventing the migration of the implant along the oesophagus. The outer side is smooth (B), which hinders neighbouring tissue attachments. The green line is a Nitinol ring (C), which is widely used in medicine because of its superelasticity and shape memory. The original idea comes from Havard J. Haugen [77], but the implant design is improved in this study.

When eating, the peristaltic movement of muscle will partially open the implant and allow for food to smoothly pass through. After eating, the implant will supply a pressure from outside with the main contribution from superelastic Nitinol ring, thus reducing the LOS volume.

The porous inner side of the implant and superelastic Nitinol ring are the key components of the implant design. Earlier studies have shown that porous structure with pore diameters of 100-300 μm, interconnective pores of 10-30 μm and a porosity higher than 70 %, would allow ingrowth of fibroblast and a vascularisation [71,201,212,219]. The ingrowth or partial ingrowth of cellular tissue is critical for preventing the migration of the implant along the LOS. The Nitinol ring supplies an additional pressure from outside to LOS because of the special superelasticity and shape memory which keeps the implant in its original form. The pressure is adjustable through varying the axial diameter of the Nitinol ring.

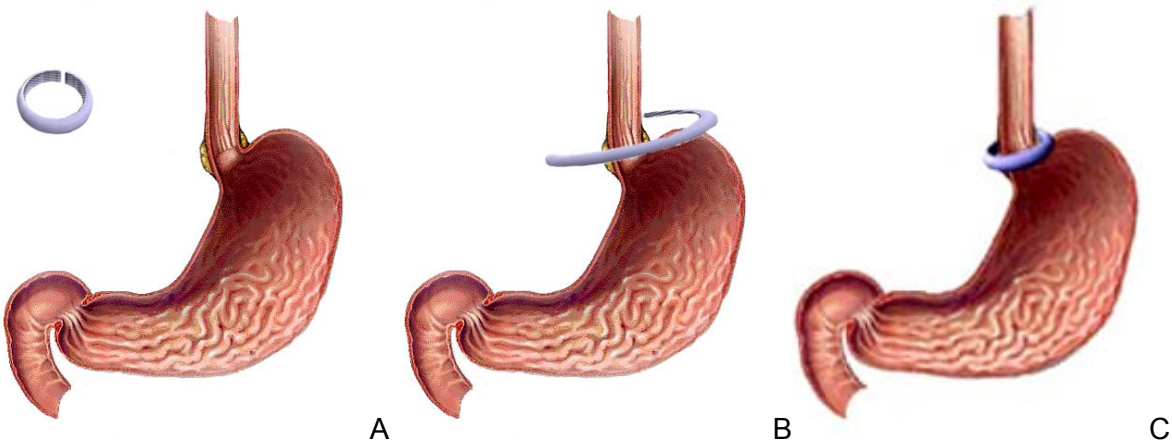

Fig. 1.7: Placement of the implant around the oesophagus at LOS
The implant is very flexible and can be stretched out (A and B). In this way the implant is placed around the LOS manually by the surgeon. (A particular applicator for the implant was also developed by the company partner Medi-Globe GmbH. This applicator will allow an easy operation for a less experienced surgeon. (figure according to [77])

Some certain specifications must be kept for the success of the development of the implant. As the implant was designed to be placed around the oesophagus, using a biocompatible polymer is very important for the implant. Secondly minimally invasive surgery of the implantation is another factor which plays an important role in the modern medicine. The ring should be easily implanted manually by the surgeons; the placement of the implant is shown in Fig. 1.7. Furthermore, an applicator was designed for the implant by the project partner (Medi-Globe GmbH, Achenmühle, Germany). With the help of the applicator a surgeon without much experience can also perform the surgery easily.

1.3 The MuCell® Process, a useful foaming method

As mentioned above, the production of the porous inner side of the implant is one of the key milestones of the development. On the other hand, since the GORD is a very common disease in Western Europe and North America [108], the yearly need of GORD implants in Germany could be very high and the number is estimated to be 10000. Thus a large scale production is necessary, there are two basic requirements of the process of the implant production: the porous structure of inner side of implant must be adjustable and a proper pore diameter with high porosity can be achieved with varying the process parameter; secondly, the productivity of the processing method must be high; the potential of this process should suffice for the yearly need in Germany and later for the European market.

Considering the above mentioned requirements, finding an appropriate foaming process is consequently decisive for this project. At present, various techniques are used to produce a

plastic product with microcellular structure. As techniques used for medical scaffold following some fabrication routes are listed in Tab. 1.1

Fabrication route	Advantages	Disadvantages
Thermally induced phase separation [120]	High porosities (~95 %) Highly interconnected pore structures Anisotropic and tubular pores possible	Long time to sublime solvent Shrinkage Small scale production Use of organic solvents
Solvent casting/particle leaching [3]	Controlled porosity Controlled interconnectivity	Structures generally isotropic Use of organic solvents
Solid free-form [189]	Porous structure can be tailored to host tissue Protein and cell encapsulation possible Good interface with medical imaging	Resolution needs to be improved to the micro-scale Some methods use organic solvents
Microsphere sintering [78]	Graded porosity structures possible Controlled porosity Can be fabricated into complex shape	Interconnectivity is an issue Use of organic solvents
Scaffold coating [160]	Quick and easy	Clogging of pores, sometimes organic solvents used, coating adhesion to substrate can be too weak
Electro-spinning [36]	High porosities High interconnectivity	Use of organic solvents Long cycle-time

Tab. 1.1: Foaming methods used in medical applications for fabrication of scaffolds
These methods are commonly used to produce scaffolds with high porosity and interconnectivity. None of them is 100 % satisfying. Using organic solvents lead to a damage of biocompatibility of the scaffold; long cycle-time limits the productivity of the process.

None of the methods in Tab. 1.1 is suitable for this project by reason of using organic solvents, which leads to a critical reduction of biocompatibility of the implant, or long cycle-time of production, which does not match the yearly need of the implant.

Since no suitable method from traditional processes can be found, an industrial microcellular foaming process which is named MuCell® technology was considered as the fabrication process of the implant [215]. The MuCell® technology can be used on extrusion, injection molding or blow molding machines. The atmospheric gases, such as carbon dioxide (CO_2) and nitrogen (N_2), are used as blowing agent, which is injected in the plasticization section of the injection molding or extrusion (Fig. 1.8). The plastic granules are plasticized by the rotation of the screw designed particularly for MuCell® with a long plasticizing section (L/D: approx. 25:1) and a homogenizing section for gas/melt mixture. During plasticizing time the blowing agent is injected into the polymer melt through the gas injector. Under high pressure in the cylinder and rotation of the screw the blowing agent is completely dissolved and dispersed in the polymer melt. After plasticizing the gas/melt mixture is injected into the mold

and with the pressure drop the dissolved gas expands to produce the microcellular foam structure. The process is schematically shown in Fig. 1.9.

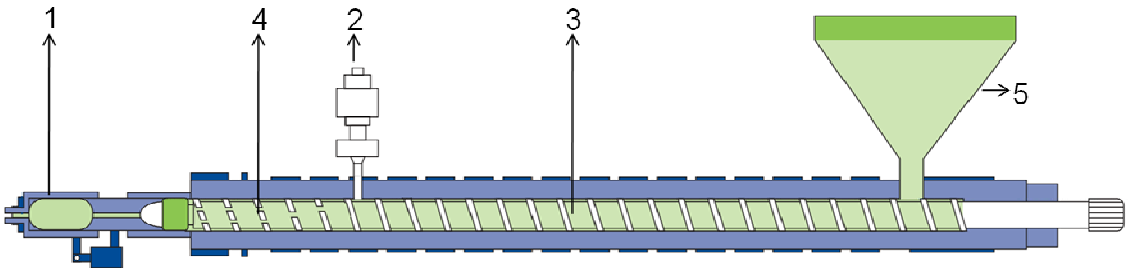

Fig. 1.8: **MuCell® plasticizing unit.**
1. Needle valve nozzle 2. Gas injector 3. MuCell®-plasticizing screw (L/D ratio: 25:1) 4. Homogenizing section for gas/melt mixture 5. Plastic granules without blowing agent. (figure according to [136])

Normally microcellular foams are defined as uniform cells with diameters of less than 100 microns. Such cell structures are produced when the cell nucleation rate is both extremely high and much greater than the diffusion rate of the blowing agent into cells. Conventional foaming technologies use physical blowing agents with nucleation agents (i.e. talc or calcium carbonate) or chemical blowing agents that induce heterogeneous nucleation in the material at a fixed and relatively small number of sites. The actual number of cell sites is related to the quantity of nucleating agent added; the homogeneity of the mixing of blowing agent and polymer melt has an obvious effect on the uniformity of the cell size. As result the lack of cell size uniformity was often observed by using conventional foaming technology.

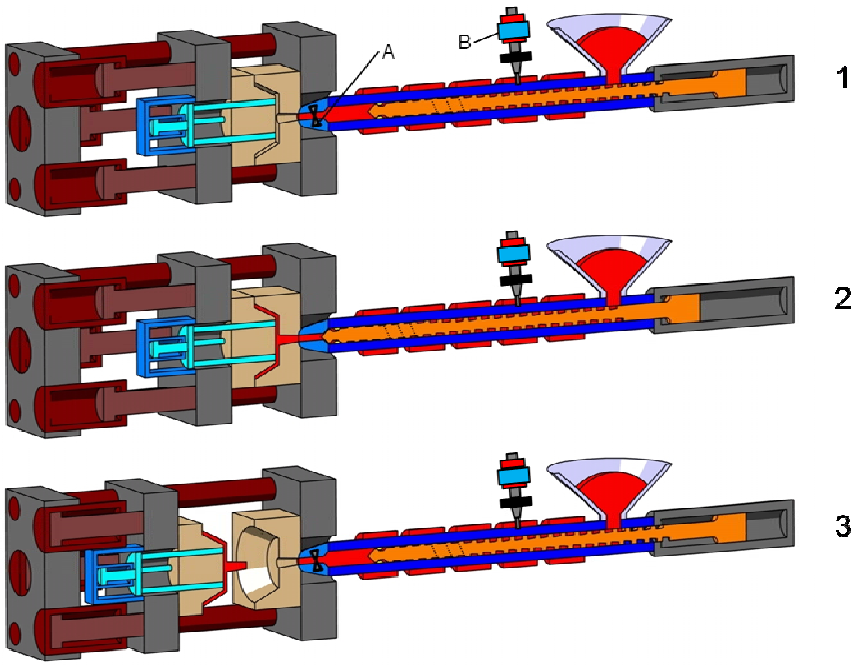

Fig. 1.9: **Schematical process of the MuCell® technology**
1. The plasticizing process takes place after the injection of the previous shot and during the mold cooling phase. The needle valve nozzle (A) is closed in this stage. The melt builds up in front of the screw. The gas injector (B) introduces blowing agent into the melt during the plasticizing process. Under heat and pressure in the cylinder, the gas is completely dissolved and dispersed in the polymer melt. 2. The needle valve nozzle opens and the melt is injected. The finely dispersed gas in the melt nucleates and expands to produce a microcellular foam and the cavity is then fully filled. At the same time the plasticizing process takes place with the gas injection. 3. After the stage 2, in which the cooling and plasticization are finished, a molded part with a solid outer skin and microcellular foam core has been formed and the mold opens for the ejection of the molded part. (figure according to [136])

A high nucleation rate needs a considerable thermodynamic instability that is achieved by first dissolving a blowing agent into the molten polymer at high temperature and high pressure thus creating a single-phase solution and then lowering the pressure quickly to below the saturation pressure. To reach the desired high rate of nucleation, the saturation level of the dissolved blowing agent and/or the rate at which the instability is achieved must be high. Compared with the conventional foaming technology the MuCell® technology has a particular way in which the cells are nucleated. The physical blowing agent (N_2 or CO_2) is injected into the polymer melt above both its critical pressure P_c and critical temperature T_c, i.e. in a supercritical state (Fig. 1.10). The gas in supercritical state is also called supercritical fluid (SCF), which is actually like liquid and which has a better miscibility with polymer melt than gas. With using a special gas delivery system and homogenizing section for gas/melt mixture MuCell® technology can facilitate an appropriate amount of blowing agent, a rapid creation of the single-phase solution, thus creating a high nucleation rate which is difficult to achieve by conventional foaming technology. As result a very small and uniform cell size is easy to

achieve. Fig. 1.11 shows the difference of the cell structure made from MuCell® (left) and from conventional foaming technology (right).

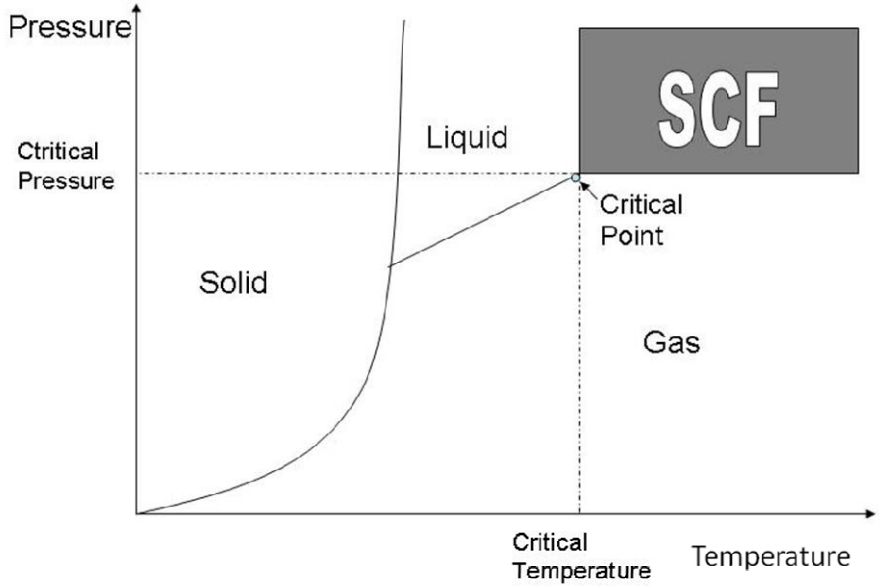

Fig. 1.10: Material phase diagram
A supercritical fluid (SCF) is any substance at a temperature and pressure above its thermodynamic critical point

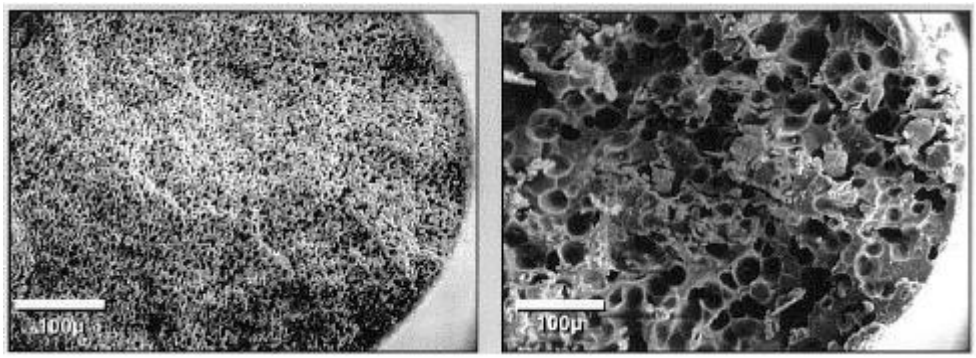

Fig. 1.11: Comparison of the porous structure made by MuCell® technology and the conventional foaming process with a chemical blowing agent
The right figure shows a porous structure of injection molded PP (Polypropylene) part with using a chemical blowing agent; the porous structure in the left figure is produced by MuCell® process. The produced pore structure from MuCell® process is more uniform and the pore size is smaller. (figure according to [136])

MuCell® technology is widely used in automobile and furniture industries. In most cases, MuCell® technology is used to save raw materials. Some industrial products, which are made of polymer and have no strict physical property requirements, can be produced and foamed by

MuCell® technology with 20 % weight reduction compared with a normal injection molding process, without obvious physical property loss [144]. Advantages of MuCell® are:

- Reduction of viscosity. The addition of SCF into a molten polymer reduces the viscosity due to a reduction in T_g, and the reduction of viscosity follows classical viscoelastic scaling theory [106]. The reduced viscosity can result in hydraulic injection pressure reduction as compared to the conventional molding. For some polymer materials which are sensitive to processing stress the reduction of the viscosity of the polymer melt leads to a lower degradation during processing.
- Effect on part weight. For the aim of cost saving the part weight can be reduced up to 20 % without obvious physical property loss. The percentage of part weight reduction depends on the polymer and mold design. 20 % is just an experiential value for polyolefin and ratios of flow lengths to part thicknesses (L/D) are less than 100:1.[1.1]
- Effect on cycle time[1.2]. The MuCell® process generally tends to shorten the cycle time due to the elimination of hold time. The uniform internal pressure of microscopic cells provides the cavity pressure needed for filling. As byproduct a cavity pressure reduction of up to 80 % can be achieved with microcellular molding.
- Effect on temperature setting. As mentioned the viscosity of the molten polymer is reduced because of the addition of SCF, therefore the reduction of the barrel temperature profile is possible according to the polymer rheology [173], if the viscosity of the molten polymer is kept unchanged after the SCF injection. Experimentally the barrel temperature setting after the injectors may be reduced by 10 to 15° C from the last zone prior to the injector. For some temperature sensitive polymers the reduction of barrel temperature can decrease the processing stress and hence degradation of the polymer during the processing.

The aim of using the MuCell® technology in this project is to produce implants with inner porous structures where the cells of sphincter can grow into, so that the implant can be fixed around the sphincter. The physical properties of the implant itself i.e. the polymer matrix, is

---

[1.1] In this project thermoplastic polyurethane (TPU) and a specially designed mold were used to produce the implant and up to 65% part weight reduction was achieved.

[1.2] A very important factor in determining the cycle time is part thickness. It is more difficult to significantly reduce cycle times with parts having a thickness of more than 4 mm because the cells appear to act as thermal insulators, hence slowing down the rate of cooling. In this project, the molded implant has a thickness of 12 mm. The cooling time was so much prolonged that the benefit of elimination of the holding time was counteracted and the whole cycle time was not reduced, but even prolonged.

not decisive for the whole physiological function of the implant, because the Nitinol ring placed in the implant supplies the pressure from outside to keep the oesophagus closed after a food passage. According to the foaming theory the porous structure made by MuCell® is adjustable by varying the processing parameters, e.g. gas content, part weight reduction, barrel temperature, etc. (s. chapter 4.1). Since the porous structure of the implant is the key parameter for the cell ingrowth, one of two main parts of this project is to investigate the relationship between the porous structure of an implant and setting parameters of MuCell® process. The present work is considered to be the first application of the MuCell® technology to a medical implant.

2 Aim of the study

The aim of this project is using MuCell® technology to produce an implant made of polymer (thermoplastic polyurethane), which soothe or even heal the gastro oesophageal reflux disease.

The implant consists of two major parts, one inner porous structure and an outer solid core with a Nitinol ring as x-ray marker and as elastic mechanical actor. Open porous structures should have pores of 100-300 µm in diameter and porosity above 70 %. The pore needs to be interconnected with pore sizes of at least 30 µm. These features are the requirements of cell growth into the porous structure of the implant, cell metabolism and nutrient exchange within the porous part of the implant. On the other hand the biocompatibility of the polymer used for the implant has to be guaranteed after the processing.

In order to reach the goals, the project has been divided into two parts.

1. The relationship between the porous structure of the implant and parameter setting of the MuCell® technology must be quantified in detail. In order to reach the suitable porous structure all the relevant parameters need to be varied in a certain processing range. At the end the major processing parameters and their influence on the porous structure should be ascertained.
2. The implant must be biocompatible after production and sterilization. Certain surface treatments will be performed in order to increase the biocompatibility of the implant. Consequently in vitro biological tests, e.g. cytotoxicity tests and cell culture experiments, must be performed to indicate the effect of the surface treatment and sterilization on the biocompatibility of the implant.

Finally, the suitable processing parameters and surface treatments should be established for the implant production and implants should be formed.

3 Foaming Theory

3.1 Background

This chapter introduces the theoretical modeling for the production process (chapter 1.3) of the implant for treating GORD. The production of polymer porous structure results from a creation of a gas phase in the polymer matrix. The aim is that the gas is as evenly as possible distributed in the polymer matrix, so that a uniform and homogeneous porous structure can be reached. The introduction of gas into polymer melt can be resolved in different ways. The formation of a gas phase can directly take place during the synthesis of polymer, when a gaseous component is released, e.g. polyurethane foam. The introduction of gas into polymer is mostly achieved by adding a foaming agent. The substance, which releases gas due to chemical reaction (chemical foaming agent) or phase transition (physical foaming agent), is described as foaming agent. The foaming agent can be added during the polymer synthesis, like the particle foam production of polystyrene (PS); be impregnated into solid polymer under high pressure, like the production of microcellular foam with batch process; or be added into the melted polymer under pressure, like foam extrusion or foam injection molding. In recent years the methods of direct injection of gas into polymer melt have been developed rapidly and are currently applied in foam extrusion or foam injection. MuCell® is one of the mentioned foaming methods with direct gas injection into the polymer melt.

Besides MuCell® there are two similar injection molding foaming technologies industrially known. These processes use gas direct injection technology to produce foam structures, just the position of gas injection in the whole process is different. ErgoCell technology [126] (Sumitomo (SHI) Demag Plastics Machinery GmbH, Schwaig, Germany) uses an additional component between plasticizing cylinder and injection nozzle to inject the gas into the polymer melt after the plasticization of polymer. The mixing of gas and polymer melt takes place also in this component. Another technology, Optifoam™ [126] (Sulzer Chemtech AG, Winterthur, Switzerland), uses a special injection nozzle to mix the gas and polymer melt. MuCell® technology differs from the mentioned two foaming technologies in gas injection position, the middle of the plasticizing cylinder. These concepts facilitate the generation of microcellular foam structure, but the MuCell® technology is relatively better commercialized compared with the others. In this chapter the foaming theory based on MuCell® technology is discussed in detail.

The phenomena-associated pore growth is known as nucleation and can be described by the nucleation theory [39]. This nucleation theory is also named as the classical nucleation theory that has been extensively reviewed [1,179]. Various extensions of this theory have been reported [17,33,56,91,95,118,156,211]. Models based upon intermolecular potentials [139,166] and molecular dynamics [222] were developed. Generally, the growth of a cell is

described by the continuum conservation equations. Studies of pore growth in infinite [12,150,185] as well as in finite liquid domains [5,8] have been reported.

A pore growth model of a polyvinylchloride (PVC)/CO_2 system was developed by Shafi et al. [175]. The classical nucleation theory was used as a basis for the development of their model. Haugen [77] modified this theory to fit a thermoplastic polyurethane (TPU)/water system processed in an injection moulding machine. But this modified model is based on using salt as water carrier and nucleation agent and is therefore not applicable to this project. Since no single model was found suitable for a thermoplastic polyurethane (TPU)/CO_2 system with MuCell® technology, which was used in this project, a pore growth model based on the foam formation process of MuCell® technology was established in this chapter to explain the connection of material with process parameters and foam structure.

3.2 The foaming process with MuCell® technology

The foam formation process is shown in Fig. 3.1 for better understanding of the MuCell® technology. This foam formation process consists of four steps:

- Creation of a single phase mixture of polymer melt with gas
- Cell nucleation
- Cell growth
- Cell stabilization

The polymer is dosed through a hopper into the cylinder by the turning of the screw, by high temperature and pressure, the polymer is plasticized. During the plasticizing phase the gas is injected under high pressure through an injector into the polymer melt. The gas is absorbed and dissolves in the polymer melt due to high pressure, high temperature in the cylinder and shearing of the screw. At the end of the plasticizing phase a single phase of mixture of polymer melt-gas-solution appears. The mixture is ejected out of the nozzle after the plasticizing phase. Thereafter, the pressure decreases rapidly and thus reduces the solubility of the gas in the polymer melt, the cell nucleation is then initiated. This process takes place in the mold. Subsequently cell growth begins in the polymer due to diffusion of the gas out of the polymer melt-gas-solution mixture. The foam formation process terminates in the so-called cell stabilization. This results from a decrease of temperature below a critical point that is defined as gas transition temperature T_g for the amorphous thermoplastic and as crystallization temperature T_m for the semi-crystalline thermoplastic. Under T_g or T_m the polymer has a phase change from molten phase to solid state, so that the long chain molecules of polymer are fixed as well as the porous structure.

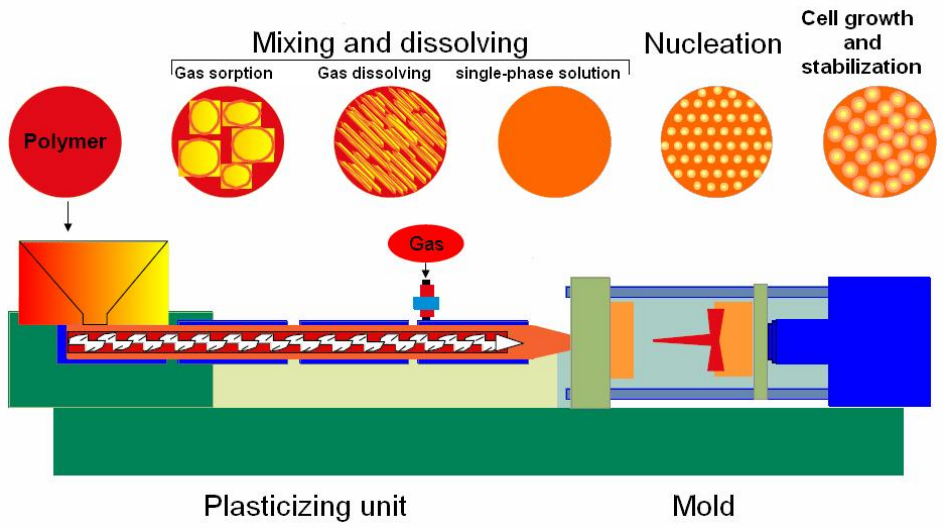

Fig. 3.1: **Foam formation process of MuCell®**
From left to right: The polymer is dosed through a hopper into the cylinder. In the cylinder the gas injected through the injector is adsorbed by the polymer melt under a high pressure. After the gas sorption the gas dissolves in the polymer melt and a single-phase of polymer melt-gas-solution appears. The nucleation takes place in the mold when the mixture is injected out of the nozzle. At the end of the process the cells grow and stabilize subsequently in the mold. (figure according to [162])

3.2.1 Creation of a single phase of polymer melt-gas-solution

Dissolving of the gas in the polymer melt is the basic prerequisite for creation of a homogeneous foam structure. The solubility of gas in the polymer melt depends on the interaction between polymer and gas, as well as between temperature and pressure in the cylinder. The maximal content of gas that can dissolve in the polymer melt at respective conditions is known as saturation concentration. Because only a certain gas concentration in the polymer melt can be reached depending on the temperature and pressure, it is necessary to harmonize the process parameters with the amount of gas added, so that all added gas can dissolve in the polymer melt. Undissolved or excess gas leads to a formation of large cavities in the foam structure. In addition to the solubility of gas in the polymer melt the diffusion plays also an important role for the formation of a single phase of polymer melt-gas-solution. A high local concentration of gas molecules leads to an exceeding solubility of gas in the polymer and furthermore a separate gas phase can be observed. To avoid this high local concentration, the gas must as evenly as possible distributed in the polymer melt, which results from gas diffusion. Through the intensive mixing that occurs in the cylinder by screw rotation the diffusion of gas can be shortened.

The gas injected into the polymer melt leads to a change in rheological properties of the polymer melt. The addition of gas acts like a plasticizer and causes a fall of glass transition temperature, and thereby reduces the viscosity of the polymer melt [103]. The amount of the

glass transition temperature shift or viscosity decrease depends on the polymer-gas-combination. The smaller the molecule weight of gas is, the more intense the decrease of viscosity will be.

If it is necessary to determine the viscosity of polymer melt-gas-solution experimentally, the standard rheometer needs some modifications to prevent the release of the dissolved gas out from the mixture during measurement. Another method is to use an online-extrusion-rheometer that has a measuring device similar to a high pressure capillary rheometer directly installed in the extruder. Numerous polymer-gas-combinations were investigated and it could be proved that the shape of the viscosity curve does not alter. The viscosity reduction resulted from the addition of gas can be principally compared with a viscosity reduction by increasing the temperature [68,69,103].

Various mathematical and empirical models were developed for the determination of the glass transition temperature [27,60,198]. A linear reduction of the glass transition temperature with increasing gas content was found out from numerous polymer-gas-combinations [26,27]. It was also proved that the reduction in viscosity is not only attributed to the decrease of glass transition temperature [69,103]. An additional "diluting effect" of gas has been expected for the contribution of the viscosity decreasing, because the free volume was enlarged by the reason of gas mixing [70,75].

3.2.1.1 Solubility of gas in polymers

The knowledge of about the interdependency of solubility of gas in polymer with temperature and pressure in the cylinder is very important for the production with a good porous structure. Complex models based on different assumptions were established for the determination of the saturation concentration [24,112,205]. A practical model, which is used to describe many gas-dissolving processes, is named Henry's law.

$$C = \frac{m_{gas}}{m_{polymer}} = S \cdot p \qquad \text{Eq. 1}$$

C is the saturation concentration of gas; m_{gas} and $m_{polymer}$ are gas and polymer mass; p is the partial pressure; S is the solubility coefficient which is the reciprocal of the Henry-Coefficient H. The solubility coefficient S is constant by the low temperature and pressure, whereas by the high temperature and pressure the solubility coefficient S is a function of temperature and pressure [49,50].

$$S = S(p,T) \qquad \text{Eq. 2}$$

The temperature dependency of solubility coefficient can be explained through the Arrhenius equation.

$$S = S_0 \exp\left(-\frac{\Delta E_s}{RT}\right) \quad \text{Eq. 3}$$

S_0 is a pre-exponential factor that is extrapolated from an infinite temperature; ΔE_s is the enthalpy of solution, R is the gas constant and T is the temperature. The experimental determinations of S_0 and ΔE_s were performed for many polymer-gas-combinations [49,50,103,170]. Since the enthalpy of solution ΔE_s of most polymer-gas-combinations is negative, the solubility of gas in polymer decreases with the rise of temperature.

3.2.1.2 Diffusion of gas in polymers

After dissolving the gas in the polymer melt the gas must spread as evenly as possible in the polymer melt through the diffusion, so that a homogeneous polymer-gas-solution can be reached. The driving force of the gas diffusion in polymer melt is the concentration gradient of gas. Due to the thermal motion of polymer molecules in molten state the gas molecules can move through the intermolecular space according to the concentration gradient. The speed of diffusion processes is described by the Fick's law [209]. The diffusion flux *dm/dt* is in the direction of the concentration gradient (x-coordinate) and proportional to the concentration gradient *dc/dx*, the density ρ and cross section A.

$$\frac{dm}{dt} = D_{diff} \cdot A \cdot \rho \cdot \frac{dc}{dx} \quad \text{Eq. 4}$$

D_{diff} is the diffusion coefficient and similar to the solubility coefficient, therefore, D_{diff} can be described by the Arrhenius equation.

$$D_{diff} = D_{diff,0} e^{-\frac{E_d}{R \cdot T}} \quad \text{Eq. 5}$$

The pre-factor $D_{diff,0}$ is the maximum diffusion coefficient at infinite temperature; E_d is the activation energy for diffusion. Both factors were experimentally determined for various polymer-gas-combinations and listed in many references [20,49,174].

According to Eq. 5 the diffusion coefficient and the corresponding diffusion increase with rise of the temperature, which can be attributed to the increase of mobility of molecules by the rising of the temperature. Consequently the diffusion of gas can be accelerated by increasing the melt temperature. However, for most of the polymer-gas-combinations the solubility of gas in polymer decreases with the rise of melt temperature.

There is another way to reduce the diffusion time, by using a mixing device to bring two substances into a shear field. The shear deformation leads to a better dispersion of gas in polymer melt. Thereby, the path of diffusion decreases and the diffusion is accelerated due to the larger contact area between gas and polymer melt. The diffusion path can be reduced up to 100 µm under the influence of the shear deformation [147]. The diffusion coefficient of CO_2 and N_2 in polystyrene, polyethylene and polypropylene is in the range between 10^{-4} to 10^{-5} cm^2/s for a normal processing temperature of 200° C [148,149]. The time of gas diffusion through the polymer melt is normally less than 10 s.

3.2.2 Cell nucleation

Cell nucleation describes an onset of a phase transition in the polymer-gas-combination. In the polymer foaming the cell nucleation is initiated by a rapid change of thermodynamic equilibrium of polymer-gas-solution. This can be done by both temperature increase and pressure decrease. In both cases the gas solubility in polymer melt reduced and the dissolved gas leaves of the solution to form a second phase. The initiation of cell nucleation occurs in general by a pressure drop since it is not possible to get a rapid temperature increase in polymer melt for a homogenous nucleation over the entire flow cross section due to the low thermal conductivity of the polymer melt.

The nucleation can be basically divided in two different mechanisms. When the nucleus formation occurs in a completely homogenous polymer melt without any impurities or additives, it is called homogenous nucleation. On the other hand if a second phase such as impurities, additives or blowing agent exists in the polymer-gas-solution, therefore, the nucleus formation occurs on the surface between the particles and solution, this mechanism is named as heterogeneous nucleation. A heterogeneous nucleation occurs by the use of the chemical blowing agent, because the solid residues from decomposition of the chemical blowing agent act as particles in the polymer melt. In this chapter both homogenous and heterogeneous nucleation mechanisms are introduced.

3.2.2.1 Homogenous nucleation

The change of free energy is considered as the nucleation energy required for the formation of a nucleus. According to the nucleation theory a decrease of free energy is the prerequisite for the formation of a stable nucleus. The free energy ΔG_{hom} of homogenous nucleation can be described by the following equation:

$$\Delta G_{\mathrm{hom}} = -V \cdot \Delta p + A \cdot \gamma \qquad \text{Eq. 6}$$

Where V is the volume of a single gas bubble; Δp is the pressure difference between the inside of the gas bubble and the polymer-gas-solution; A is the surface of the gas bubble and γ is the

interface tension of the interface between gas bubble and polymer-gas-solution. Because spherical gas bubbles are formed due to the lowest surface tension, the Eq. 6 can be redrafted as follows:

$$\Delta G_{\text{hom}} = -\frac{4}{3} \cdot \pi \cdot r^3 \cdot \Delta p + 4 \cdot \pi \cdot r^2 \cdot \gamma \qquad \text{Eq. 7}$$

where r is the radius of the gas bubble. If the free energy ΔG is plotted against the gas bubble radius, a maximum of the free energy is clear to be seen in Fig. 3.2. With a small bubble radius the surface tension dominates and therefore the change of free energy ΔG_{hom} increases with the radius initially. In this area a shrinking of the bubble is easier than a growth to occur due to positive free energy change, resulting in a collapse back upon themselves. Only when the critical radius r^* is exceeded, the bubbles can grow stably, because with increase of the radius the free energy ΔG_{hom} decreases. The critical radius is defined as the radius in which dissipation of the free energy as a function of the radius is zero. As result the critical radius r^* can be described by Eq. 8:

$$r^* = \frac{2\gamma}{\Delta p} \qquad \text{Eq. 8}$$

The nucleation energy ΔG^*_{hom} required for the homogeneous nucleus formation corresponds to the free energy for the formation of a gas bubble with the critical radius r^*.

$$G^*_{\text{hom}} = \frac{16 \cdot \pi \cdot \gamma^3}{3 \cdot \Delta p^2} \qquad \text{Eq. 9}$$

With the help of the nucleation energy the nucleation rate can be described with the Boltzmann distribution [32].

$$N_{\text{hom}} = f_0 \cdot N_g \cdot Exp(-\frac{\Delta G^*_{\text{hom}}}{R \cdot T}) \qquad \text{Eq. 10}$$

Here f_0 is a factor that describes the frequency of gas accumulation on the nucleus. N_g is the number of gas molecules in the solution. The nucleation rate is a measure for the number of nuclei initiated per time and volume unit. The total number of initiated nucleis per volume unit is named the nucleation density.

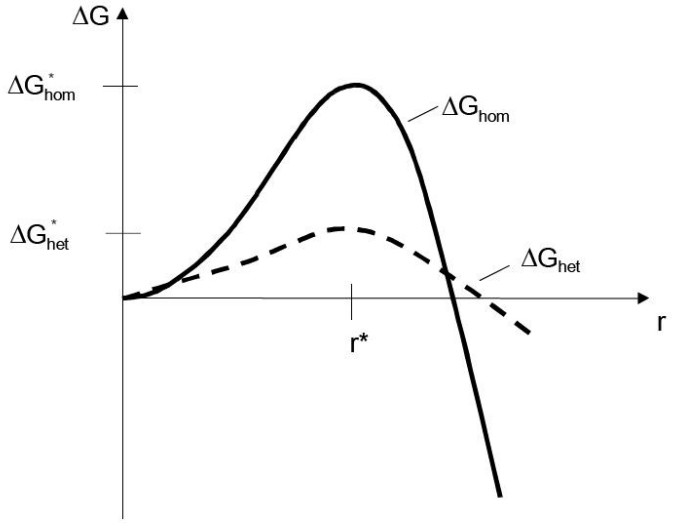

Fig. 3.2: The free energy of homogeneous and heterogeneous nucleation [34]

According to Eq. 9 and Eq. 10 it is obvious that a low surface tension and high pressure difference between the solution and environment lead to a reduction of nucleation energy, as well as a higher nucleation rate. The nucleation rate can also be increased by a higher temperature or larger gas content in the polymer melt.

3.2.2.2 Heterogeneous nucleation

The heterogeneous nucleation differs from the homogeneous nucleation by the presence of the dispersed solid particles in polymer-gas-solution. The influence of the interface between the polymer-gas-solution and particles can be described by an additional function *g(θ)* for the calculation of the nucleation energy of homogeneous nucleation.

$$\Delta G^*_{het} = \Delta G^*_{\mathrm{hom}} \cdot g(\theta) = \frac{16 \cdot \pi \cdot \gamma^3}{3 \cdot \Delta p^2} \cdot g(\theta) \qquad \text{Eq. 11}$$

ΔG_{het} is the heterogeneous nucleation energy, the function *g(θ)* depends on the the contact angle of the gas on the solid particle surface and is described as:

$$g(\theta) = \frac{1}{4} \cdot (2 + \cos\theta) \cdot (1 - \cos\theta)^2 \qquad \text{Eq. 12}$$

Since the value of *g(θ)* is only between 0 and 1, the heterogeneous nucleation energy is lower than the homogeneous nucleation energy or at maximum up to the same value. Thereby the nucleus formation is easer for a smaller contact angle, i.e. for a worse wettability of the surface of blowing agent particles.

The nucleation rate of the heterogeneous nucleation can be described with the following Equation [32]:

$$N_{het} = c_{het} \cdot f_1 \cdot Exp(-\frac{\Delta G^*_{het}}{R \cdot T}) \quad \text{Eq. 13}$$

Here c_{het} corresponds to the concentration of a blowing agent in the polymer melt and f_1 is similar to f_0, a factor of the frequency of gas accumulation at the nucleus. Compared with the homogeneous nucleation the heterogeneous nucleation rate is additionally affected by the blowing agent concentration and the size of the blowing agent. Actually, the more the blowing agent is added and the smaller the particle is, the better the nucleation is. In order to reach an even cell nucleation a homogeneous distribution of blowing agents in the polymer melt is indispensable.

3.2.3 Cell growth

The cell growth process describes the stabile growth of the cell nuclei, which means the bubbles that have reached the critical size for a stable growth. In the beginning, the bubble growth process is dominated by the hydrodynamic force. It is assumed that the bubbles begin to growth independently from each other. Thus the bubble growth can be described as an isolated bubble in an infinite viscoelastic medium. The driving force of the bubble growth is the pressure difference between the inside of the bubble and the medium. The growth speed is controlled in this stage by the surface tension of the bubbles and by the viscoelastic properties of the polymer melt. The gas diffusion has no effect in this stage [192].

In the beginning of the cell growth, the time-dependent radius $R(t)$ of a spherical gas bubble in the infinite viscoelastic medium can be described by the following Equation [12,102]:

$$\rho\left[\frac{3}{2}\left(\frac{dR(t)}{dt}\right)^2 + R(t)\frac{d^2R(t)}{dt^2}\right] + \frac{4\eta_E(t)}{R(t)}\left(\frac{dR(t)}{dt}\right) = p_1 - p_2 - 2\gamma \quad \text{Eq. 14}$$

Here ρ and η_E correspond to the density and elongational viscosity of the viscoelastic medium; p_1 and p_2 are the pressures in the gas bubble and medium; γ is the surface tension. The third term on the left side of Eq. 14 describes the influence of the viscoelastic properties of the medium on the growth of bubble radius. The elongational viscosity is used as the characteristic of viscoelastic properties of the medium, because a strong elongation strain on the gas bubble exists during cell growth. The potential influence of the shear from outside on the gas bubble is ignored in this equation, because the cell growth in the foam injection molding occurs outside the nozzle of the injection molding machine and therefore no shear strain exists. Eq. 14 was initially used for Newtonian fluids which show a pure viscous

behaviour. The consideration of the complex viscoelastic behaviours of the polymer melt is described through the term with elongational viscosity. Several models were developed for the description of the elogational viscosity which depends on the elongation rate, time and temperature [117,206].

In the selection and application of the models it must be taken into account, that during cell growth the polymer melt is undergone by a biaxial elongation strain (Fig. 3.3). The tensile force in the cell wall extends in all directions because of the three-dimensionality of the cell and therefore a biaxial elongational strain appears. Furthermore the elongational viscosity depends also on the remanent gas content in the polymer melt. Although the escape of gas from the polymer melt is a time-dependent process, it can be well assumed that the gas concentration quickly decreases immediately after leaving out from the nozzle, so that the description of the cell growth relates to the pure polymer melt [70].

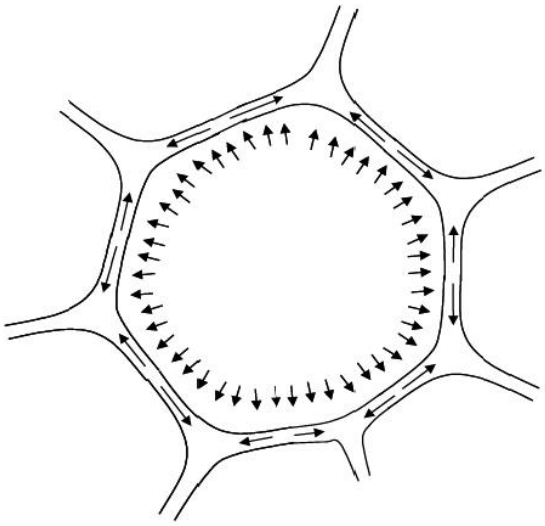

Fig. 3.3: Schematic description of the cell growth

However using Eq. 14 to describe the cell growth at the beginning is critical, because the gas transfer in the growing bubble via diffusion and not via isothermal effect, for example the heat release by the desorption of the gas from the polymer-gas-solution, are not taken into account [192]. Nevertheless, Eq. 14 is very suitable for assessing the influencing factors on the beginning of the bubble growth. Thus it is obvious that a high elongational viscosity can reduce the speed of cell growth, whereas a low surface tension leads to an increase of cell growth speed.

If the growing bubble reaches a certain size, growth can not be maintained by the pressure difference [192]. This means that the speed of gas supply into the bubbles is smaller than the value required due to the pressure difference and hydrodynamic force. The moment of

appearance of this phenomena is when the gas from the boundary layer of the gas bubble escapes into the bubble itself. The gas required for the further growth process must diffuse from farther region into the gas bubble. At this stage the cell growth is controlled by the diffusion of the gas.

The single gas bubble can be still regarded as isolated, but the medium around the bubble affects bubble growth due to the increase of the bubble size (Fig. 3.4). The inner circle is the growing bubble. This bubble is surrounded by a spherical shell which describes the surrounding medium, from where the gas diffuses into the growing bubble. Due to the diffusion of gas, the gas concentration in the polymer melt which directly surrounds the gas bubble, decreases. From the Fig. 3.4 it is evident, that the gas concentration in polymer melt is lowest at the surface of the gas bubble and increases with larger distance from the bubble.

It is necessary to use a coupled differential equation, which takes the mass transfer in the gas bubble into account, in order to describe cell growth controlled by gas diffusion. The conservation of mass, momentum and energy must be considered and related to each other with the cell growth. In recent references there are a variety of models that describe the diffusion-controlled cell growth in detail [5,8,89,155]. An appropriate model description can help to understand foaming process in addition to the mathematical description. Fig. 3.4 shows that before a direct interaction between two growing bubbles appears, the shell of respective bubbles will contact firstly.

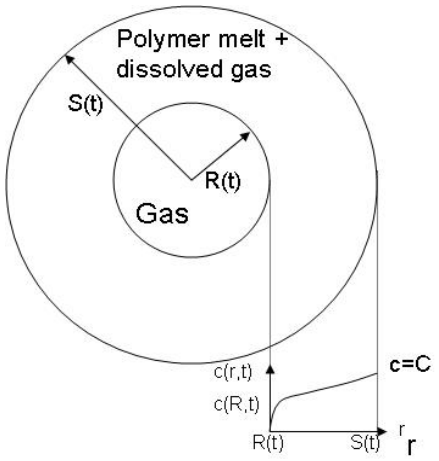

Fig. 3.4: Schematic illustration of growth of a single pore
The growth occurs as gas diffuses from the surrounding polymer into the bubble with radius R(t), the bubble is surrounded by a polymer melt shell with radius S(t). In this diagram the gas concentration in the shell is schematic illustrated, where C is the saturation concentration of the gas in polymer melt. (Figure according to [8]).

When the gas bubbles and relevant shells which join together are equal in size, the spread of the shell will stop and the cells can continue to grow until the gas existing in the shell diffuses into the gas bubbles. Consequently the bubbles have a similar size at the end of the foaming process. This is only a decent approximation when the cells are nucleated at the same time and average distance between the nuclei is equal. Based on this deduction it is obvious that a high nucleation rate and a well-proportioned distribution of nuclei are very important and necessary for a homogeneous pore structure.

If the gas bubbles with different sizes contact with each other, the gas is in favour of diffusing into the bigger bubbles due to energetic reasons. There is a balance (Eq. 15) between the surface tension γ needed for the bubble surface A and volume change V induced by the gas pressure p in the gas bubble.

$$\gamma \cdot dA = p \cdot dV \qquad \text{Eq. 15}$$

If the gas bubbles are seen as balls, the Eq. 15 can be changed with the bubble radius r.

$$\gamma \cdot 8 \cdot \pi \cdot r \cdot dr = p \cdot 4 \cdot \pi \cdot r^2 \cdot dr \qquad \text{Eq. 16}$$

So the gas pressure in the bubble is:

$$p = \frac{2 \cdot \gamma}{r} \qquad \text{Eq. 17}$$

Consequently the gas pressure in a smaller bubble is higher than the pressure in a bigger bubble for an identical surface tension and the pressure difference between the pressure in the polymer-gas-solution and gas bubble of the smaller bubble is lower. This is the reason why the gas is in favour of diffusing into the bigger bubbles when two bubbles with different size contact are present. For the same reason the coalescence of bubbles, which means the association of small cells to large cells and the corresponding reduction of the cell surface, occurs relatively easily compared with the total volume of the cells.

Another reason for the cell-coalescence can be ripping of the cell walls. In the course of the cell growing the spherical bubbles grow steadily against each other firstly. The distance between the bubbles become less and less, that means, the thickness of the polymer melt which surrounds and divides the cells become smaller. The cells are compressed at the place where they meet and change from spherical to polyhedron shape which is shown in Fig. 3.3. Single cells are then separated from each other only by very thin films of melt, the cell walls.

As already mentioned the polymer melt has received a biaxial elongation strain during cell growth. If the polymer melt strength is too low, there may be a rupture of the cell walls and the corresponding association with the neighboring cells. In addition to the coalescence of the cells, i.e. the complete association of two cells, the rupture of cell walls can lead to the formation of an open-cell structure. The cells keep their original form after the rupture of the cell walls; however, the cells are no longer completely surrounded by a polymer melt film, but linked with each other. Such effects are unexpected in the manufacture of closed-cell foams followed by a reduction in mechanical strength and in thermal insulation of the product. On the other side the open-cell structure has its importance as scaffold in the field of medicine.

The last effect on cell growth must be taken into account, that is, gas loss into the environment. The gas pressure in cells is far lower than the gas pressure of the surrounding area, so gas is easy to diffuse out from cells. The higher the temperature and the more slowly the cooling of polymer melt of polymer melt are, the larger the gas loss is. As mentioned above, the speed of gas diffusion decreases with the reduction of the reduced temperature of polymer melt. A quick cooling of the outer skin of the foam can likewise decrease the gas loss. If the gas loss in the environment per time unit is too large, it can even lead to a partial or complete collapse of the cell structure.

3.2.4 Cell stabilization

Cell stabilization, i.e. foam stabilization means the fixation of the foam structure. This will occur if the viscosity of the polymer melt is so significantly increased that the pressure in cells is no longer sufficient for the further extension. Thus, the cell walls are consequently so stable that the diffusion process can not change the foam structure any more. The increase of the viscosity is caused by the cooling of the foams. There are two cooling effects in the injection molding process, the one is the extern cooling which means the temperature controlled inner

surface of the mold, the other additional cooling effect is the isentropic expansion of the gas [137]. The foam structure of amorphous polymers will be fixed when the glass transition temperature is achieved, because the viscosity of polymer melt has a great increase. For semi-crystalline polymers the initiation of crystallization leads to a huge rise of viscosity and thus stabilizes the foam structure.

The time between the beginning of cell growth and the freezing of the foam structure has a decisive influence on the foam structure. If the foam stabilization is very rapid, the cells have only very short time to grow, so that the formed cells are very small. Only a part of gas can diffuse into the cell due to the short growing time and the porosity of the foamed structure will therefore be low. However, if the duration of the fixation is prolonged, a large part of gas can escape from the foamed structure into the environment due to the low pressure outside and the formed cells can also collapse.

It has been proved in various studies that additives such as foaming or nucleation agents have an influence on the crystallization behaviour of thermoplastic polymers [128,138,202,221]. Gas dissolving in polymer melts, such as CO_2 or N_2, reduces the crystallization temperature. The reduction of the crystallization temperature due to dissolved gas can be attributed to a higher mobility of the polymer molecules induced by an increased free volume. The reduction of the crystallization is proportional to the gas concentration, therefore it must be considered that during the cell growth the effect of dissolved gas in polymer melt on the crystallization temperature becomes less due to the gas concentration which decreases.

In the case of using a chemical foaming agent an increase of the crystallization temperature can be observed despite of the gas release from the chemical foaming agent, because the solid residues released from decomposition of the chemical blowing agent act as the nucleation agent. The nucleation agent facilitates not only the nucleation of gas bubbles but also the nucleation of crystallite [128,138,202]. Like cell nucleation the nucleation of crystallites is also divided in two different mechanisms, homogeneous and heterogeneous nucleation. The nucleation energy can be reduced due to the addition of nucleation agent. Consequently the number of nuclei increases and crystallites grow faster. The addition of the nucleation agent generally leads to an increase in the crystallization temperature, which is particularly important for the cell stabilization, because as mentioned above, the time of cell growth is short due to the high crystallization temperature, which results in a low porosity of the foamed structure.

Besides the foaming agent the process of injection molding has also influences on the crystallization behaviour of polymers. When the polymer melt flows through the nozzle, shear and elongation strains are applied to the polymer chain in flow direction and an orientation of the polymer chain can be induced, which reduces the nucleation energy of the formation of crystallites [81,199]. The flow induced crystallization depends on material parameters such as

molar mass distribution, the shear and elongation strain on polymer melt in the nozzle, particular the polymer melting temperature. The lower the difference between the melting temperature and crystallization temperature is, the greater the possibility of flowing induced crystallization is.

3.3 Model modification

Since late 2000, Sejin Han, R. Zheng et al. of Moldflow Corp. and Jingyi Xu and Levi Kishbaugh of Trexel, Inc. have worked together to study and develop a simulation model for the microcellular injection molding process. The effects of cell growth on material properties and flow have been investigated. Some simulation results such as melt pressure and final cell size distribution are compared with experimental results. The results of this study have been previously reported [144]. The latest reported results show good agreement with the experimental results in terms of cavity pressure and the final bubble-size distribution. But a perfect agreement on cell density, average pore diameter and interconnectivity was not found. Following are suggested model modifications.

3.3.1 Rheology of mixture

In order to describe the viscosity of the polymer-gas-solution, a modified Cross-WLF equation is proposed:

$$\eta(\dot{\gamma},T,p,\phi)=\eta_0(T,p)f(\phi)\left[1+\left(\frac{\eta_0(T,p)\cdot\dot{\gamma}}{\tau^*}\right)^{1-n}\right]^{-1} \qquad \text{Eq. 18}$$

where η_0 is the zero-shear viscosity which is a function of temperature and pressure, n and τ^* are model parameters, ϕ is the volume fraction of the gas, and f is a function of the volume fraction of the gas. The zero-shear viscosity is given in Eq. 19

$$\eta_0(T,p,\phi)=D_1\cdot\exp\left(-\frac{C_1(T-T_0)}{C_2+(T-T_0)}\right) \qquad \text{Eq. 19}$$

with $T_0 = D_2 + D_3{*}p$, and $D1$, $D2$ and $D3$ are model parameters.

In the injection molding process, the dissolved gas acts as an internal plasticizer, and the plasticizing effect of the gas can reduce the bulk viscosity, the following equation is used to describe this effect:

$$f=(1-\phi)^{\alpha} \qquad \text{Eq. 20}$$

where α should be determined from experimental data. The volume fraction of the gas can be calculated by

$$\phi = \frac{4\pi R^3/3}{V_{shell} + 4\pi R^3/3} = \frac{4\pi R^3/3}{1/(\rho N_w) + 4\pi R^3/3} \quad \text{Eq. 21}$$

where V_{shell} is the volume of the polymer melt shell (s. Fig. 3.4) and N_w is the reciprocal of the unit mass of the shell.

3.3.2 Macroscopic flow

The microscopic model of the cell should be coupled with the macroscopic flow through the fluid pressure around the cell for solving the injection molding problems [99].

It is assumed, for mathematical convenience, that the foaming stage starts after the injection nozzle is closed. Before the nozzle is closed, the mold filling analysis is therefore the same as for conventional cases. After the closing of the nozzle the bubble expansion is the driving force behind the fluid flow. The pressure equation is given as follows:

$$\frac{\partial}{\partial t}\int_0^b \ln(\rho_{cell})dz - \nabla(S, \nabla p) = 0 \quad \text{Eq. 22}$$

With

$$S = \int_{-h/2}^{h/2} \frac{z^2}{\eta} dz \quad \text{Eq. 23}$$

where $\nabla_{(x,y)}$ denotes the gradient operator with respect to the midplane, h is the thickness of the mold cavity, and z is the local thickness coordinate. Note that both the cell viscosity η and the cell density ρ_{cell} depend on the bubble size. The cell viscosity is given by Eq. 18, and the cell density is given by

$$\rho_{cell} = \frac{m_{cell}}{V_{shell} + 4\pi R^3/3} = \frac{3\rho}{3 + 4\pi R^3 N_m \rho} \quad \text{Eq. 24}$$

As mentioned there are various models for the theoretical description of foaming theory i.e. the growing of pores, but no one is fully suitable for the MuCell® technology. The modifications above are also just partially fitted for MuCell® used in this project. Experiments of the process parameters must be performed, the results need to be compared with the theoretical description to demonstrate the validity of the model and modifications. This work

is one of most important parts of this project. The experimental method and results discussion will be found in chapter 4 and 5.

4 Materials and methods

4.1 Experimental strategy

Many factors can influence the foam structure in a foaming injection molding process (Fig. 4.1), such as polymer raw material, blowing agent, additive, after treatment and process control [103]. Since in this study the MuCell® process and only thermoplastic polyurethane were used to generate the foam structure, the parameters which could be altered were blowing agents and manufacturing parameters.

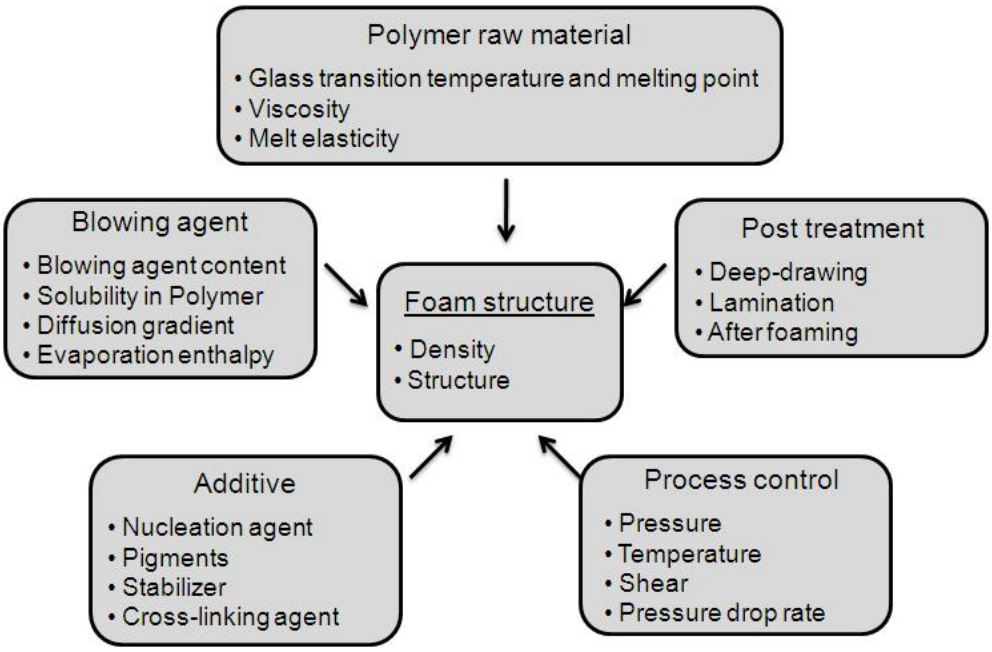

Fig. 4.1: Influencing factors on the cell morphology in the foaming process

As there are several process control parameters and blowing agents to investigate, it is necessary to focus on some key processing parameters. Fig. 4.2 shows the main control factors and classification based on their effect on cell nucleation and growth [97]. Level I indicates the first factors that directly affect cell nucleation and growth; Level II shows second factors which influences the first factors. These factors can be controlled easily even though they are dependent variables. The factors that are indicated on dark background are those which were examined in this study. The choice of the changeable parameters was made based on the knowledge given by nucleation theory and literature search [97,144]. This information also enabled the choice of parameter range. These ranges are presented in Tab. 4.1. The experiments were done by varying one of these parameters while keeping the others constant.

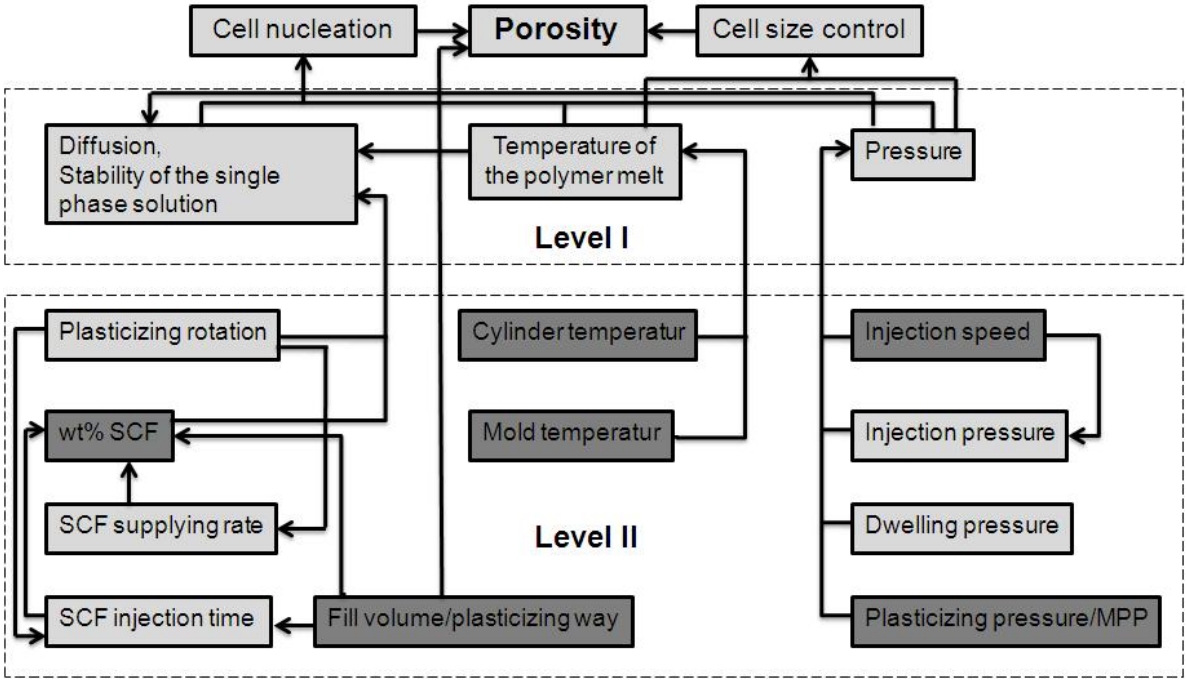

Fig. 4.2: Classification of process control parameters for cell nucleation and growth
The factors that are indicated on dark background are those which were examined in this study. Level I indicates first factors that directly affect cell nucleation and growth. Level II indicates second factors that affect first factors.

Variable Parameters	Examined range
CO_2 concentration	1-6 % wt
Degree of weight reduction	35-65 %
Injection speed	30-300 mm/s
Plasticizing pressure/MPP	160-220 bar
Plasticizing temperature	180-210° C
Mold temperature	25-85° C

Tab. 4.1: Variable parameters for injection molding process[4.1].

As mentioned in chapter 4 the main driving forces for cell nucleation are the height of the pressure drop and the pressure drop rate, both given by injection speed and plasticizing pressure, as well as the amount of SCF in the solution. The plasticizing temperature affects the solubility of gas in polymer melt, furthermore both mold and cylinder temperature have an

[4.1] The microcellular process pressure (MPP) is an active pressure that keeps the SCF in polymer melt. This pressure is actually the plasticizing pressure. Plasticizing temperature is normally a temperature gradient along the cylinder from nozzle to the hopper. Here the plasticizing temperature means the nozzle temperature, at which the polymer-gas-solution is injected into the mold.

effect on the cooling time that has a decisive influence on the foam structure. The degree of weight reduction compared with compact moulded part decides the end porosity of the foam structure.

The other fixed parameters that were kept constant throughout all experiments are shown below.

Fixed parameters	Value
Cooling time	120 s
Dwell pressure	450 bar
Beginning dwell pressure	0.5 mm
Duration of dwell pressure	0.5 s
Clamp tonnage	200 kN
Plasticizing rotation	40 min^{-1}
Injection pressure	0-3000 bar

Tab. 4.2: Fixed parameters for injection molding for all experiments.

4.2 Materials

Since the MuCell® process was chosen as the standard producing process, it is important to find a suitable polymer material which fits the requirements of the implant and process. The polymer must have a high biocompatibility and biostability from the medical view. On the other hand this polymer should be well processable for the injection molding process and easily available from the market based on the great need of the implant. Such polymers which are just available on laboratory scale are not suitable for this application. At last, this polymer must have higher mechanical properties such as good elasticity after processing according to the applicator designed by Medi-Globe for the operation.

Medical grade thermoplastic polyurethane TPU (Texin® 985, Bayer, Pa, USA) was chosen as raw material for the implant due to its excellent mechanical properties, biocompatibility and biostability. TPUs are non-crosslinked polymers and can be generally described as a linear thermoplastic that exhibit an elastic behaviour due to their copolymer structures. They consist of short, alternating blocks of soft and hard segments, as shown in Fig. 4.3. The polymer structure is defined by these components. The soft segment determines the elasticity and the flexibility of the TPU and is typically a polyether-diol in light of its hydrolytical stability in biomedical applications comparing with the polyesterdiol. The hard segments which give the polymer its thermoplastic attributes are composed of an aromatic or aliphatic diisocyanate such as TDI, MDI or HDI. TPUs exhibit a broad range of physical properties, due to the options available in selection the chemistries and molecular weights of the various

components, and the ratios in which they are reacted. The properties range from very brittle and hard materials to soft, tacky, viscous ones [109,204].

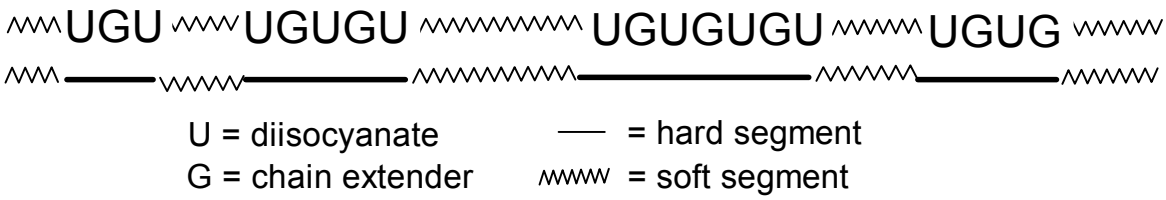

Fig. 4.3: Segmented polyurethane structure

Fig. 4.4 shows the synthesis of Texin 985 using an aromatic bifunctional reagent diisocyanate (MDI) and a high-molecular weight polyetherdiol. A short chain-extending diol increases the hard segment as well as the molecular weight of the TPU [204].

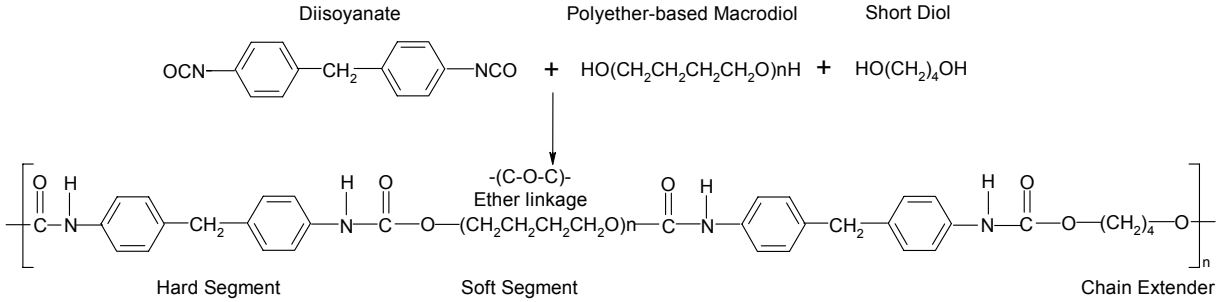

Fig. 4.4: Synthesis of Texin 985
The polymerization of thermoplastic polyether-urethanes uses an aromatic bifunctional reagents diisocyanate (MDI) and a high-molecular weight polyether-diol. The short chain-extending diol increases the polymer molecular weight.

4.3 Polymer processing

4.3.1 Machinery

An injection molding machine (KM 125-520C2, KraussMaffei Technologies GmbH, Munich, Germany) with a temperature control unit for cooling the mold (90S/6/TS22/1K/RT45, Regloplas, St. Gallen, Switzerland) was used for the production of the samples.

The injection molding machine was equipped with a MuCell® package by the Trexel Inc., Woburn, MA, USA. The package contains a special plasticizing unit (SP220 MuCell® plasticizing unit with a screw diameter of 25 mm and an adaptor for SP220 plasticizing unit, KrausMaffei Technologies GmbH, Munich, Germany) with one SCF injection valve (25 mm, series II injector, Trexel Inc., Woburn, MA, USA). It also includes an SCF metering system

that consists of an SCF delivery system (TE-3 series II injector, Trexel Inc., Woburn, MA, USA) and piping as well as instrumentation. The delivery system takes in gaseous CO_2 or N_2, compresses the gas to a supercritical state and then accurately meters the SCF into the barrel of the injection molding machine. Dependent on the needed flow rate of SCF different mass flow elements were used.

To ensure stable conditions for molding the polymer granules had to be thoroughly dried [13]. A drying and conveyor system was used. It consists of a conveyor device (FX 2014, Simar Fördertechnik GmbH, Vaihingen/Enz, Germany), a gas ring vacuum pump (2BH1500-7AH06, NASH ELMO Industries GmbH, Bad Neustadt, Germany). According to the operation guide [13] the granules were dried for at least 2 hrs at 85° C.

4.3.2 Blowing agent

The choice of blowing agent affects the expected microcellular structure. Carbon dioxide has a much greater solubility in polymer melt than nitrogen (Tab. 4.3). The result of greater blowing agent concentration in the polymer melt is generally greater density reduction. However, due to the similar diffusion rates of CO_2 or N_2 in polymer melt, N_2 tends to generate smaller cells at the same concentration in molten polymer than CO_2. The driving force for N_2 to devolve from the molten polymer/blowing agent single-phase solution is greater than for CO_2 and thus more nucleation sites form with the N_2 blown molten polymer. Because of the similar diffusion rates, the nucleation sites grow at the same rate with both CO_2 and N_2 and thus N_2 leads to smaller cell sizes. Therefore, to achieve a structure with a high porosity and relatively large pores, CO_2 was used as blowing agent (CO_2 protective gas DIN-32525-C1, Westfalen AG, Münster, Germany).

Polymer	CO_2 (%)	N_2 (%)
PE	14	3
PP	11	4
PS	11	2

Tab. 4.3: **Estimated maximum of solubility at 200° C/27,6 MPa**
CO_2 has generally greater solubility in polymer melt than N_2, but no information about their respective solubility in TPU was found in literature [171].

4.3.3 Implant design (i.e. mold design)

In order to produce the implant two particular molds have been designed and manufactured. Mold A had been designed just for the preliminary test of the feasibility of the foaming process and parameter research. This mold was made of aluminium alloy (Al Zn Mg Cu 1.5) taking account of the production cost. The mold was equipped to produce six implants at a time. Mold B was designed for the production of the implant and has an improved construction based on the results from mold A. Considering the production of implants mold B was made of steel due to a high requirement of stability, durability, abrasion resistance and good thermal conductivity. Based on the result from mold A the shape of molded part was changed for more suitable foamed structure. The technical drawings of molded parts from mold A and mold B are shown in Fig. 4.5.

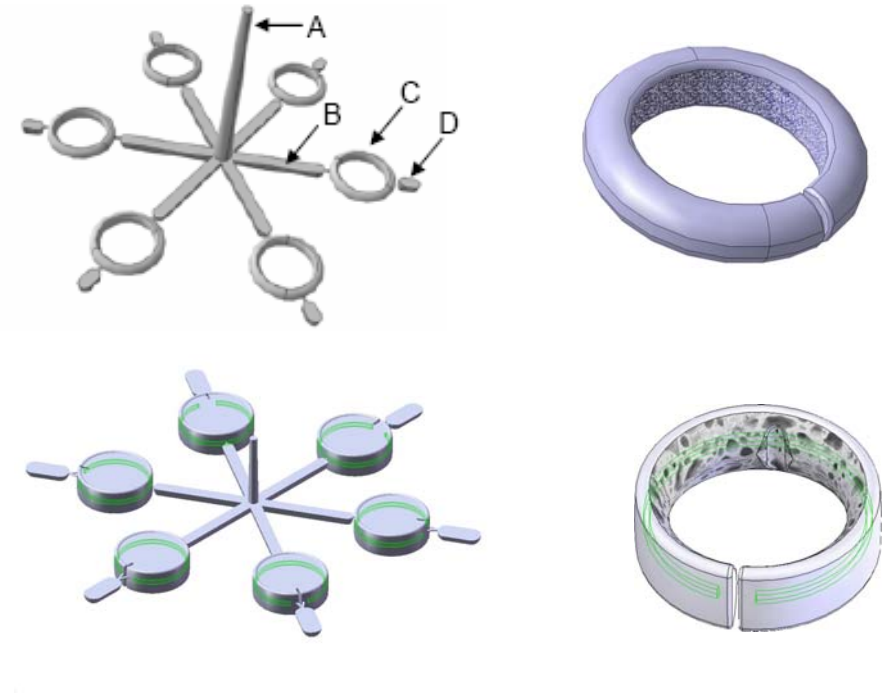

Fig. 4.5: Injection molded parts and single implant after cutting from tow molds
The upper part shows the molded parts and single implant from mold A; lower part is the molded parts and single implant after removing inner side from mold B. A) the sprue B) runners C) implant D) runners. Left is the molded parts; right is the implant after cutting out the inner skin. The green line in implant from mold B is the Nitinol ring.

For the mold A the molded part was later cut to remove the inner skin of the implant. This implant prototype has an inner ring radius of 25 mm, which corresponds to a large oesophageal diameter. The removing of inner side of implant was performed by water jet cutting machine (Perndorfer cutting system, Perndorfer Maschinenbau, Neumarkt, Austria). The parts from mold B have an improved shape design based on the results from mold A. The

implant has an embedded Nitinol ring between the inner porous side and outer smooth side. As mentioned in chapter 1 the Nitinol ring supplies an additional pressure from outside and keeps the implant around the LOS (low oesophageal sphincter). Secondly the molded parts have a solid structure compared with those from mold A. This solid structure can offer a better foam behaviour in the MuCell® process and lead to a preferable porous structure such as a bigger pore diameter, higher porosity etc.. This phenomenon will be discussed in detail in the next chapter.

The technical drawing of mold B is shown in Fig. 4.6. The highlight of mold B is an extra hydraulic core pulling unit besides the ejector unit, which can ensure a successful inlaying of the Nitinol ring in the implant. Two hydraulic motors operate the ejector pins forward or backward during the whole process. After opening of the mold, the hydraulic motors move the ejector pins forward and the Nitinol ring is placed around the pins due to its superelasticity, then the mold is closed and the ring stays in the cavity of the mold. After the injection of polymer melt into the mold the ring is embedded in the implant and the hydraulic motors begin to operate the ejector pins backward, the ring is left in the implant. The velocity and initial point of back moving of the ejector pins can be controlled by the hydraulic system to ensure the successful embedding of Nitinol ring.

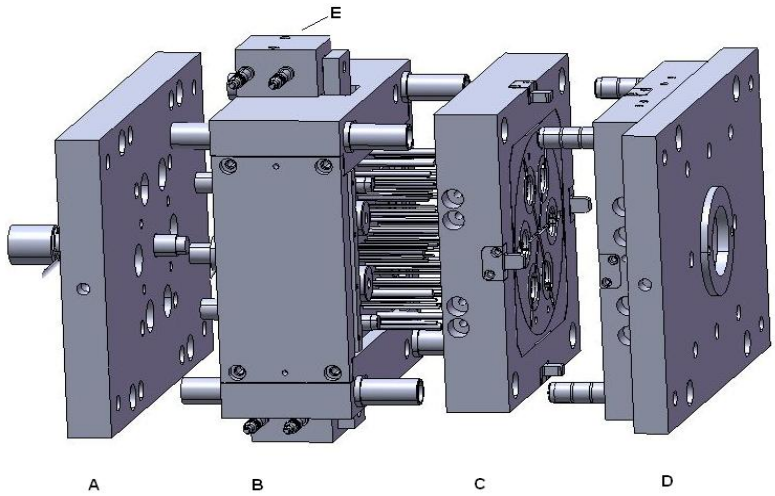

Fig. 4.6: CAD model of the mold B
From left: A) The clamping plate at moveable mold part. B) The ejector unit and hydraulic core pulling unit. The ejector unit has ejector pins, retainer and ejector plate. The hydraulic core pulling unit has hydraulic system (E), ejector pins and ejector plate. C) Mold plate with cooling plate at moveable mold part; D) mold plate with cooling plate and clamping plate at unmoveable mold halve. The cylinders between each plate are centring sleeves to ensure superimposing of all plates.

4.4 Characterization of macro- and microstructures

4.4.1 Microscopy

Scanning electron microscopy SEM (Jeol JSM-6060LV, JEOL Ltd., Tokyo, Japan) was used for the observation of the pore morphology of the cross section of implant. The samples were sliced with a scalpel and then coated with a thin gold layer by using a sputter-coater (SCD 005, BAL-TEC AG, Balzers, Lichtenstein) under high vacuum with a current range between 5-15 kV.

Characteristics of porous structure such as pore size and porosity can be calculated by counting the average cell number and size of several SEM-images from one sample. One area with certain size was chosen and all pores were measured manually with help of the software of the digital microscope (VHX-500, Keyence Corporation, Osaka, Japan). The average diameter of pores was calculated as $D_{measured}$. Due to the fact that the pores shown in the micrographs are two-dimensional projections of three-dimensional objects, their maximum diameter may not be represented in the image. Following equation was used for determination of the maximum spherical diameter, named corrected median pore diameter, from the measured pore diameter.

$$D_{Corr} = \frac{D_{measured}}{0{,}616} \qquad \text{Eq. 25}$$

The pore density was determined using the same SEM-images. If the pore number in a certain measured area is counted, the ratio of pore number to measured area in pore number per cm^2 is uncritical to be identified. To transform the two-dimensional pore density to three-dimensional pore density in pores number per cm^3 the following equation was used:

$$N_f = \left(\frac{n}{A}\right)^{\frac{3}{2}} \qquad \text{Eq. 26}$$

Where n and A are pore number and measured area. In the literature, however, the pore density is usually not specified by pore density per foamed polymer, but unfoamed part [82,105], because the pores number depends on cell nucleation as well as the porosity of foamed polymer. The volume fraction of gas in foamed polymer V_f can be calculated from the density of foamed polymer ρ_f and the density of unfoamed polymer ρ_0:

$$V_f = (1 - \frac{\rho_f}{\rho_0}) \quad \text{Eq. 27}$$

The pores in foamed polymer were consequently nucleated in unfoamed polymer *(1-V_f)*. For the calculation of the pores number per cm^3 of unfoamed polymer the following equation was used:

$$N_0 = \frac{N_f}{1 - V_f} = N_f \cdot \frac{\rho_0}{\rho_f} \quad \text{Eq. 28}$$

In this thesis the given pore density is based on the Eq. 28.

4.4.2 Porosimetry

Mercury intrusion porosimetry (AutoPore VI 9500, Micrometritics GmbH, Mönchengladbach, Germany) was used to determine pore size distribution and porosity of the samples. The porous materials were placed in a solid penetrometer with 6 ml bulb volume (model 07-044506-01, Micromeritics Norcross, GA, USA). The intrusion was filled with mercury at a pressure of 3,45 kPa and the samples were penetrated with mercury until a maximum pressure of 30 MPa, at which time the total intrusion volume reached a plateau. The intruded mercury volume per gram sample was measured by the porosimeter and was assumed to be equal to the pore volume (V_{pore}). The porosity P was then calculated as:

$$P = \frac{V_{pore}}{V_{pore} + (1/\rho)} \cdot 100\% \quad \text{Eq. 29}$$

The density of TPU (ρ) was given by measuring the density of TPU granula using density analyzer. The porosimeter can also measure the pore size according to the Washburn equation:

$$D = \frac{4\gamma|\cos\theta|}{P} \quad \text{Eq. 30}$$

where D is the pore diameter, γ is the surface tension of mercury, θ is the contact angle between mercury and the scaffold material, and P is the pressure.

Density analyzer (GeoPyc® 1360, Micrometrics GmbH, Mönchengladbach, Germany) was used to determine the density and porosity of the samples. This methods compared with mercury intrusion porosimetry is much easier to operate and the cycle time of determination is very short.

4.4.3 Microcomputed tomography (MicroCT)

MicroCT (SkyScan 1172, SkyScan, Kontich, Belgium) was used to non-destructively and quantitatively measure the three-dimensional (3D) porosity and porous interconnectivity of implants: three 8 mm×11 mm cylindrical samples from each implant (n=3) at 7 μm resolution using a voltage of 59 kV, and a current of 167 μA. Image reconstruction and analysis were conducted using the software package provided by SkyScan. The raw images of scaffolds were first reconstructed to serial coronal-oriented tomograms using a 3D cone beam reconstruction algorithm. A thresholding analysis was then performed to determine the threshold value for which grayscale tomograms of implants were most accurately represented by their binarized counterparts in terms of porosity. An optimal threshold value of 55-255 was applied for all 3D reconstructions and quantitative analysis in this study.

Representative 3D reconstructions of porous implants were generated based on the binarized tomograms to visually show the 3D models of implant structures. A cylindrical volume of interest (VOI) with a diameter of 5 mm and a height of 10 mm was selected in the center of a sample to eliminate potential edge effects. Implant porosity was then calculated as:

$$\text{Porosity} = 100\ \%\text{-vol \% of binarized object (implant material) in VOI} \qquad \text{Eq. 31}$$

In this study, interconnectivity was quantified as the fraction of the pore volume in an implant that was accessible from the outside through openings of a certain minimum size. A shrink-warp process was performed between two 3D measurements to shrink the outside boundary of the VOI in a scaffold through and openings whose size is equal to or larger than a threshold value (14-70 μm were used in this study). Interconnectivity was calculated as follows:

$$\text{Interconnectivity} = (V - V_{shrink\text{-}warp})/(V - V_m) * 100\ \% \qquad \text{Eq. 32}$$

where V is the total volume of the VOI, $V_{shrink\text{-}wrap}$ is the VOI volume after shrink-wrap processing, and V_m is the volume of implant material.

In this study the whole MicroCT test was performed with help from Dr. Havard Haugen, in collaboration with the Faculty of Dentistry, University Oslo.

4.4.4 Comparison of different measuring methods

First of all MicroCT is the most precise technique for pore characterization and it has demonstrated various key advantages. The numerous parameters can be calculated and this depends on the computational capability of the software and hardware, which leads to a high investment or cost. It is the best but also the most expensive method.

Using SEM-images to calculate pore diameters and porosities of cellular structures of foamed polymers is widely used in scientific work. It is very easy to perform and has low cost compared with MicroCT. Earlier the pore diameter was always measured manually on the image and analyzed with office excel, the accuracy of result depends on how to estimate the pore structure. In some complicated cases the estimation of pore structure is even impossible. Now there are some programs that help people measuring and analyzing the pore structure automatically, but an inextricable problem is that the program can not accurately distinguish the pore structure due to the indistinct figure of foamed and unfoamed area of polymer, sometimes the figure of the pore must be marked per hand on the image.

Using porosimeter to analyze pore morphology is also a convenient method. The operation of this instrument is easy, the analysis of pore structure can be automatically measured, the cost compared with using MicroCT is low. But in this case the foamed TPU is very flexible and mercury intrusion may lead to a breaking of pore structure and consequently false result. For the rigid porous structure such as porous ceramic or metal this method is perfectly suitable.

In this project the pore diameter and pore density were measured by the SEM-image method, the porosity and interconnectivity were measured by MicroCT, at the same time the porosity was also measured by porosimeter and density analyser to compare.

4.5 Thermal and rheological analysis

A differential scanning calorimeter (DSC, Jupiter Netzsch Gerätebau GmbH, Selb, Germany) was used to determine the melting points, glass transition temperatures and crystallitity of the polymer samples. Each sample weight 25 ± 0.2 mg was heated three times from -100° C up to 190° C at a heating rate of 10 K/min. Cooling runs were done at the same rate.

A capillary rheometer (Rheograph 2003, Göttfert, Buchen, Germany) was used to test the shear viscosity of the TPUs. The TPU granules were tested under different temperatures, shear velocities and L/D (Length/Diameter) of die to indicate the relationship between shear flow and viscosity of TPU melt.

4.6 Surface treatment of implants

Polymers have been widely accepted for in vivo and in vitro medical applications for a long time because they are relatively inexpensive and easily molded or formed into complex shapes. Unfortunately, fabrication procedures that require bonding are difficult to achieve, and biological interface reactions within the body or in the laboratory can limit their in vivo and in vitro performance.

Some surface treatments offer the techniques for easing these limitations by modifying the surface of these polymers. By altering just the first few atomic layers, the surfaces of most

medical polymers can be rendered wettable so that adhesive bonding can be achieved to troublesome materials such as polyolefins, silicones, and fluoropolymers. In this study the contact surface of implant was treated by plasma activation and titan-coating. The biological analysis was performed on the implants with and without surface treatment to indicate the effects of surface treatment on the biocompatibility of TPUs.

4.6.1 Plasma treatment

Plasma treatment as surface bio-activation technology is widely used in the field of medicine [11,28,168]. Given enough energy, any gas can be activated into the plasma state, which includes ions, electrons, excited species and free radicals. There are many temperature and pressure conditions where this phenomenon will take place, but for use in polymer area, a low temperature (10-100° C) and low pressure (<0.001 bar) are commonly used, because the surface reaction with polymers are feasible without bulk interaction.

Plasma surface treatment usually refers to a plasma reaction that either results in modification of the molecular structure of the surface or atomic substitution. Gases such as oxygen and nitrogen are used, for some special aims gases such as ammonia, argon and helium are also used. Oxidizing species such as oxygen, water vapor, or nitrous oxide are often used to leave functional oxygen-containing groups on the surface. These groups greatly enhance wetting, improve adhesive bonding, and, in some instances, create acidic surfaces. In at least one instance, sterilization of components has been reported with the use of strong oxidizers such as ozone or hydrogen peroxide vapors.

In this work the implants were treated with a low pressure (0.3 mBar, 10 min., 90 % capacity) oxygen plasma process (TETRA 30 LF PC, Diener electronic GmbH + Co. KG, Nagold) to enhance the hydrophilicity and cell adhesion on the implant surface, further for the cell ingrowth into the porous structure of implant.

4.6.2 Titanium coating

Titanium and its oxides are known as well established biomaterials for various medical applications. In bulk form, it is used for the fabrication of implants [152], whereas in the form of porous structures, it is used as a support for living cells [182].

Since most polymers show hydrophobic properties and bioinertness, the coating of TiO_2 film on the polymer surface to enhance the biocompatibility and bioactivity of polymer implant surface has been widely studied in recent years. It was proved that after coating of TiO_2 film the polymer implants show a great hydrophilicity, wettability and bioactivity [21,142]. In this work the implants were coated with a thin TiO_2 film using a patented coating process by GfE Medizintechnik GmbH (GfE Medizintechnik GmbH, Nürnberg, Germany). The surface of

implants was evenly coated with a thin TiO_2 film in nanometer scale at low temperature and pressure to protect the bulk properties of polymer implant.

4.7 Chemical analysis

Molecular weight analysis of the polymers were measured in a gel permeation chromatography (GPC) system (600E, Waters GmbH, Eschborn, Germany) with a refractive index detector, Waters 410, a column oven Jetstream, 717 plus Autosampler, three Waters Styragel HT columns 2, 4 and 6 delivered in dimethylformamide, DMF. The Waters Empower chromatography software was used to acquire and process data. The solution for the analysis was HPLC Grade DMF with an additional 0.05 M LiBr to circumvent the hydrophobic interactions between the solvent and polymer. The columns were calibrated with twelve polystyrene standards (Sigma-Aldrich Chemie GmbH, Munich, Germany). All measurements were done at 85° C to ensure a suitable viscosity of the test fluid. All samples were filtered through a 0.45 µm hydrophilic polypropylene membrane filter (Acrodisc 13 GHP, Waters) and analysed 5 times.

4.8 Biocompatibility analysis (*in vitro*)

4.8.1 Cell types

The oesophagus is composed of several different cell types, such as muscle cells, epithelia cells and fibroblasts [213]. Since it is expected that the implant is fixed onto the oesophagus with ingrowth of cells of oesophagus into the porous structure of the implant, the fibroblasts are considered to be the most important cells for the ingrowth [104,172]. Because fibroblasts from oesophagus were not available from the cell bank ATCC Manassas, a permanent cell line (Detroit 551, CCL-110, ATCC, Manassas, USA) was used in this study and was cultivated in MEM-Earle-Medium (Biochrom AG, Berlin, Germany) with supplementary ingredients (Appendix A). This fibroblast is very similar to the fibroblasts from oesophagus [116] and has a finite lifespan of about 25 serial passages [187].

4.8.2 Cell culturing

Subcultivation of monolayer culture

The cultivation of cells used in *in vitro* experiments took place in Petri dishes (T25 and T75, TPP, Trasadingen, Switzerland) and corresponding medium (DMEM, Biochrom AG, Berlin, Germany). A cell culture incubator (Heraeus Kendro Laboratory Products GmbH, Langenselbold, Germany) was used for cell cultivation at conditions of 37° C and 5 % CO_2 atmosphere. For subcultivation, culture medium was removed from the Petri dish and washed twice with phosphate buffered saline (PBS-Dulbecco, Biochrom AG, Berlin, Germany).

Trypsin (Trypsin EDTA solution, Biochrom AG, Berlin, Germany) was used for the removing cell monolayer out from the Petri dish.

A preliminary test was performed by using different cell numbers (3000, 5000, 10000 cells/ml cell suspension) for different cultivation times (3, 5 and 7 days), to determine the time of 100 % confluence of cells proliferation. After testing it was found that a cell number of 10000 cells/ml cell suspension in Petri dish T25 with 7 days cultivation time is the best conditions for the cell cultivation.

Vitality and cell number measurements

Cell vitality was controlled with using a microscope (Axiovert 25, Carl Zeiss, Jena, Germany). The Casy® 1-Cell Counter Analyser System, Model TT (Schärfe System GmbH, Reutlingen, Germany) was used to determine the cell number. The cell suspension was diluted one to one hundred by a weak electrolyte (Casy®ton, sterile filtered, Schärfe System GmbH, Reutlingen, Germany). Subsequently the diluted suspension was drawn into a capillary with a constant flow velocity. A defined electrical resistance appears after voltage is applied to the capillary by two platinum electrodes and the filling of the capillary volume by fibroblasts will change this resistance because a vital cell functions as an isolator. Resistance is thereby decreased. Its number can be sued as a scale for living cells [134]. Vital cells that were monitored were within a size variant of 10-40 µm.

Cell seeding

The porous TPU samples were cut in certain size that suits the size of 24 Well plates, so that after insertion of samples into wells the buoyancy can be avoided. Subsequently a drop of cell suspension with 2×10^5 cells, which were counted according to the procedure previously described, was given to each sample and the Well plates were placed in culture incubator for 60 minutes to ensure the cell seeding on the sample surface. After this 1 ml medium was added to each sample and the Well plates were placed in incubator for further seeding. The cell seeding procedure is shown in Fig. 4.7.

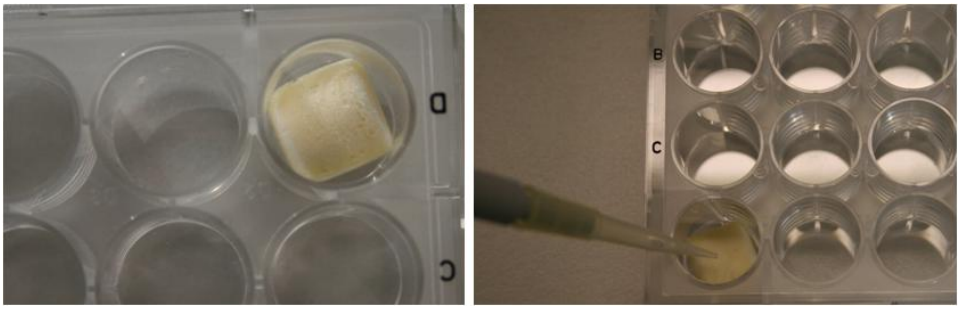

Fig. 4.7: The cell seeding on the surface of the implant
The ring was cut in quadrangle to fit the 24 Well plates, so that the piece of implant would not float in the given medium. 2×10^5 cells were given onto the surface of the implant piece, then the Well plate was placed in incubator for 60 minutes and at the end 1 ml medium was given to each sample.

4.8.3 Cytotoxicity test (*in vitro*)

An *in vitro* cytotoxicity test based on the European norm ISO 10993-5 and 10993-12 was performed for the biological evaluation of the material used for implants. The test methods for determining the cytotoxicity can be divided into three groups [214]:

- Tests with direct contact of sample material
- Tests with indirect contact of sample material
- Tests with extract from sample material (Eluate)

The choice of test methods depends on several aspects such as function of the implant, material and the place of implantation. In this study tests with direct contact as well as extract of sample material were performed. In these ways the substance released from implants after processing can be tested and compared; on the other side, the effects of different treatment and sterilization on the implant surface can also be indicated.

Tests with extract from sample material

Sterile, porous samples (750 mg) from the implant with different surface treatments were incubated in culture medium for 7 days. The culture medium after incubation was added to 96 Well plates and a cell suspension with 6000 cells was given to each well for 1, 3 and 7 days at 37° C in a 5 % CO_2 atmosphere, shown in the Fig. 4.8. 10 %vol. of cell proliferations reagent WST-1 (Roche diagnostics GmbH, Mannheim, Germany) was added directly into the medium. After 90 minutes the behaviour of these fibroblasts were analysed.

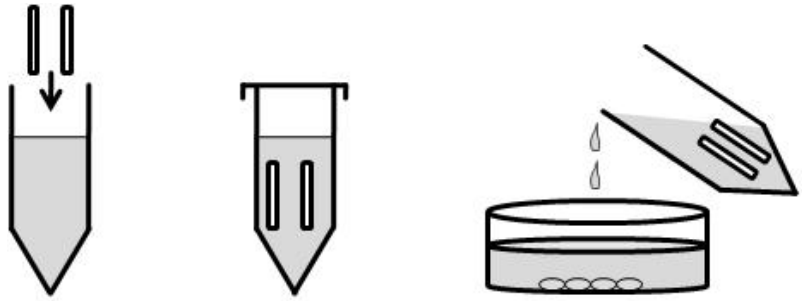

Fig. 4.8: Schematic presentation of the cytotoxicity test with extract from implant
Left: 750 mg sample pieces were incubated in culture medium. Middle: 7 days incubation. Right: the culture medium was added to a 96 Well plate with a monolayer of fibroblasts.

Tests with direct contact of sample material

The samples with seeded cells according to the procedure previously described in *cell seeding* were taken out of incubator after 1, 3 and 7 days and 10 %vol. of cell proliferations reagent WST-1 (Roche diagnostics GmbH, Mannheim, Germany) was added directly into the media. After 90 minutes the media from each sample were drawn out of 24 Well plates and added into 96 Well plates for further photometric measurement.

For the two methods the control was the culture medium with WST-1 reagent. The photometric measurement took place in a 96 Well plate with 450 nm (reference wavelength 620 nm) on an ELISA reader (Sunrise, Tecan GmbH, Crailsheim, Germany). The absorption of the control was subtracted from the measured samples. The photometric measurements of the samples were performed three times and with the same parameters as the control. An average optical density (OD) with standard deviation was calculated. The difference in OD percentage from the samples was compared to the control well, which was taken to be 100 % WST-1, is the standard assay used in cytotoxicity test and is recommended by EN ISO-10993.

4.8.4 Histological methods

Scanning electron microscopy SEM

In order to observe optical fixation of cell growth on the implant surface with SEM, the sample must be treated by following procedure. After cell seeding the samples were washed twice with PBS and immersed in 3 % glutaraldehyde (VWR, Darmstadt, Germany) at 4° C for two days. Subsequently the samples were dehydrated using a graded ethanol (VWR, Darmstadt, Germany) series from 50 % to 99 %, two times ten-minute incubation periods for each step. At the end dehydration was completed by critical point drying using CO_2 (CO_2 protective gas DIN-32525-C1, Westfalen AG, Münster, Germany). After dehydration the samples were sputtered and examined in SEM. (s. capital 4.4.1)

Vitality experiments of the cultivated fibroblasts

A LIVE/DEAD® Viability/Cytotoxicity Assay Kit (26611W, Invitrogen GmbH, Karlruhe, Germany) with the reagents Calcein AM (4mM in DMSO) and Ethidiumhomodimer-1 (EthD-1, 2mM in DMSO/H_2O 1:4) was used to test the vitality of the fibroblast in the TPU samples. Calcein AM can diffuse into the vital cells and react with the cytoplasma. After an esterase activity the Calcein AM can be converted to Calcein, which shows green under fluorescent microscope. Non-vital fibroblasts show no esterase activity but the nuclei of dead cells shows red under fluorescent microscope due to reaction of cell-membrane and Ethidiumhomodimer. The wavelength of excitation for Calcein is 490 nm with emission at 515 nm, 534-558 nm with emission at 590 nm for Ethidiumhomodimer. The visualisation s of the different fluorescent colours were performed using a fluorescent microscope (Axiovert 200, Carl Zeiss, Jena, Germany). The images were recorded with an AxioCam digital camera and assessed with the software AxioVision 4.6 (Carl Zeiss, Jena, Germany).

The LIVE/DEAD® test took place in the µ-Slide VI (ibidi GmbH, Munich, Germany) designed for high-end microscopic analysis of fixed or living cells, especially for multiple immunofluorescence stainings. The procedure of test is shown in Fig. 4.9. The cell suspension was diluted to the desired cell density. 30 µl cell suspension with 6000 cells was added into the channel of the µ-Slide, the reservoirs were covered with the supplied lid. Subsequently the µ-Slide was incubated at 37° C and 5 % CO_2 as usual for 90 minutes so as to ensure the cell attachment. Afterwards each reservoir was filled with 60 µl of extract from different sample (s. chapter 4.8.3). After 1, 3 and 7 days of incubation time the extract was moved out and a LIVE/DEAD®-coloration-solution was added into the reservoir. This solution is a mixture of PBS with 2 µM Calcein-AM and 4 µM Ethidiumhomodimer. Each channel with two reservoirs was filled with 150 µl coloration-solution and the µ-Slide was incubated at 37° C and 5 % CO_2 for 10 minutes. After incubation the µ-Slide was observed by fluorescent microscope.

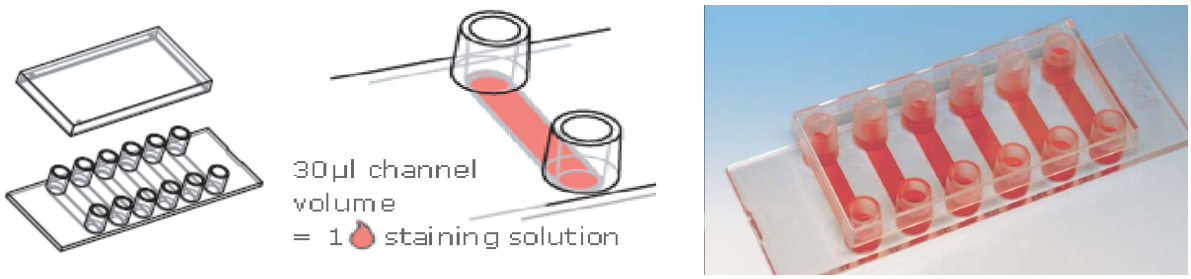

Fig. 4.9: **LIVE/DEAD® test of cell vitality**
Left: µ-Slide for cell vitality test. Middle: 30 µl cell suspension with 6000 cells was added into the channel. Right: after 90 minutes incubation time for cell attachment each reservoir was filled with 60 µl extract from different samples for further incubation.

4.9 Animal tests (*in vivo*)

It is necessary to assess the biocompatibility and functionality of the implant on animals, before the implant is applied to human. In this study animal testings on rabbits and pigs were performed at MITI-group (Minimal Invasive Interdisciplinary Therapeutic Intervention, Klinkum rechts der Isar, TU München, Munich, Germany) and biological evaluation was performed at MedTech (Lehrstuhl für Medizintechnik, TU München, Munich, Germany).

4.9.1 Tests with rabbits

The *in vivo* tests (according to DIN EN 10993-6) were performed to testify the function of implant for cell ingrowth. 12 pieces of implant were subcutaneously implanted in the dorsal region of rabbits. The test plan is shown in Fig. 4.10. The implants were moved out after 2, 6, 12 and 26 weeks. Due to the flexibility and porous structure of TPU samples the histological preparation of implant with tissue based on paraffin wax embedding is not suitable here and the big hole is easy to see in the sections. To solve this problem and observe the cell ingrowth in the pore structure of implant the histological preparation were made using cold polymerization of PMMA (poly-methylmethacrylate). Paragon-colouring was used for identification of cells as well as tissue from implants. The detailed process is shown in Appendix B. The preparations were observed using light microscopy (Axiovert 200, Carl Zeiss, Jena, Germany).

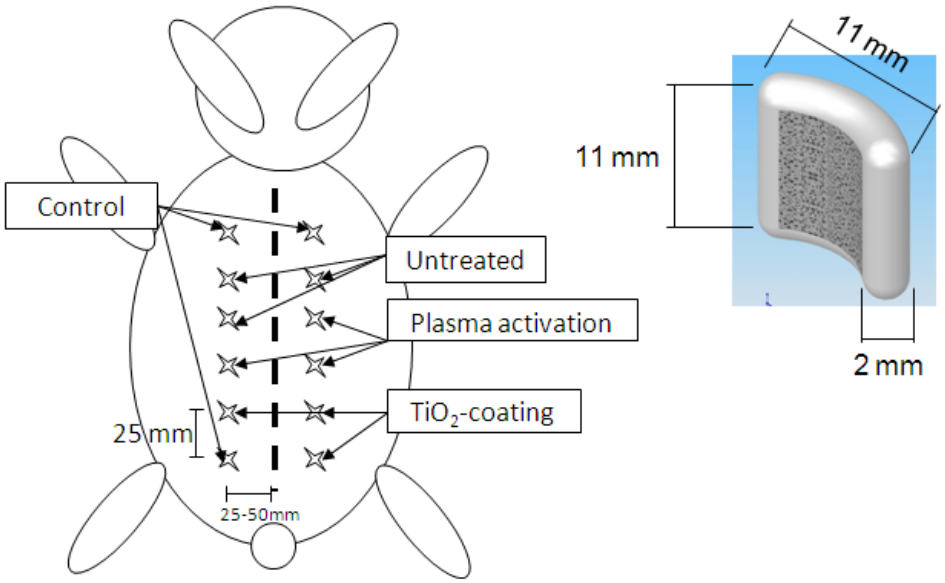

Fig. 4.10: Test plan on a rabbit (positioning of specimen)
12 pieces of implant were implanted under the skin of the back of rabbit. 4 of 12 are PE without porous structure as control, 4 untreated, 4 with plasma treatment and 4 with TiO_2-coating. For each implantation time there were three rabbits available.

4.9.2 Tests with mini pigs

The *in vivo* tests on pigs were performed for the test of functionality of the implant. Before the implantation the myektomie (partial resection of oesophagus of pig) on pigs was performed to induce a reflux disease on pigs. The ring shaped implant with and without Nitinol ring were placed around the sphincter through the operation. The pH-meter monitors the pH value of oesophagus of the pigs per radio communication. After a defined period the implant with gastric section was taken out for the further research of cell ingrowth and biocompatibility of the implant. The Fig. 4.11 shows the operation for the ring implantation by surgery.

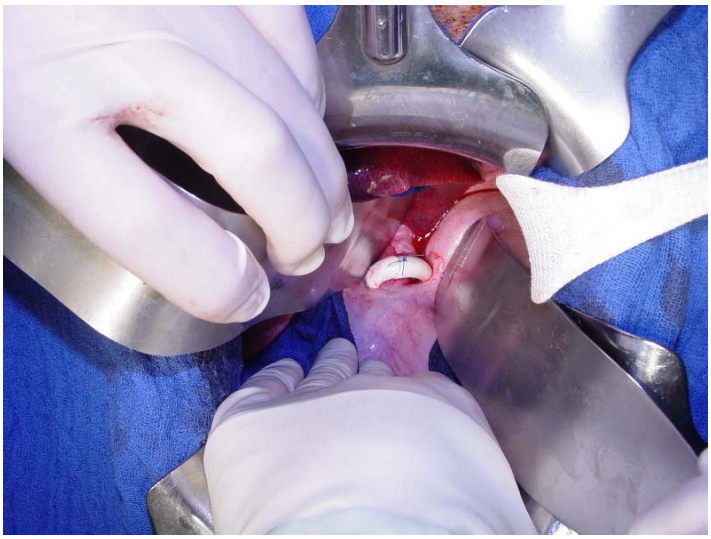

Fig. 4.11: Operation on a pig for the ring implantation

5 Polymer processing and pore morphology

5.1 Influence of the processing parameters on pore morphology

As mentioned in the foregoing chapters the MuCell® process was chosen as the process of implant production. In chapter 3 the theoretical model of MuCell® was detailed described. From the foaming theory of MuCell® it is well known that in the foaming process many parameters such as temperature, pressure and gas concentration can affect the cell nucleation and growth as well as final pore morphology. This phenomenon makes it possible to produce an expected pore structure by adjusting the parameters in the foaming process.

The experimental strategy to indicate the relation between the processing parameters and pore morphology of foamed polymer was described in chapter 4.1, in this chapter the results will be presented and discussed.

5.1.1 Influence of the weight reduction and gas content

The weight reduction percent and gas content are the two most important parameters which affect the foamed structure of polymer in MuCell® technology. The gas content of polymer-gas-solution directly decides about the amount of nucleus formation and the degree of weight reduction gives a space for the formation of foamed structure. The higher gas content can lead to a larger foaming potential, but the gas solubility in polymer melt has a limit; on the other side, without enough free volume for the foaming the porous structure can not form. Hence the influence of the weight reduction and gas content will be discussed together. In this work the values of the constant and variant parameters can be seen in Tab. 5.1. The gas content has varied from 1 % to 6 %. At very single gas content, the degree of weight reduction has also varied from 35 % to 65 %. The pore morphology at every parameter was investigated by using the methods described in chapter 4.

Variant Parameter	**Value**
Degree of the weight reduction	35 % - 65 %
Gas content	1 % - 6 %
Constant parameters	
Injection speed	120 mm/s
Mold temperature	25° C
Plasticizing pressure	170 bar
Plasticizing temperature	190° C

Tab. 5.1: Constant and variable parameters while varying the gas content and the degree of weight reduction

The degree of the weight reduction depends on, how many percent of mold cavity is filled compared with compact injection. It is possible to fill the mold cavity usually from 100 % to 45 % with proper gas content and the mold cavity can be fully filled by the foamed material at the end. Fig. 5.1 shows the SEM images of the porous structure of implant after cutting. The difference of the porous structure between the different degrees of weight reduction is clear to see.

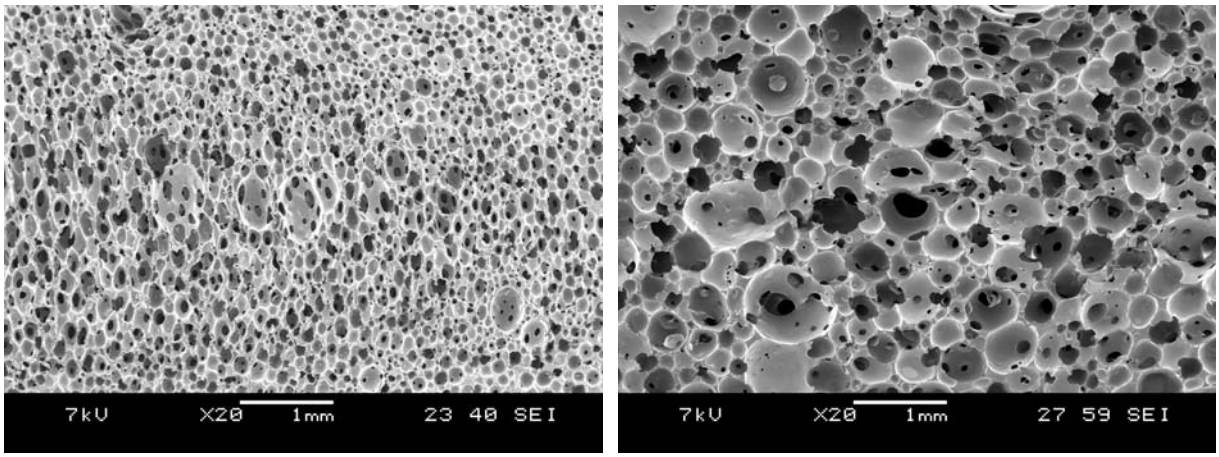

Fig. 5.1: Pore morphology at 35 % (left) and 55 % (right) degree of weight reduction

The SEM images of porous structure at 35 % and 55 % weight reduction have shown the effect of degree of weight reduction. With the low degree of weight reduction the pore diameter is smaller than the value at higher degree, which matches the result from mercury intrusion porosimetr in Fig. 5.2. The integrated area below the curve means the number of the pores with corresponding pore size, therefore the pore size distribution is in proportion to the area below. It was to see that the high weight reduction has more pores with larger size than low weight reduction, which corresponds to the SEM images, at the same time the porosity increased also with the rise of the degree of weight reduction.

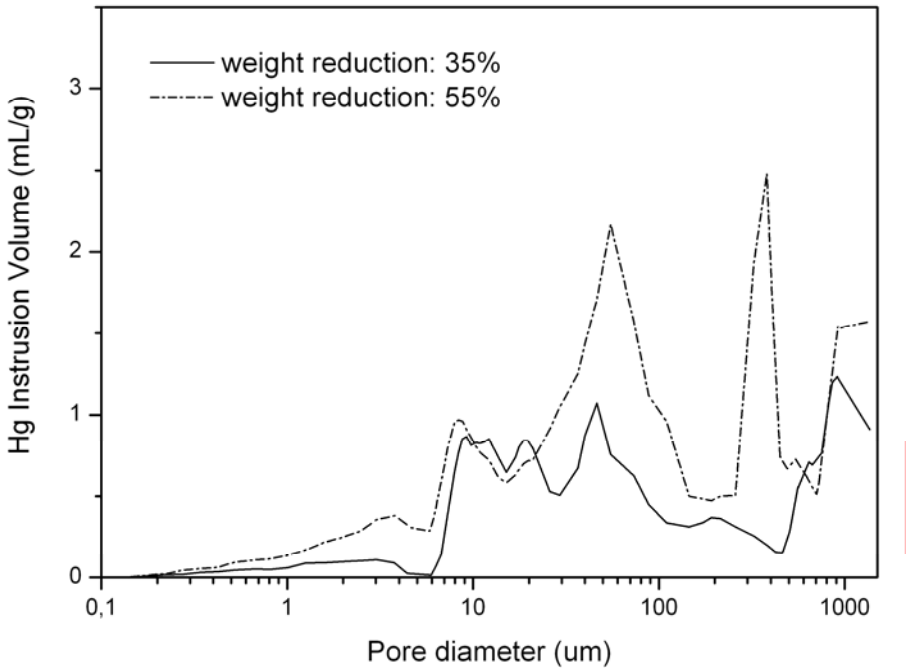

Fig. 5.2: Pore size distribution depending on the degree of weight reduction.

The SEM images in Fig. 5.3 show the pore morphology at different gas content with constant weight reduction of 55 %. The change of pore morphology was obvious, with rise of the gas content the pore size decreased obviously.

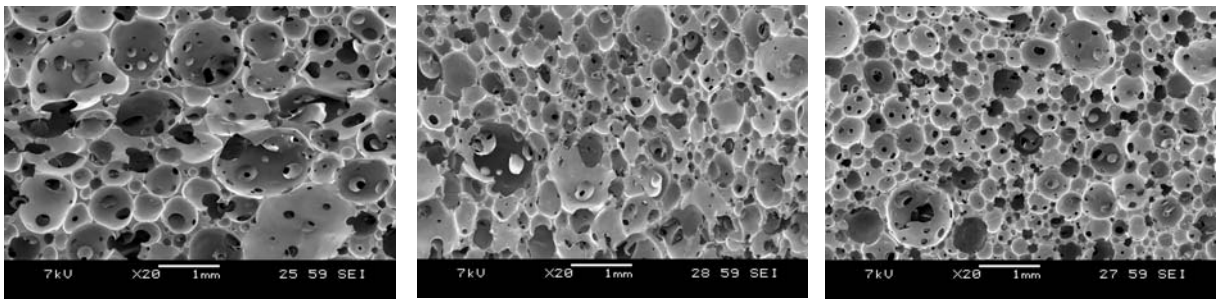

Fig. 5.3: Pore morphology at different gas contents
Gas content from left to right is 1 %, 3 % and 6 %.

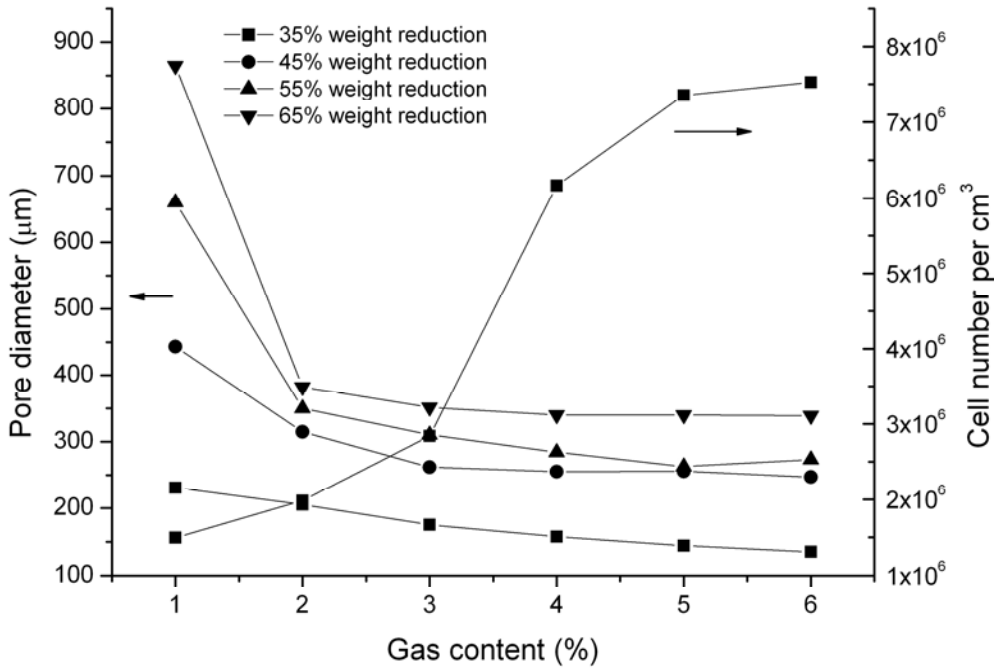

Fig. 5.4: Pore diameter and cell density at different gas contents and weight reduction
Every value is the average value from 4 different samples produced with the same parameters. The standard deviation was not drawn in the curve because of the disturbance of curves observation.

The quantitative comparison is shown in Fig. 5.4. The curve of every degree of weight reduction shows that the pore size has a similar change trend, reduction of pore size with increasing gas content. The rise of gas content led to more nucleus formation and consequent more pores. As result the mean pore size decreased because of the unchanged free volume for the foam structure. The mean pore size dropped quickly from gas content 1 % to 2 %, then the change rato was slowed down and became evenly up to 6 %. At the same gas content, the mean pore size increased also with the rise of weight reduction. At 1 % gas content the mean pore size was increased from 230 µm to 864 µm and this change range was larger than at high gas content 6 %, 135 µm to 339 µm. The cell density of the foamed sample indicated the reason of mean pore size change on the other side. The cell density of weight reduction 35 % was increased from 1.4×10^6 to 7.5×10^6 per cm^3 between the gas content ranges from 1 % to 6 %. All the other degrees of weight reduction showed similar cell density curves.

Another important factor of pore morphology is the porosity which indicates the foaming degree of the foamed samples. The effect of gas content and weight reduction on the porosity is shown in Fig. 5.5.

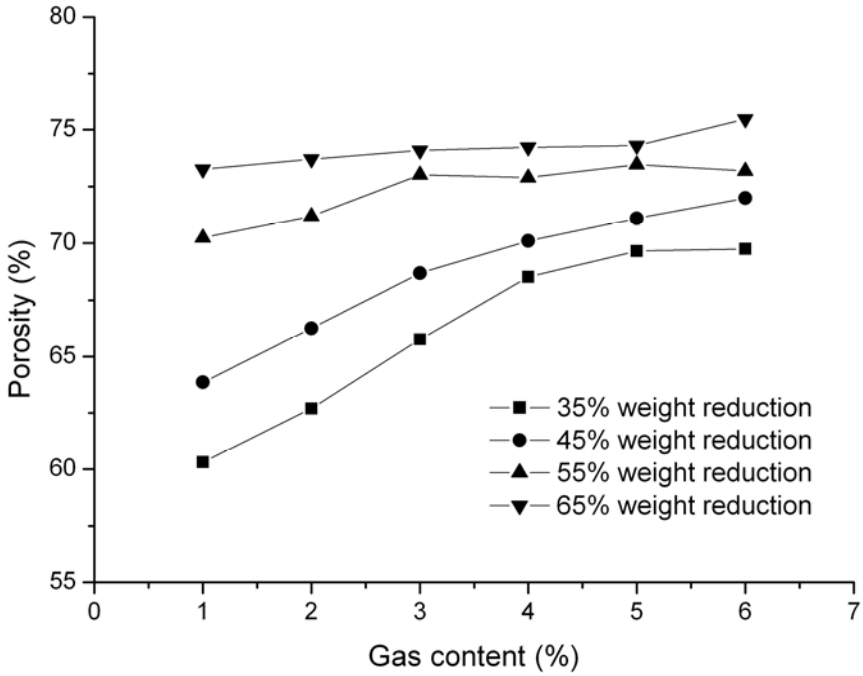

Fig. 5.5: Porosity in relation to the gas content and the weight reduction
Every value is derived from four different samples. The standard deviation was not shown in curves because of the disturbance of observation.

The porosity changes are similar to the finding with the mean pore size. The rise of gas content leads to an increase of porosity, which corresponds to the relevant rise of cell density. The porosity of 35 % weight reduction had a range between 60 % and 69 % with rising gas content and the increase of weight reduction up to 65 % shifted this porosity range to higher value, between 73 % and 79 %, which means rising both gas content and weight reduction leads to a higher porosity in the MuCell® process.

As mentioned in this study, an implant with high porosity, proper pore size and interconnection for the cell ingrowth is expected. The values of interconnection size in relation to the gas content and weight reduction are shown in Fig. 5.6. The change trend of the interconnection size was just as same as the finding of the mean pore size. Rising gas content led to a decrease of both mean pore size and interconnection size, for example by 35 % weight reduction, the range of interconnection pore size was between 108 µm and 40 µm. By higher weight reduction of 65 % the interconnection pore size was shifted to the range of 131 µm to 52 µm.

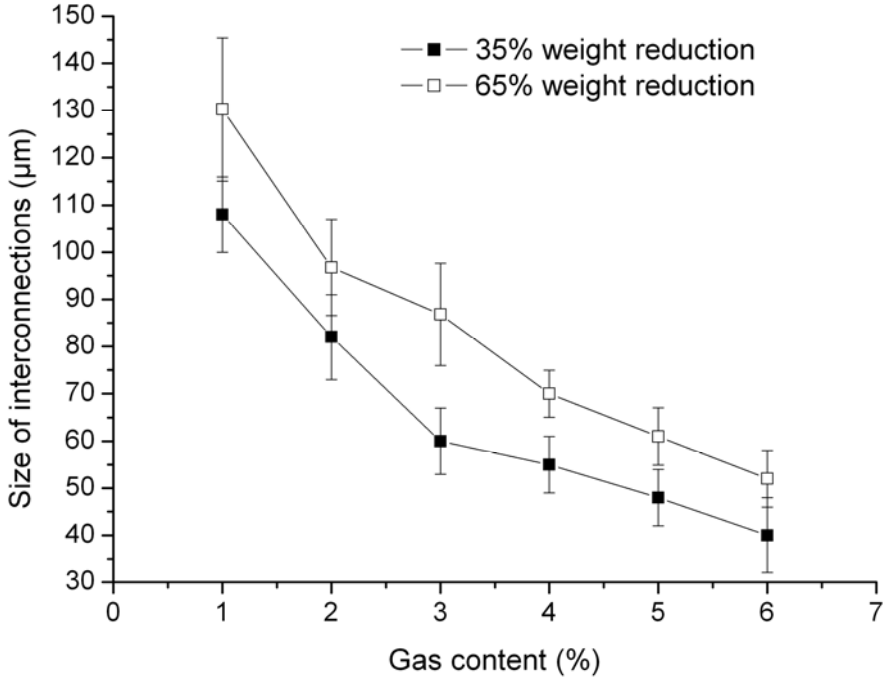

Fig. 5.6: Size of interconnections in relation to gas content and weight reduction

Fig. 5.6 shows the interconnection size of porous structure of foamed part just in 2-dimensional definition, but a 3-dimensional description of relation between the interconnectivity and gas content and weight reduction is more significant. Fig. 5.7 shows the relative porosity depending on interconnection size of foamed sample.

The relative percentage of porosity compared with normally measured porosity means the porosity which consists of all the connective pores larger than defined interconnective pore size. This value shows the interconnectivity of foamed sample and is one of the most important characteristics of the porous structure. If the defined interconnection size is 0 µm, all the pores were counted in the porosity, which means 100 % measured porosity are effective. With rising of the defined interconnection size from 0 to 70 µm (interval 14 µm) the amount of connective pores as well as relative porosity was decreased. By the weight reduction of 65 % with gas content 1 % the relative porosity decreased from 100 % to 68 %, but with gas content 6 % this range was between 100 % and 5.5 %. Therefore the increase of gas content could lead to not only a lower interconnectivity but also a quick drop of the interconnectivity of foamed sample. In the same way a low weight reduction of 45 % with gas content 3 % means less free volume for the pore formation, therefore, the interconnectivity (from 100 % to 1.5 %) showed a faster drop in comparison to the same gas content but higher weight reduction of 65 %, relative porosity from 100 % to 28 %.

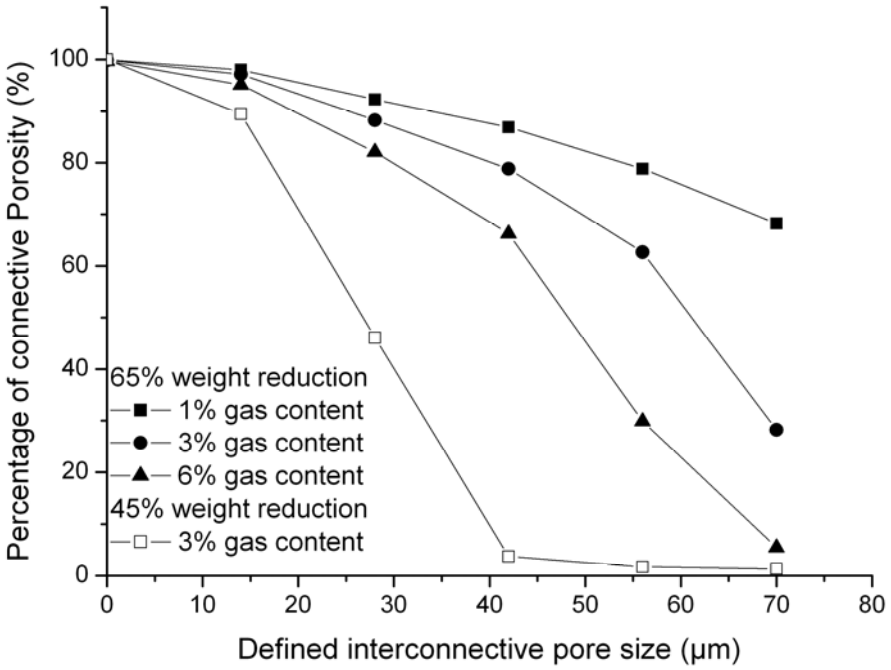

Fig. 5.7: Relative porosity depending on the interconnective pore size at different weight reduction and gas content from micro CT
The interconnective pore size dependent porosity means the percentage of porosity which consists of all connective pores bigger than defined interconnective pore size.

5.1.2 Influence of the injection speed

The injection speed of process is the velocity at which the polymer-gas-solution is injected through the nozzle into the mold. As mentioned in chapter 3 the main driving force of cell nucleation in MuCell® process is the pressure decrease in a very short time. The injection speed of polymer-gas-solution directly decides the pressure of the mixture at the point out of the nozzle as well as the pressure drop range, therefore the effect of injection speed on the porous structure of foamed part was expected. Tab. 5.2 shows the injection speed range and all constant parameters during the test, the corresponding pores morphologies are found in Fig. 5.8. From SEM image of morphology a significant decrease of pore diameter with rising of injection speed was observed. The quantitative description found in Fig. 5.9 shows the same change.

Variant Parameter	Value
Injection speed	30 - 300 mm/s
Constant parameters	
Degree of the weight reduction	55 %
Gas content	2 %
Mold temperature	25° C
Plasticizing pressure	170 bar
Plasticizing temperature	190° C

Tab. 5.2: Constant and variable parameters while changing the injection speed

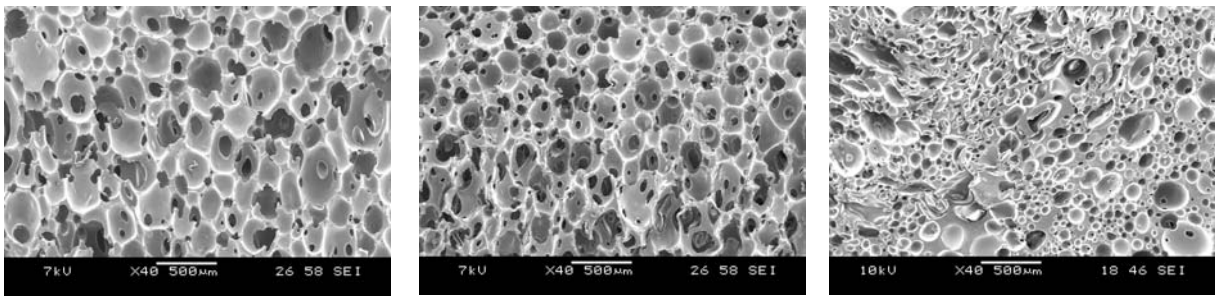

Fig. 5.8: Pore morphology at different injection speeds
Pore morphology at 30 mm/s (left), 150 mm/s (middle) and 300 mm/s (right)

It was found that the mean pore size at high injection speed was smaller than at low injection speed. This change can be attributed to the varying of pressure induced by injection speed, because the pressure drop of polymer-gas-solution is the main driving force for the cell nucleation. More cell nucleation was achieved with high pressure drop in mold induced by high injection speed. As result the smaller mean pore size and higher cell density was observed. In this case the mean pore size decreased from 340 µm to 246 µm with injection speed rise from 30 mm/s to 300 mm/, whereas the cell density increased from 5.8×10^5 to 1.6×10^6 per cm^3. Theoretically this change trend should be independent of used material and also was observed by PS (Polystyrene) [96,97,114], but nothing was found about other commercial materials such as PE (Polyethylene) or PP (Polypropylene).

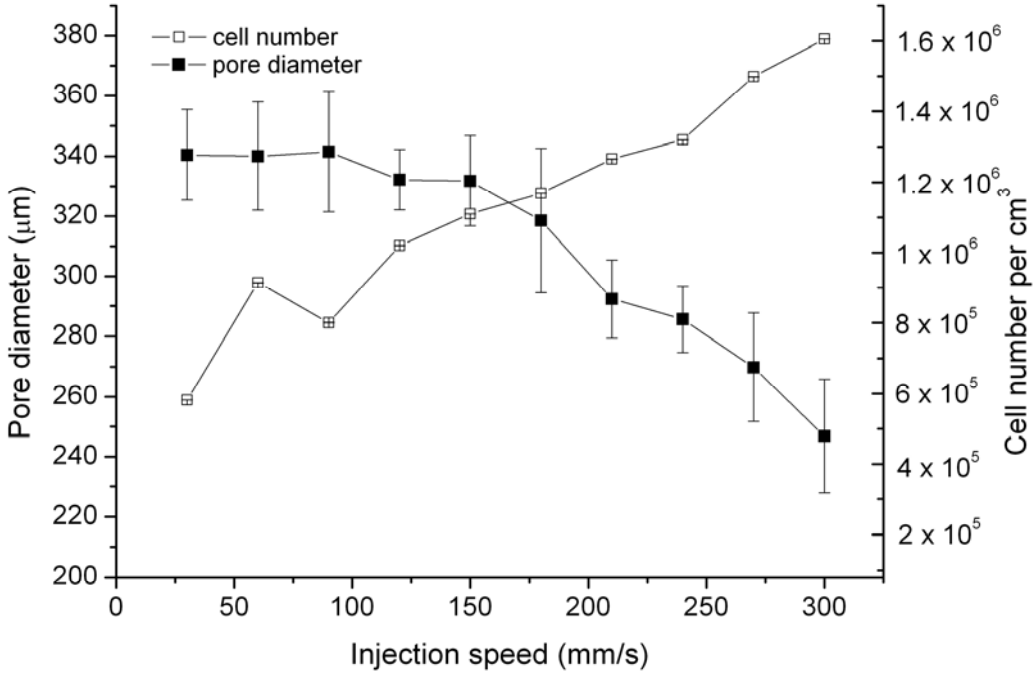

Fig. 5.9: Pore diameter and cell densities at different injection speeds

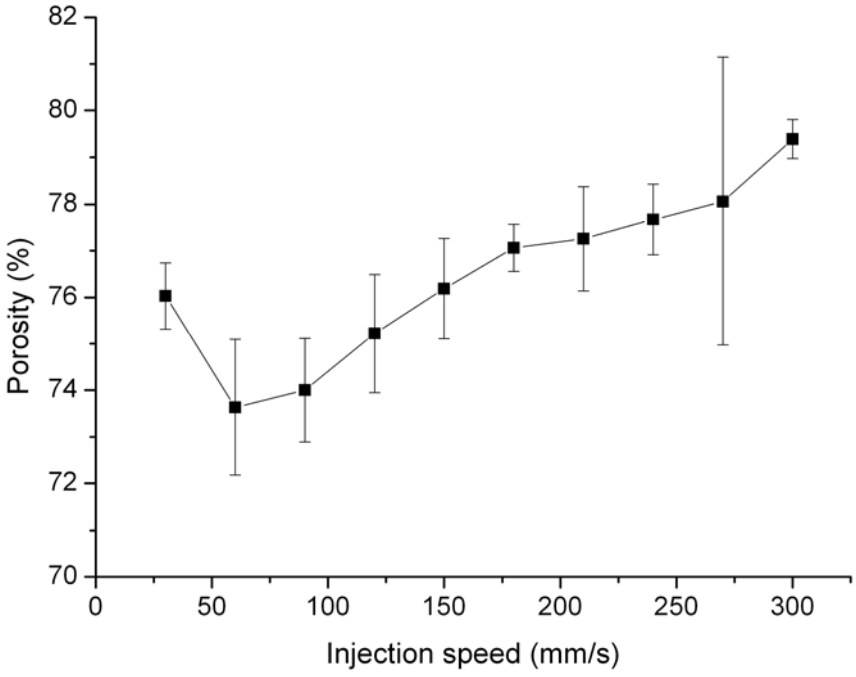

Fig. 5.10: Porosities at different injection speeds

In Fig. 5.10 the porosity at different injection speed is illustrated. At injection speed range from 30 mm/s to 60 mm/s the porosity showed a slight drop, from 76 % to 73 %, but after

60 mm/s the porosity increased continuously from 73 % to 79 %. The reason may be the deviation between the actual value and setpoint of injection speed on the machine. It was found that at low injection speed area the actual value was always higher than setpoint and the deviation was going to small at high injection speed area. The large deviation at the low injection speed area (< 60mm/s) can probably lead to the unusually change of porosity at the low injection speed, but it was just a assumption.

The interconnective pore size did not show a regular change (Fig. 5.11). A peak of 135 µm as mean pore size was found at the speed of 150 mm/s, whereas at the speed range of 30 – 120 mm/s and 210 – 300 mm/s the size of interconnections stayed in a small range of 107 – 116 µm. No relevant report was found about this phenomenon by other materials, so that the generality of this rule needs to be further researched.

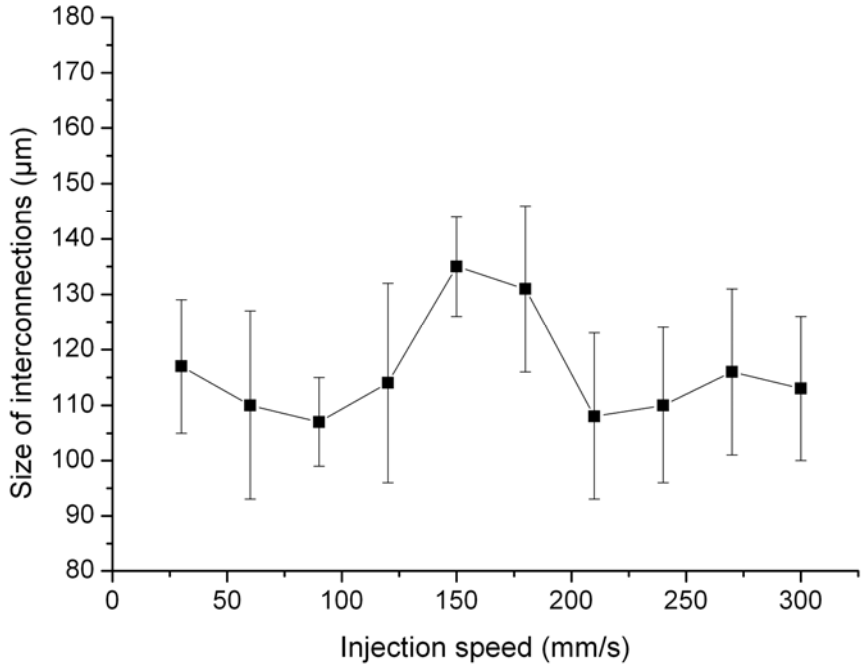

Fig. 5.11: Size of interconnections at different injection speeds

Fig. 5.12 shows the percentage of connective porosity depending on the defined interconnection size for different injection speed and testified the measuring of interconnection size. It was clear to see that injection speed change had nearly no effect on the relative porosity except at the speed of 150 mm/s. The curve of injection speed 150 mm/s showed a higher percentage of connective porosity at every defined interconnective pore size, which corresponded the larger interconnective pore size measured in Fig. 5.11.

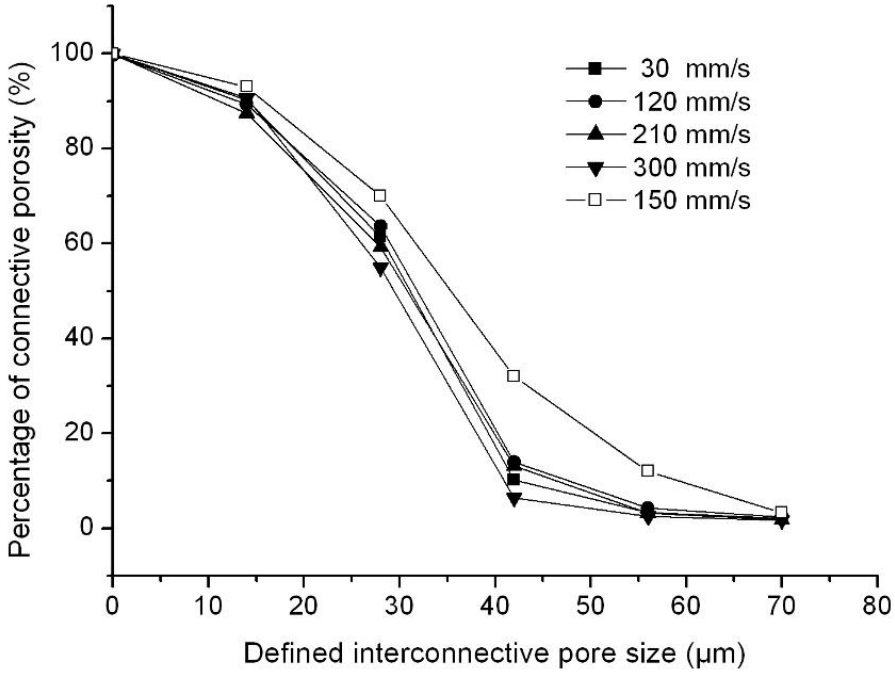

Fig. 5.12: Relative porosity depending on the defined interconnective pore size for different injection speed

5.1.3 Influence of the plasticizing temperature

The plasticizing temperature is normally a temperature gradient along the cylinder from nozzle to hopper. Here the temperature of nozzle, at which the polymer-gas-solution is injected into the mold, was taken as the cylinder temperature. The cylinder temperature decides the solubility and solution speed of gas in polymer melt. For example higher temperature induces possibly a more homogeneous, faster gas dissolution in polymer melt. That gives the possibility to change the morphology of foamed part through varying the cylinder temperature. The parameters are found in Tab. 5.3. The SEM images of different morphology are shown in Fig. 5.13.

Variant Parameter	**Value**
Plasticizing temperature	180° C, 195° C, 210° C
Constant parameters	
Degree of the weight reduction	55 %
Gas content	2 %
Injection speed	120 mm/s
Mold temperature	25° C
Plasticizing pressure	170 bar

Tab. 5.3: Constant and variable parameters while varying plasticizing temperature

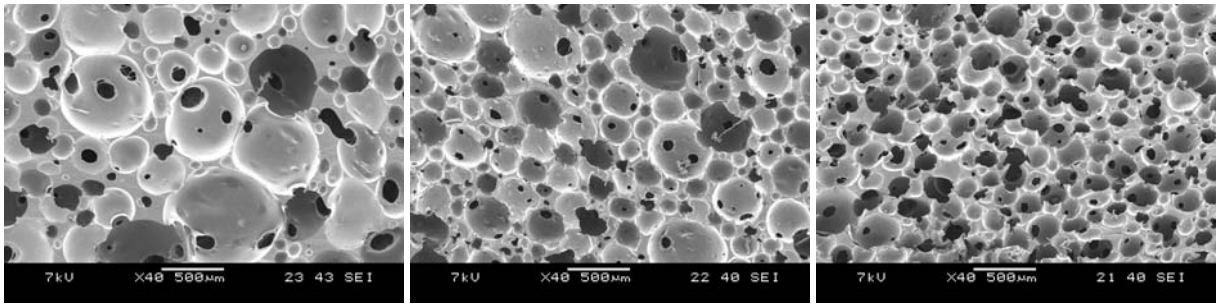

Fig. 5.13: Pore morphology at different plasticizing temperatures
Pore morphology at plasticizing temperature of 18° C (left), 195° C (middle) and 210° C (right)

From the SEM images it is observed that with rising plasticizing temperature the pore diameter shows a significant decrease, which is quantitatively illustrated in Fig. 5.14. The mean pore size has slightly decreased from 353 µm to 304 µm by temperature elevation from 180° C to 210 °C, whereas the cell density increased quickly from 3.3×10^5 to 8.8×10^5 per cm^3. The similar result was also reported by producing soft rubber foams of poly(ethylene-co-vinyl acetate) with using CO_2 as SCF foam agent in expansion process [84].

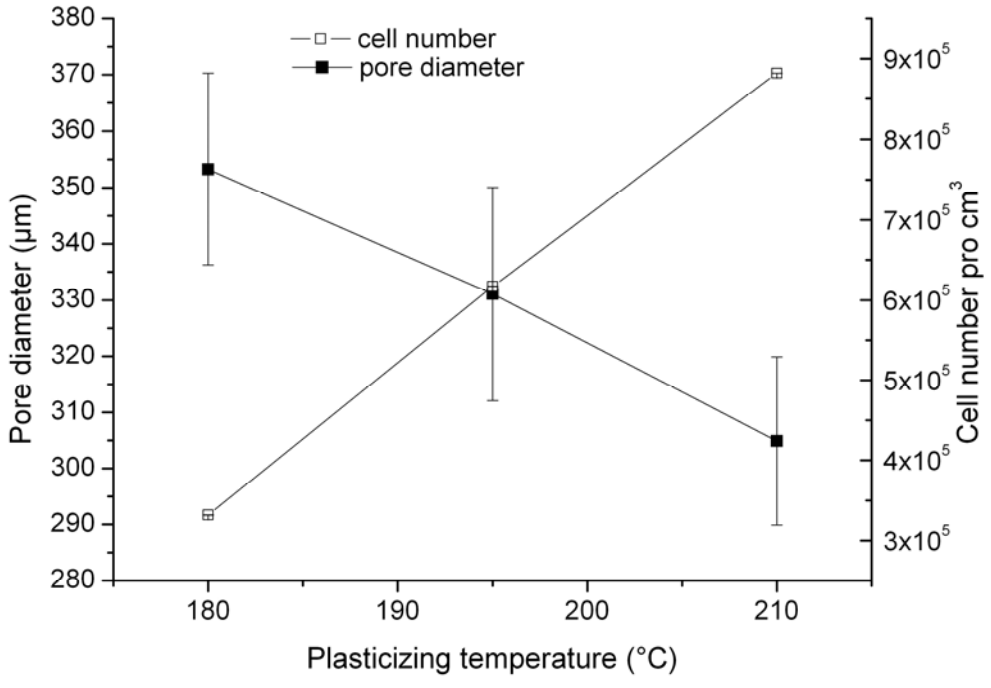

Fig. 5.14: Pore diameter and cell density at different plasticizing temperatures

The porosity and interconnection size of different plasticizing temperature is shown in Fig. 5.15. The temperature dependent porosity shows a slight increase from 68 % to 71 % corresponding to the reduction of mean size and rise of cell density. The interconnection size

indicates a slight decrease from 129 µm to 113 µm. These small changes in porosity and interconnection size can be normally disregarded if compared with the results from influences of weight reduction and gas content. No relevant report was found about these phenomena.

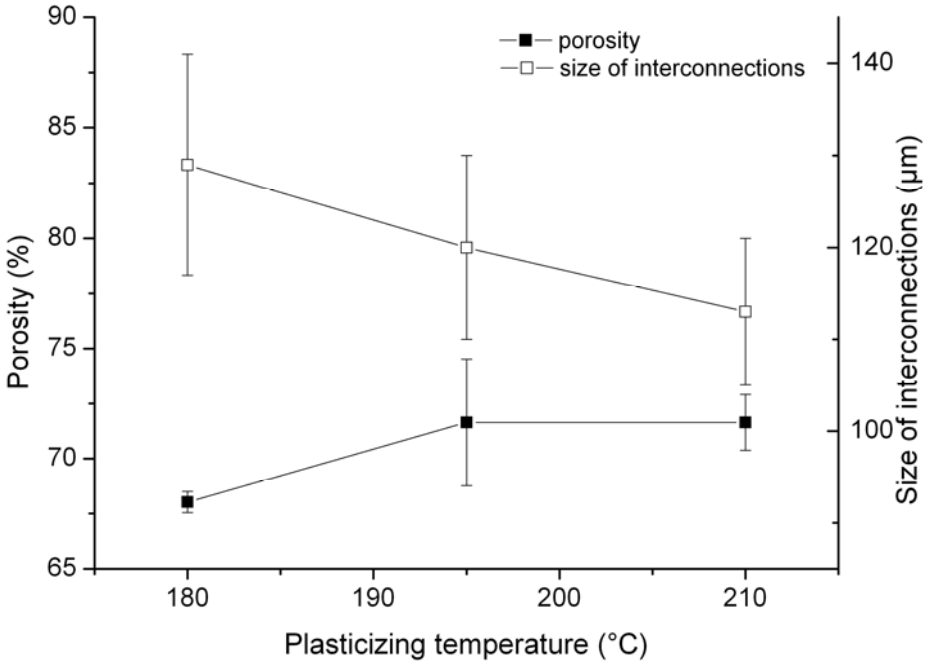

Fig. 5.15: Porosities and interconnection sizes at different plasticizing temperatures

Despite the changes of porosity and interconnection size at different plasticizing temperatures, the percentage of connective porosity shows different results (Fig. 5.16). At low plasticizing temperature of 180° C the connective porosity was significantly larger than at high temperature of 195° C and 210° C, which showed relative the same values and the change trend. The foamed sample at high plasticizing temperature had almost no connective porosity if effective pores were defined having interconnective pore size larger than 42 µm, but at temperature of 180° C this connective porosity was even at 29.69 % with 70 µm interconnective pore size, which meant a relative better interconnectivity for cell ingrowth.

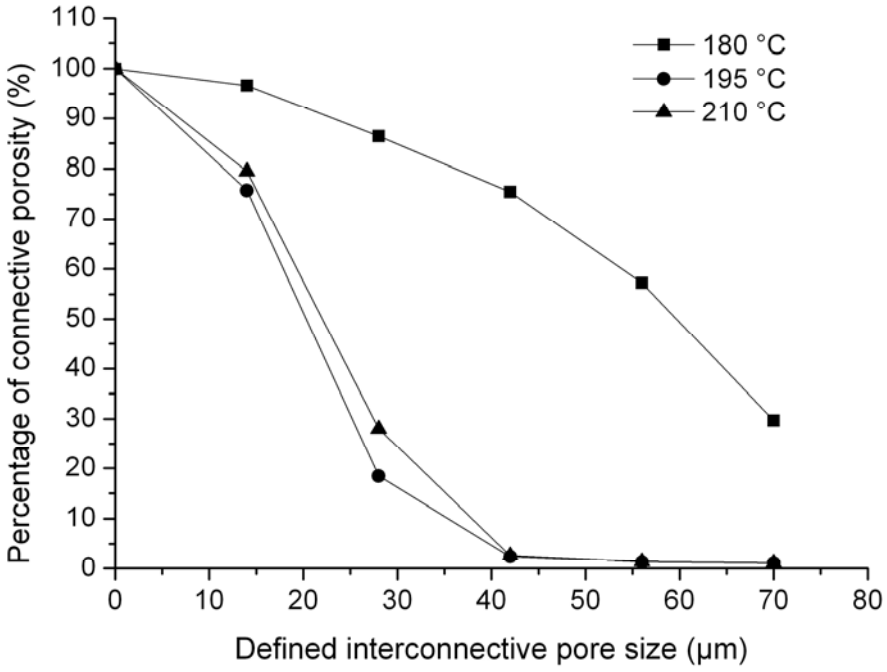

Fig. 5.16: Relative porosities depending on defined interconnective pore size at different plasticizing temperatures

5.1.4 Influence of the plasticizing pressure

The plasticizing pressure is the pressure at which the polymer is plasticized and gas is injected into the polymer melt. From the foaming theory it is known that the pressure and temperature are decisive for the gas dissolution in polymer melt. For a homogeneous single phase of mixture of polymer melt-gas-solution certain pressure i.e. plasticizing pressure must be maintained. The parameters by varying the plasticizing temperature are found in Tab. 5.4. The plasticizing pressure varied from 110 bar to 200 bar with interval of 30 bar. The SEM images of sample morphology at different plasticizing pressures are shown in Fig. 5.17.

Variant Parameter	**Value**
Plasticizing pressure	110 bar, 140 bar, 170 bar, 200 bar
Constant parameters	
Degree of the weight reduction	55 %
Gas content	2 %
Injection speed	120 mm/s
Mold temperature	25° C
Plasticizing temperature	190° C

Tab. 5.4: Constant and variable parameters while varying the plasticizing pressure

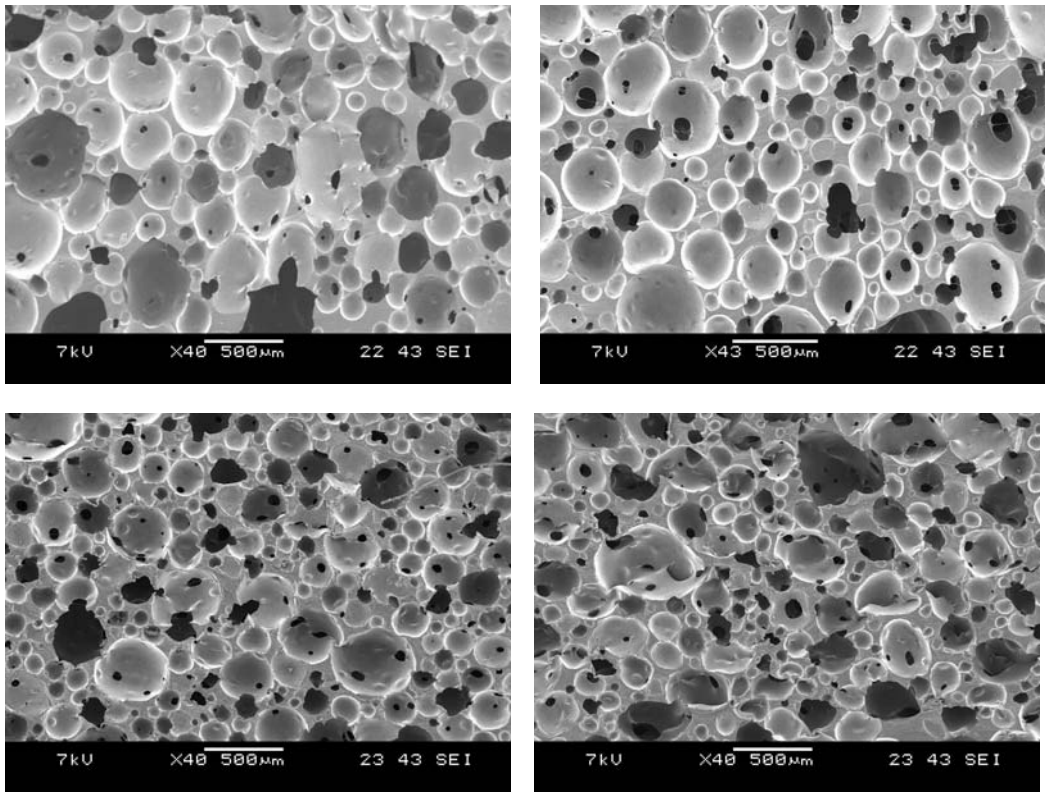

Fig. 5.17: Pore morphologies at different plasticizing pressures
Pore morphology at 110 bar (top left), 140 bar (top right), 170 bar (bottom left) and 200 bar (bottom right)

From SEM images it was found that the pore morphology has changed to small with rise of the plasticizing pressure. Quantitative curves were shown in Fig. 5.18. The mean pore size has decreased from 330 µm to 275 µm with changes of plasticizing pressure from 110 bar to 200 bar, corresponding to a cell density increase from 4.4×10^5 to 9.1×10^5 per cm^3. This can be explained by the more homogeneous gas dissolution with higher degree induced by high pressure. The same effect of pressure on the mean pore size and cell density was also reported in several literatures [35,37,84]. Most people have attributed this effect to the better dissolution behaviour of gas in polymer melt at high pressure.

But unlike the described results, that porosity was normally in direct proportion to the cell density, the porosity of foamed sample at different pressures indicated a slight drop from 75 % to 68 % with plasticizing range up to 140 bar and kept nearly unchanged up to 200 bar, despite a continuous increase of cell density (Fig. 5.19). Concurrently the interconnective pore size did not show a regular change, but just two plateaus of 116 and 86 µm. The porosity was more sensitive to the change of plasticizing pressure at low area.

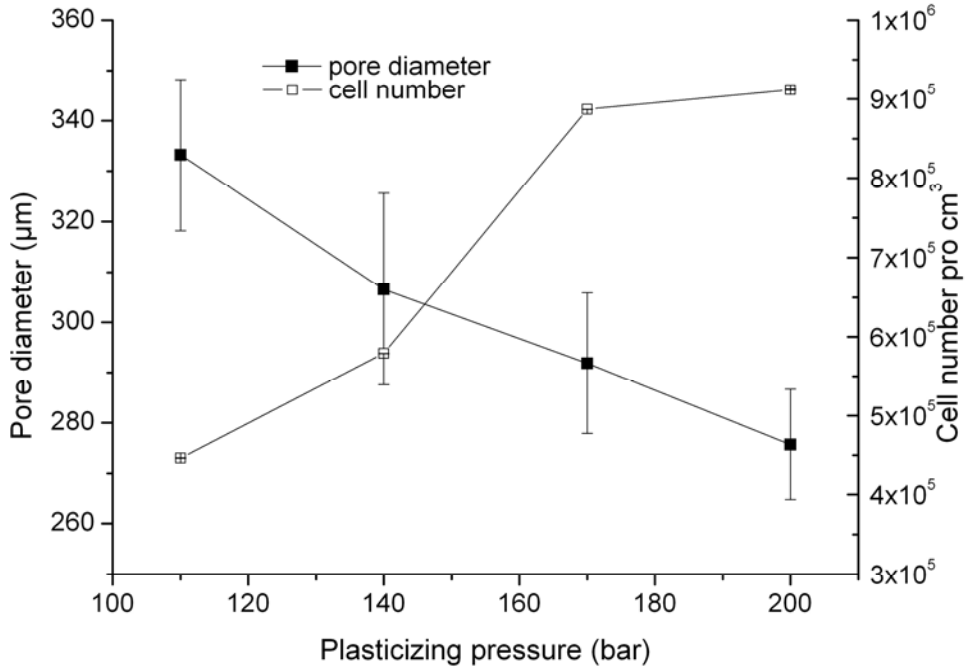

Fig. 5.18: Pore sizes and cell densities at different palsticizing pressures

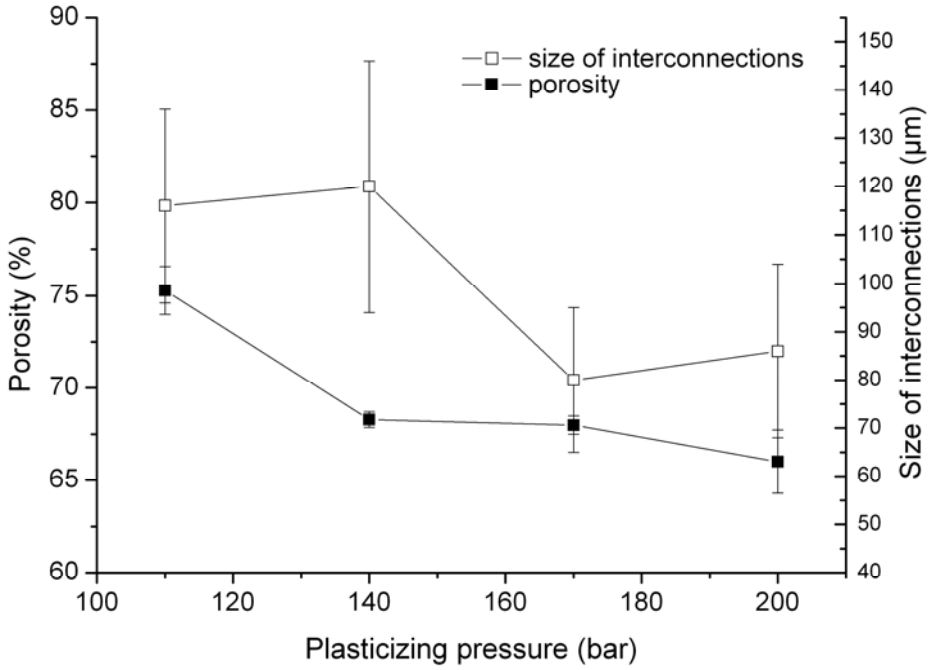

Fig. 5.19: Porosities and interconnection sizes at different plasticizing pressures

The percentage of connective porosity in relation to the defined interconnective pore size (Fig. 5.20) showed a significant change with varying the plasticizing pressure. At 110 bar the curve indicated a low interconnectivity at every defined interconnective pore size. With rise of the plasticizing pressure from 110 bar to 200 bar the connective porosity increased

continuously, though at pressure of 170 bar and 200 bar two curves had almost the same value. This gave the possibility to enhance the interconnectivity through increasing the plasticizing pressure.

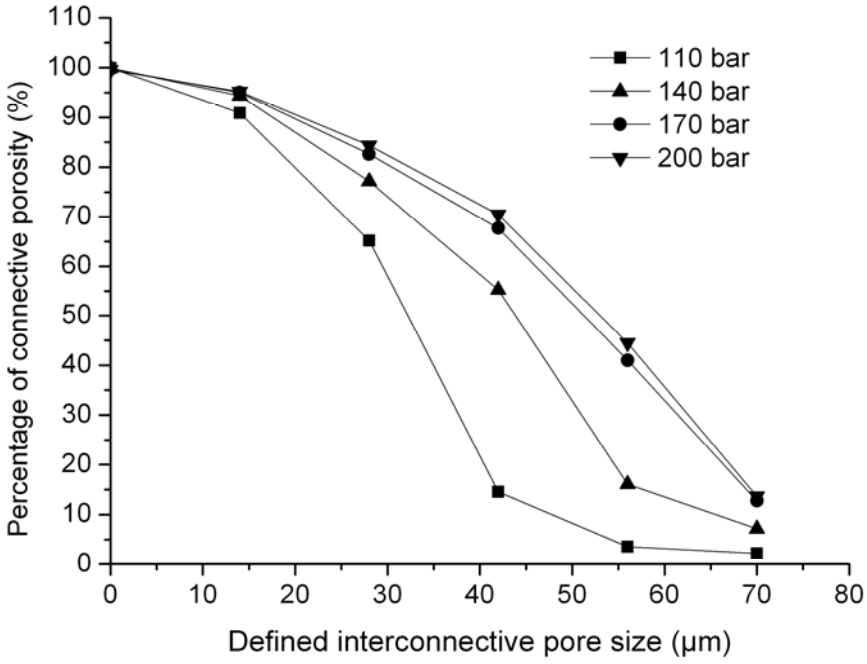

Fig. 5.20: Relative porosities depending on defined interconnective pore size at different plasticizing pressures

5.1.5 Influence of the mold temperature

The mold temperature is the environment temperature at which the cell growth and cell stabilization take place. As mentioned in chapter 3 this temperature decides the change of viscosity of injected polymer melt and consequently the cooling time of polymer melt in mold. Too short cooling time leads to an incomplete cell growth with small cell size, but a long cooling time induces also a collapse of formed cells. In such case the mold temperature must be accurately adjusted to make sure that the polymer-gas-solution in mold has a proper cooling time for desired pore morphology. The parameters by varying the mold temperature were found in Tab. 5.5. Fig. 5.21 shows the SEM images of the morphology at different mold temperatures.

Variant Parameter	Value
Mold temperature	25° C, 45° C, 65° C, 85° C
Constant parameters	
Degree of the weight reduction	55 %
Gas content	2 %
Injection speed	120 mm/s
Plasticizing temperature	25° C
Plasticizing pressure	170 bar

Tab. 5.5: Constant and variant parameters while varying the mold pressure

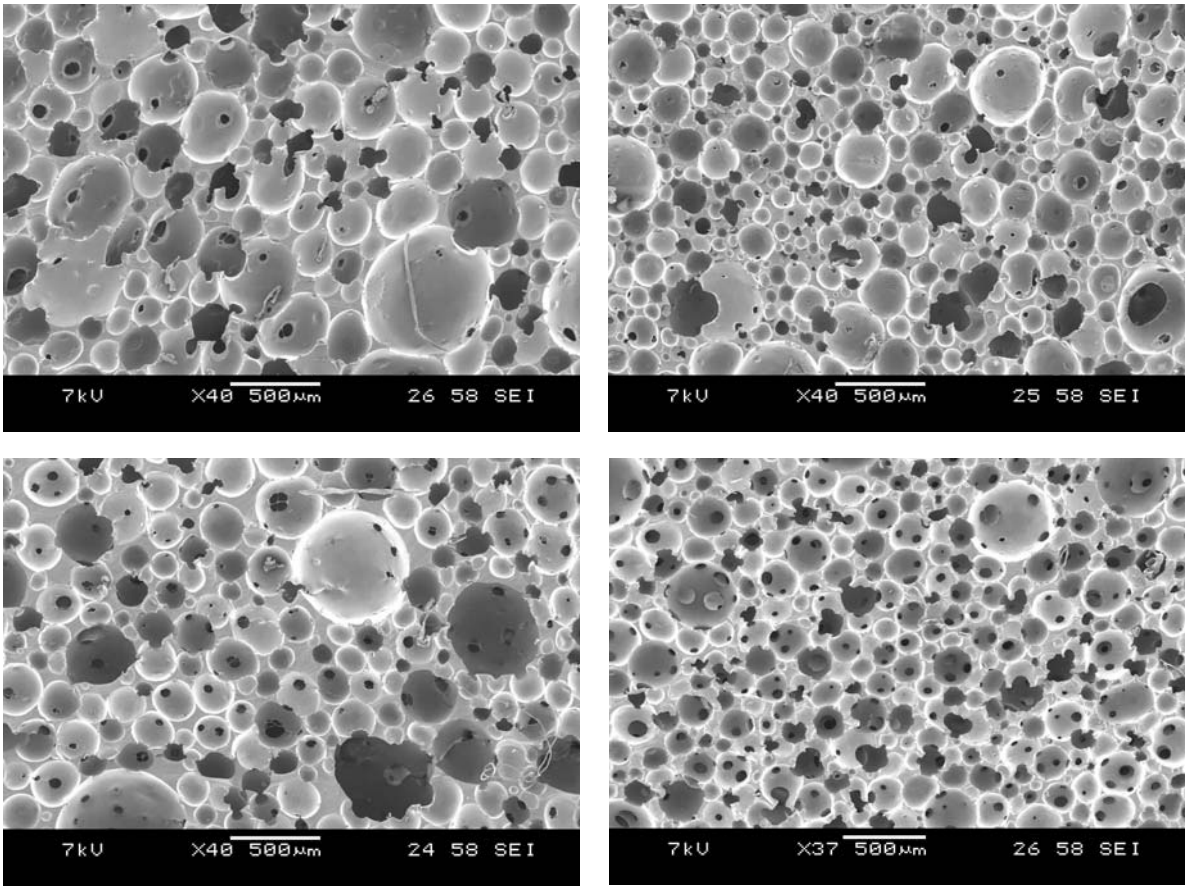

Fig. 5.21: Pore morphologies at different mold temperatures
Pore morphology at mold temperature of 25° C (top left), 45° C (top right), 65° C (bottom left) and 85° C (bottom right)

It was observed that the mean pore size has changed smaller if the mold temperature increased, which seemed to be unsuitable for the mentioned effect of mold temperature. Considering the limit of cooling system which controlled the mold temperature through water, the reachable lower limit is just 25° C. This may be the reason of large pores despite low temperature because the temperature under 25° C is not possible to test.

Fig. 5.22 shows quantitative changes of mean pore size and cell density at different mold temperature. The mean pore size has decreased from 371 µm to 240 µm by varying the mold temperature from 25° C to 85° C, whereas the cell density showed no significant change from 25° C to 65° C with value of about 9.5×10^5 and an obvious increase up to 1.15×10^6 at highest temperature of 85° C. This effect was found just on the contrary by foaming PS (Polystyrene) [96,97], but in an other case of foaming PET (Polyethylene Terephthalate) with different chemical structure the same results like this case was also found [37], although different process was used in foaming of PET. It can be consequently assumed that the influence of mold temperature on the pore morphology is rather material dependent, but further experiments need to be performed.

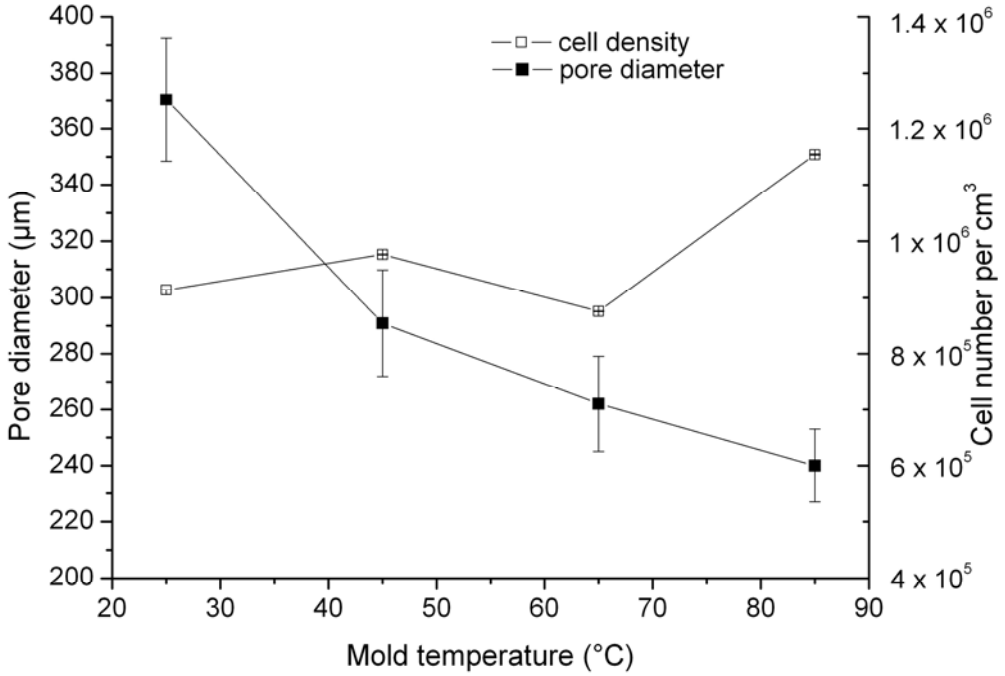

Fig. 5.22: Pore sizes and cell densities at different mold temperatures

It is found from Fig. 5.23 that the porosity has slightly decreased from 73 % to 66 % as well as the size of interconnections respectively from 110 µm to 82 µm, by varying mold temperature from 25° C to 85° C. The porosity here was also in inverse proportion to the cell density like varying the plasticizing pressure.

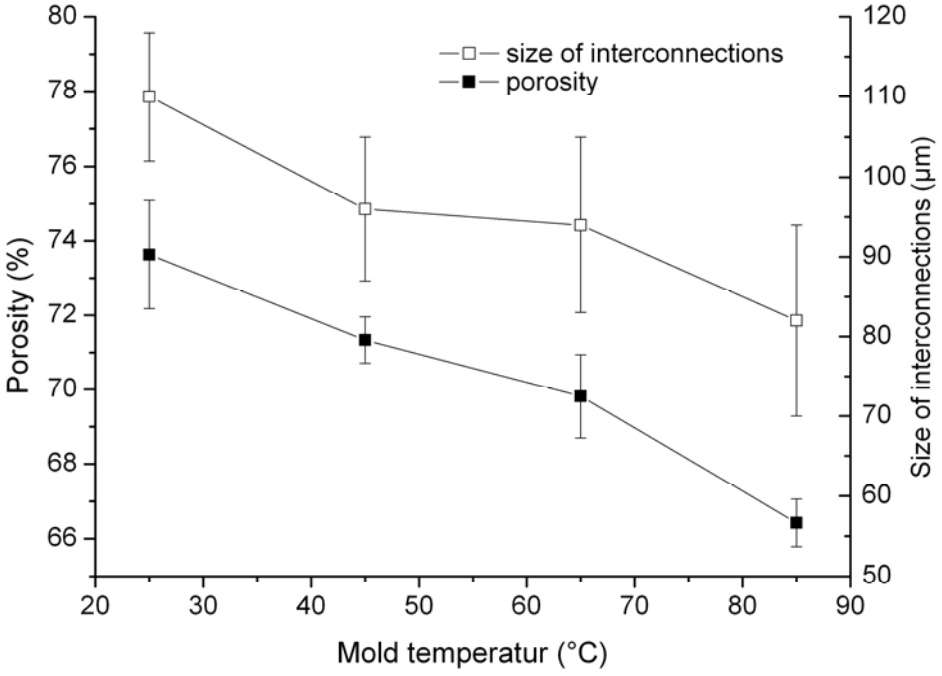

Fig. 5.23: Porosity and size of interconnections at different mold temperatures

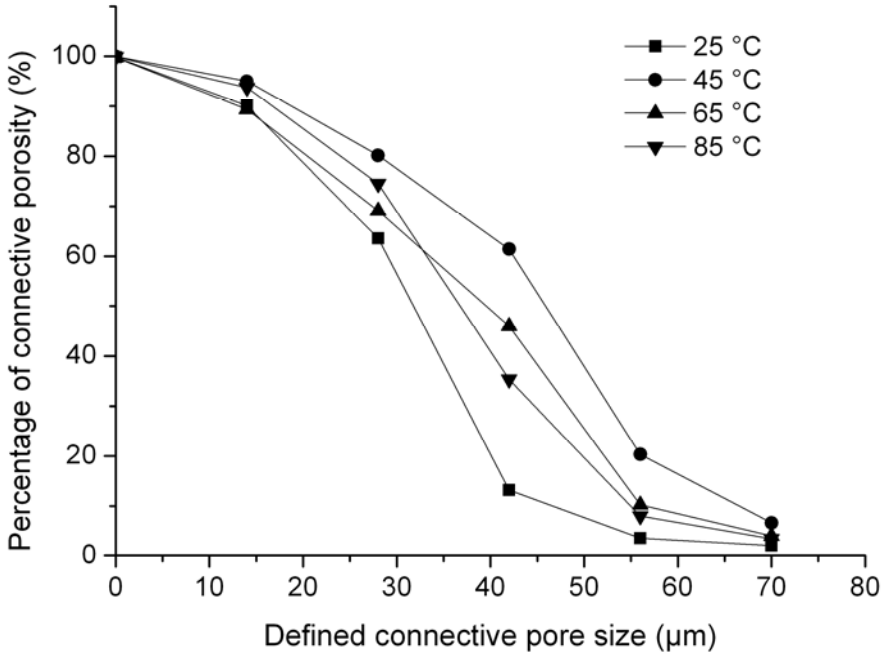

Fig. 5.24: Relative porosities depending on defined interconnective pore size at different mold temperatures

Fig. 5.24 shows the interconnectivity of foamed samples at different mold temperatures. The curve of 25° C indicated a worst interconnectivity despite the highest porosity and biggest mean pore size, but on the other hand the best interconnectivity was found at the temperature of 45° C, not the highest temperature, so that no regularity relation could be observed.

5.1.6 Standard deviation of measuring

The standard deviation of measuring was displayed in Tab. 5.6. The implants were produced with the setting of 55 % weight reduction and 2 % gas content (s. Tab. 5.1). For five sections from one implant the porosity was 71.4 ± 4.9 %. The porosity of sections from six different implants of one junction molded part showed an average value of 70.8 ± 2.8 %. Sections taken from different molded parts but at the same position showed an average porosity of 71.2 ± 1.9 %. The repeatability of whole process was proved through this standard deviation measuring and for a convincing pore morphology analysis samples taken from different molded parts with same position should be taken into the measuring.

Tested samples	Average porosity
One implant (n = 5)	71.4 ± 4.9 %
One molded part (n = 6)	70.8 ± 2.8 %
Series of molded parts (n = 6)	71.2 ± 2.9 %

Tab. 5.6: Average porosity and standard deviation
A molded part consist of six implants, the sprue and runner system (s. chapter 4)

Another issue in need of attention was the time in which the process has become stable. After varying the process parameter the process needed a certain cycles to ensure the stabilization of new setting. The number of waiting cycles depended on the dwell time of polymer melt in injection molding machine. It related to many parameters such screw diameter, injection volume, cycle time and so on. Fig. 5.25 shows the changes of molded samples after beginning of gas injection into the polymer melt. It has been proved that the dwell time in this study was at least 25 cycles, so that if the process parameter was changed, only samples after 25 cycles could be taken for the analysis.

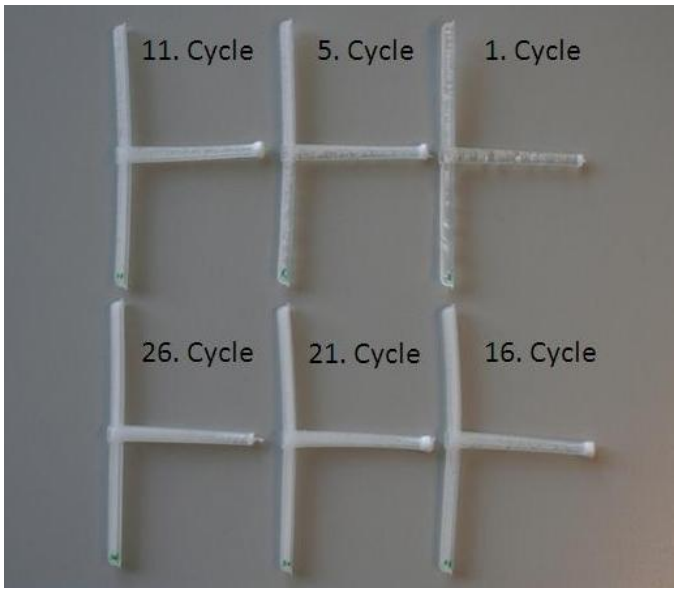

Fig. 5.25: Process stabilization after varying process parameter
After beginning of gas injection the sprues from molded parts were taken out with certain cycles. It was showed that only after over 20 cycles the sprues indicated no distinct difference. 25 cycles as dwell time would be assured for a stabilized process.

5.1.7 Short summary

In section 1 the detailed relations between parameter changes and pore morphology were described. Several important process parameters and consequent pore morphologies were investigated. It was proved that certain relationships between the process and pore structure existed and the foaming theory validity was partially testified. As brief summary Tab. 5.7 displays the influences of process parameters.

Process parameters	Pore size	Porosity	Interconnective pore size
Gas content	↓	↑	↓
Weight reduction	↑	↑	↑
Injection speed	↓	↑	relationship not obvious
Plasticizing temperature	↓	↑	↓
Plasticizing pressure	↓	↓	relationship not obvious
Mold temperature	↓	↓	↓

↓↑ obvious increase or decrease ↓↑ slight increase or decrease

Tab. 5.7: The relationships between process parameters and pore morphology
The arrow means the change trend with increased value of each process parameter. Some process parameters such as gas content and weight reduction showed a more obvious influence on the pore morphology whereas some others had just slight effect on the pore structure.

It was obvious that some process parameters such as gas content and weight reduction showed a more obvious effect on the pore morphology than some others. Subsequently for expected pore structure the parameters with fat arrow in Tab. 5.7 should be firstly considered, and then based on the results the other parameters could be adjusted as additional setting.

5.2 Influences of the mold design on pore morphology

In chapter 4 it was mentioned that two molds were designed and manufactured for the implant. The first mold had a ring shaped implant design and was just used for the preliminary test of the feasibility of the foaming process and parameter research. The second mold was designed based on the results from mold A for a better foam structure of molded implant and prospective production. The different implant designs are shown in Fig. 4.5.

The mold B has a shorter polymer melt flow and the L/D (length/thickness) of 2.8 whereas this L/D by mold A is 4.7. This means the molded part from mold B is relatively thicker but shorter. The advantage of mold B is that the energy loss of melt flow, which dominates the cell nucleation and growth, is reduced due to the shorter flow path (low L/D in the mold), as result a better pore morphology, such as bigger mean pore size, higher porosity and so on, could be expected. On the other hand the mold B has a bigger capacity which means more possibilities of parameter variation. The disadvantage of mold B is that relative thicker molded part will lead to an incomplete filling of the cavity of mold B, a long cooling time and significant shrinkage of molded part, in normal injection molding process. These problems could be partially or wholly resolved if the foaming process is applied due to the expansion of foamed polymer. In 5.3 of this chapter it will be described in detail.

Fig. 5.26 shows the comparison of the maximal porosity at different process parameters from two molds. It was observed that the mold B indicated a higher porosity at every parameter variation. The porosity at 35 % weight reduction from mold B showed a minimal elevation of ca. 6 % while the maximal porosity elevation of 14 % was found by injection speed variation. In Fig. 5.27 the differences at every single speed from two molds were illustrated. It was clear that at every single speed the porosity from mold B was always higher than the porosity from mold A. Two figures have indicated that with mold B a higher porosity of foamed sample by MuCell® was achieved.

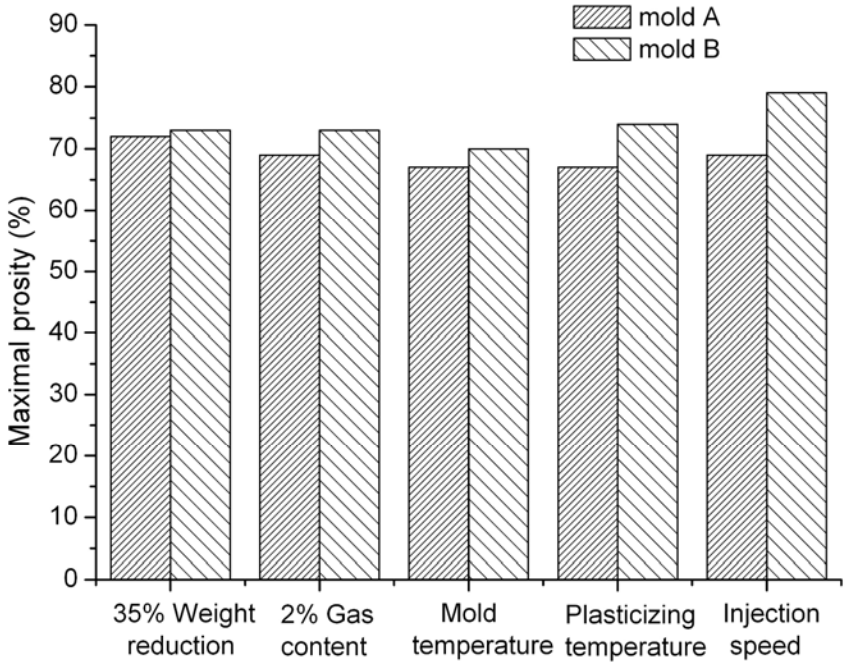

Fig. 5.26: Differences between the maximal porosity at different processing parameters
The maximal porosity at every parameter variation from two molds was compared and the differences were shown in the figure.

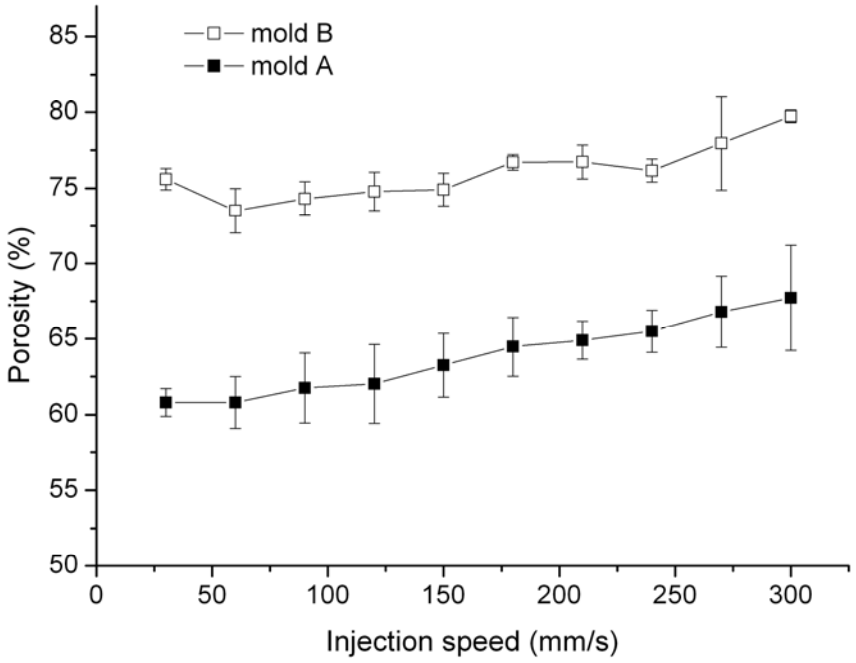

Fig. 5.27: Differences of the porosity at injection speed variation

It was also found from Fig. 5.27, that the standard deviation of porosity from mold B was significant smaller than the deviation from mold A. The same effect was found by observation of the mean pore size. Fig. 5.28 shows the mean pore size of two molds by injection speed variation. The mean pore size from mold B at every speed was higher compared with mold A, the range of increase of pore size was between 45 % and 62 %; at the same time an obviously decrease of standard deviation of mean pore size was observed on the mold B. This means that the new design of mold B can not only increase the porosity and mean pore size but also reduce the standard deviation, which shows the more uniform pore morphology.

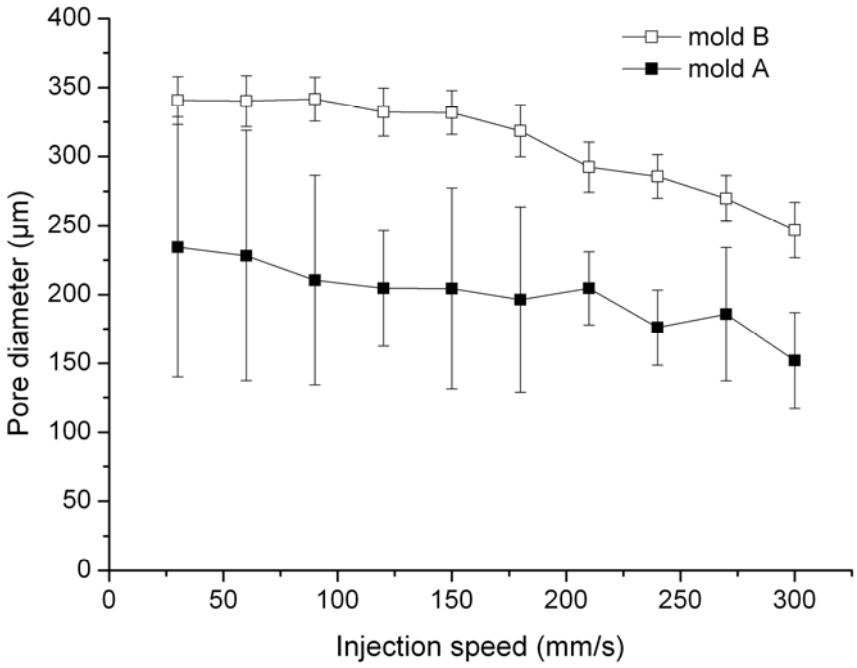

Fig. 5.28: The mean pore size from two molds at different injection speeds

So far the intent to improve the pore morphology through mold design change was achieved. The improved pore morphology such as the higher porosity, larger mean pore size and smaller deviation was found by the foamed samples from mold B. This has indicated that besides the effects of process parameters the mold design i.e. product design has also a distinct influence on the foam behaviour of foaming process, which has given the possibility to change or improve the pore morphology through a more suitable mold design if the process parameters are limited.

5.3 Benefits from MuCell® technology

As mentioned in previous chapters the MuCell® technology has many advantages such as saving the materials, reduction of the viscosity of polymer melt etc. In this section some advantages from MuCell® were described in detail.

It was already mentioned in section 2, that changes of mold B could lead to an incomplete filling of the cavity, a long cooling time and significant shrinkage of molded part. In compact injection molding those problems are very difficult to solve, but foaming process such as MuCell® may overcome the difficulty according to the foaming theory without guarantee. No similar case was found in industrial production, the information from the MuCell® supplier as well as literatures was also very limited. That meant that the risk of failure of mold design B must be taken account. In this case the functionality of MuCell® was finally proved and shown in Fig. 5.29.

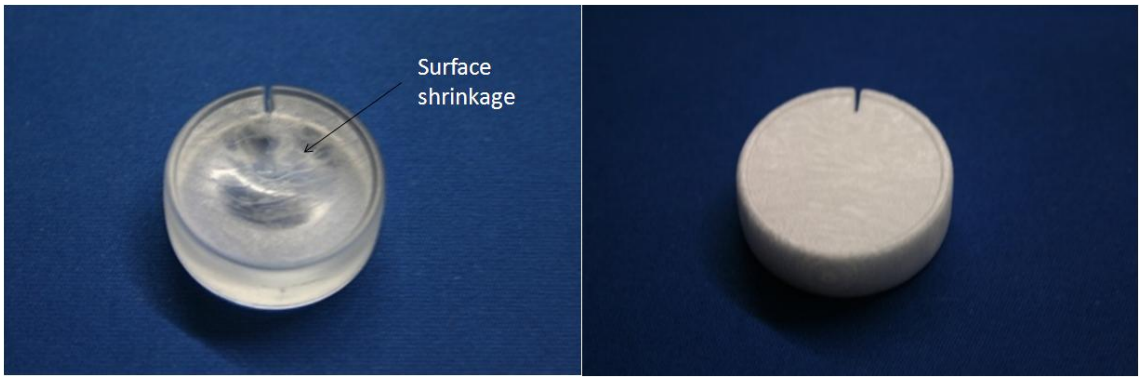

Fig. 5.29: Molded parts from compact and foaming injection molding by mold B
Left is the compact molded part by TPU, right is foamed part. The left sample showed a clear surface shrinkage, which was not possible to solve by compact injection molding, but the right foamed sample showed no surface shrinkage.

It was found that compact molded parts by mold B had an apparent surface shrinkage and it was not avoidable through varying the process parameters. But if MuCell® was applied, this problem was successfully overcome. The same result was also observed by PE (Polyethylene).

Fig. 5.30 indicates the injection pressure in relation to cylinder temperature with and without gas mixing. The injection pressure decreased if the cylinder temperature rose because the viscosity of polymer melt decreased. The same effect was found while the gas was injected, which meant the injection of gas has also reduced the viscosity of the mixture, so that the injection pressure by gas injection was lower compared with compact injection. For some temperature sensitive materials the processing temperature can be reduced without viscosity increase if the gas was mixed in, so that the temperature dependent degradation of polymer can be effectively decreased.

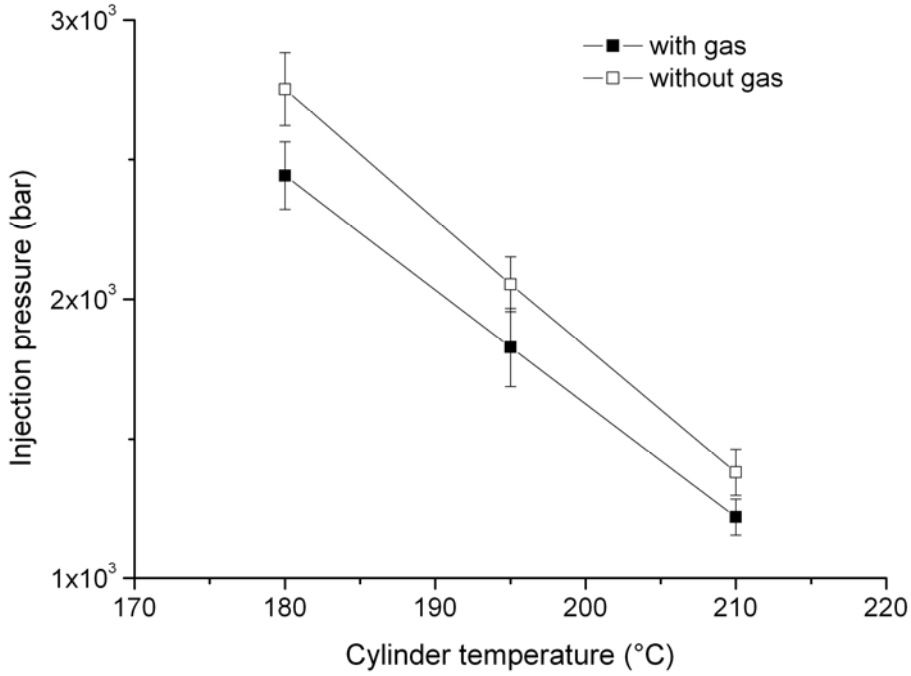

Fig. 5.30: Reduction of injection pressure due to gas mixing
The injection pressure was measured with the same injection speed.

At last the effect of gas mixing on the mold pressure is shown in Fig. 5.31. By the compact injection molding the mold was fully filled at first with pressure at the peak value, then during the cooling time the pressure reduced slowly and continuously to a very low level, whereas by the MuCell® process the pressure in mold was always very low (just several bar) and stable during the whole cooling phase. This property of MuCell® process can effectively prolong the life of mold and reduce the holding pressure during the cooling phase.

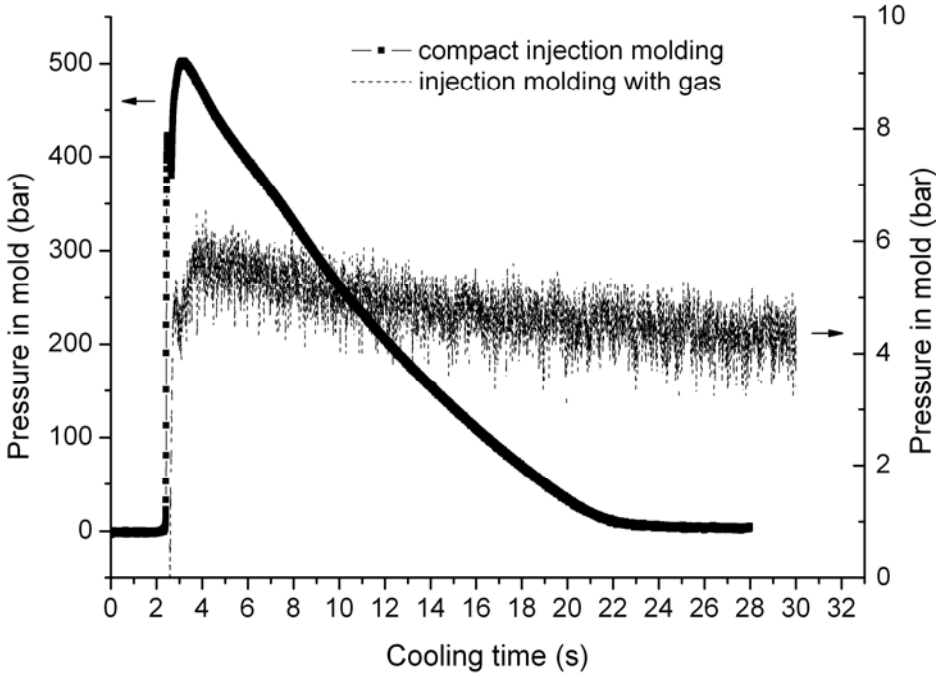

Fig. 5.31: The pressure in mold during the cooling with/without gas injection
The cooling time begins at the moment of injection of polymer melt into the mold. By compact injection molding the mold is full filled at first, consequently the pressure in mold is at the peak value, then during the cooling the pressure reduces slowly and continuously to zero. But by MuCell® the pressure in mold is stable and very low (several bar) from beginning to end.

5.4 Summary

From large numbers of trials the intent of producing implants with designed pore structure was achieved. The key parameters of MuCell® were tested to find out their influences on the foamed pore structure. Some parameters were found having to be more influencing on the pore morphology than others. The relationships from experimentation indicated approach for obtaining the expected pore structure. But it is important to note that all the relationships founded in this study are based on the MuCell® process and using TPU as raw material. Whether the relationships could be generally applied on the other foaming process and materials, need to be further researched.

Besides the process parameters the mold design has also an obvious effect on the pore structure. It was proved that an improved mold design could enhance the porosity, mean pore size and interconnections. Consequently the mold design as well as product design must be carefully considered, before the mold was manufactured, due to its high cost.

The advantages of MuCell® have been proved in this study. Through this foaming process the limitation of mold design was overcome. At the same time the reduction of temperature or

pressure in cylinder could be easily achieved through gas injection, as result a lower degradation of polymer during the process could be expected. The decrease of mold pressure, which is induced by MuCell®, could prolong the life of the mold and lead to a cost reduction for large production.

6 Biocompatibility of foamed implants

6.1 Surface treatments, sterilization and its influences on the implants

6.1.1 Surface treatments and sterilization of implants

In this chapter the biocompatibility of produced implants will be discussed in detail. The foamed implants were cut by a ring shape cutter to remove the central skinny core and reveal the inner porous structure. Fig. 6.1 shows the implant produced by MuCell® and after removal of the inner core.

Fig. 6.1: The implant (left) and the ring after removal of the core (right)

As most polymers show hydrophobic properties and bioinertness, some surface treatments of such implants may increase their biocompatibility [11,21,142,146]. In this study the plasma surface activation and TiO_2-coating were carried out for improving biocompatibility, cell attachment and ingrowth of the implants. After surface treatment the implants were sterilized by γ-rays for sterility. Different radiation dosages (25 and 60 kGray) were used for testing the effects of sterilization. For researching effects of the gamma sterilization on the plasma activated polymer surface, the plasma activated implants without gamma sterilization were chosen to be compared.

After surface treatments and sterilization the biocompatibility of the implants was tested *in vitro* and *in vivo*. At the same time the chemical and physical analyses were also performed to indicate the property changes of implants. In Tab. 6.1 the test samples are summarized.

Surface treatment method	Gamma sterilization	Sample name
Untreated	25 and 60 kGray	Inj. Mold, 25, 60 kGray
Plasma activation	25 and 60 kGray	Inj. Mold, Plasma treating, 25, 60 kGray
Plasma activation	none	Inj. Mold, Plasma treating
TiO_2-coating	25 and 60 kGray	Inj. Mold, TiO_2-coating, 25, 60 kGray

Tab. 6.1: Different surface treatments and sterilization methods
Plasma activation and TiO_2-coating were performed to increase the biocompatibility of the implants. Gamma sterilization was carried out for a high sterility assurance level. After these the implants were tested *in vitro* and *in vivo* to find out the influence of the surface treatments and sterilization on the biocompatibility of the implants.

6.1.2 Chemical and physical changes of implants after surface treatments and sterilization

Polymers consist of different long chain molecules revealing certain repeating structural units typically interconnected by covalent chemical bonds. This particular structure gives the polymers their special properties such as good flexibility by TPU. However the long chain structure shows also disadvantages: for example, the long chain molecule can be broken due to influences of one or more environmental factors, such as heat, light or chemicals. Therefore, bulk properties as well as nano-micro properties, for example the biological behaviour of polymers, can be altered due to this molecular chain break. These property changes of the polymers are also known as polymer degradation.

In this study the TPU granules were processed by injection molding, treated through different methods (plasma activation, TiO_2-coating), sterilized by γ-rays. These methods enable chemical structure changes of the TPU and consequently define its bulk properties. This may alter biological behaviours of the TPU sample. Some polymer characterizations were performed in this study to indicate the influences of performed processing, surface treatments and sterilization on the TPU implant.

Fig. 6.2 shows the ATR FT-IR (Annotated Transmission Reflex Fourier Transmission Infrared Analysis) measuring of the TPU samples after different surface treatments and sterilization. The chemical nature of surface can be qualitatively characterized through FT-IR. There is no major difference in the spectra (< 5 % transmission deviation) of all samples. Neither surface treatment such as plasma activation and TiO_2-coating, nor different γ-ray doses had influenced the chemical structure of the samples, compared with unprocessed TPU granules. The similar results were also presented in another study [77].

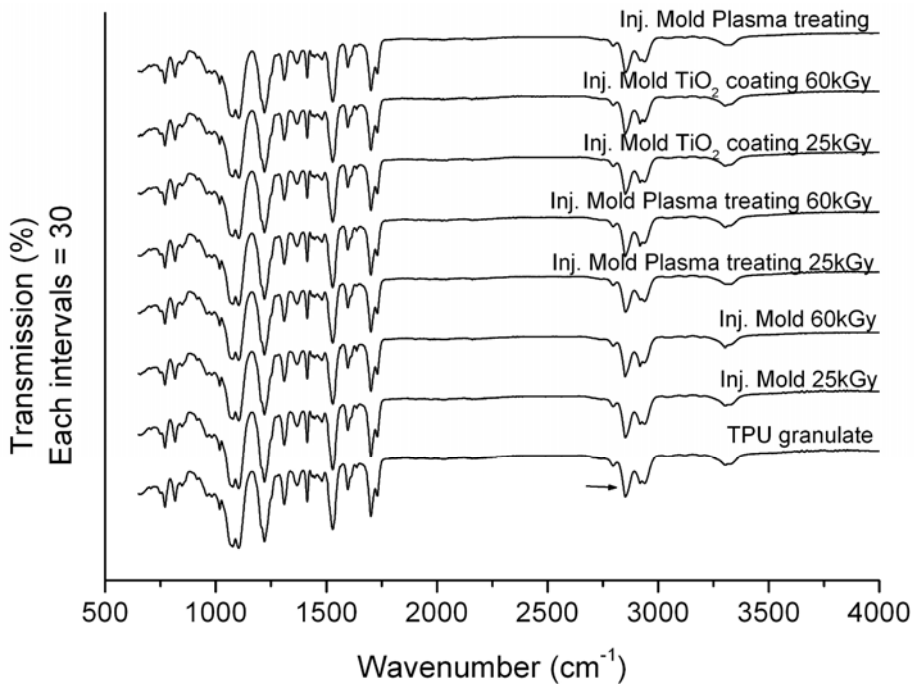

Fig. 6.2: ATR FT-IR-spectra of samples following different treatments and sterilization

Plasma activation and TiO_2-coating are widely used as surface treatment methods to improve the biocompatibility of polymers [11,21,142,146]. The general agreement is that such surface treatments can increase the surface wettability and biocompatibility as consequences.

Fig. 6.3 shows the contact angle and water adsorption test of the TPU sample surface with and without surface treatments. The contact angle measurement was performed on the surface of the injection molded TPU plate due to the difficulty of measuring the contact angle on a porous surface of foamed samples.

After surface treatments the contact angle has obviously decreased, from 103° of untreated to 64° of plasma activated, 78° of TiO_2-coating. The contact angle reduction induced by plasma activation can be attributed to surface functionalization by the interlock of polar groups such as (−C−O−C) and (−C=O) [168]. TiO_2-coating offers an increase of polar group (such as −Ti−O−) due to its chemical structure itself, at the same time a potential oxidation of polymer surface during the coating process may also lead to the rise of polar species [21,143]. The water adsorption test showed similar results compared with the contact angle test. The porous implant surface treated by plasma activation and TiO_2-coating adsorbed the water faster than the untreated surface. All these tests showed that the surface treatments such as plasma activation and TiO_2-coating were active for TPU. A consequent improvement of the biocompatibility of treated samples was expected .

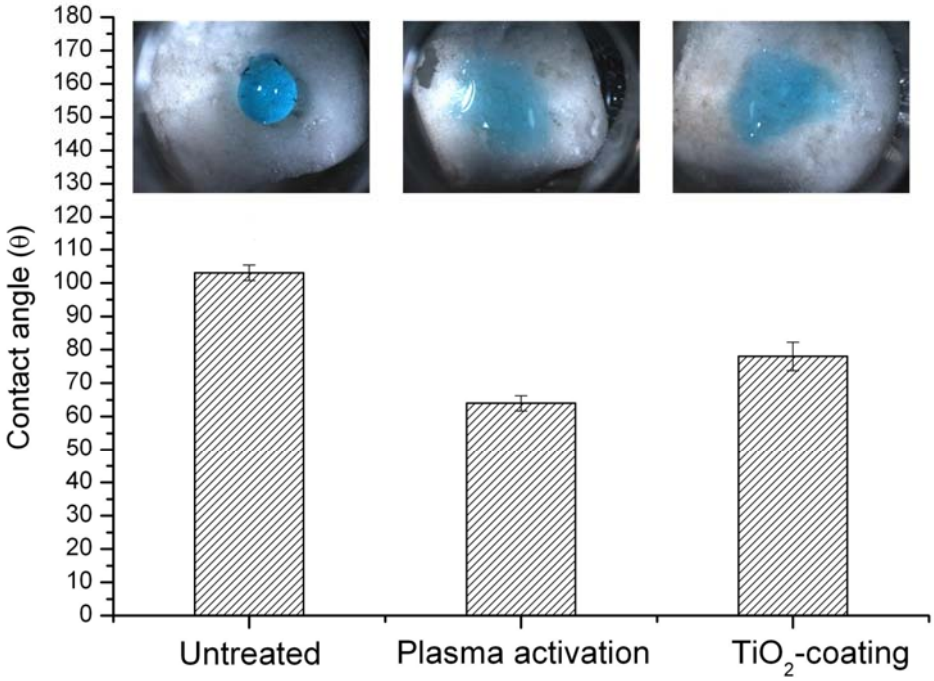

Fig. 6.3: Contact angle tests and water adsorption tests of TPU samples
After surface treatment the water contact angle of TPU surface showed an obvious decrease, which indicated a rise of wettability and consequent better biocompatibility. The water adsorption tests (images above every contact angle test) on the porous surface of foamed samples have shown the similar result. The colored water was dropped on the foamed sample surface and observed after 3 minutes. (n=3)

Since the implant used in this study has a relatively high porosity and the porous surface structure with large pore diameters (300-600 μm), the question is, whether the surface treatment can affect not only the surface but also deeper structures of the open porous structure of the implant. In this study the distribution of titanium atoms on the deeper inner pore surface was tested through SEM-EDX (Energy Dispersive X-ray Spectroscopy) and shown in Fig. 6.4. The implant after TiO_2-coating was dipped in liquid N_2. Then the implant was disrupted manually to expose a fracture for the SEM-EDX testing.

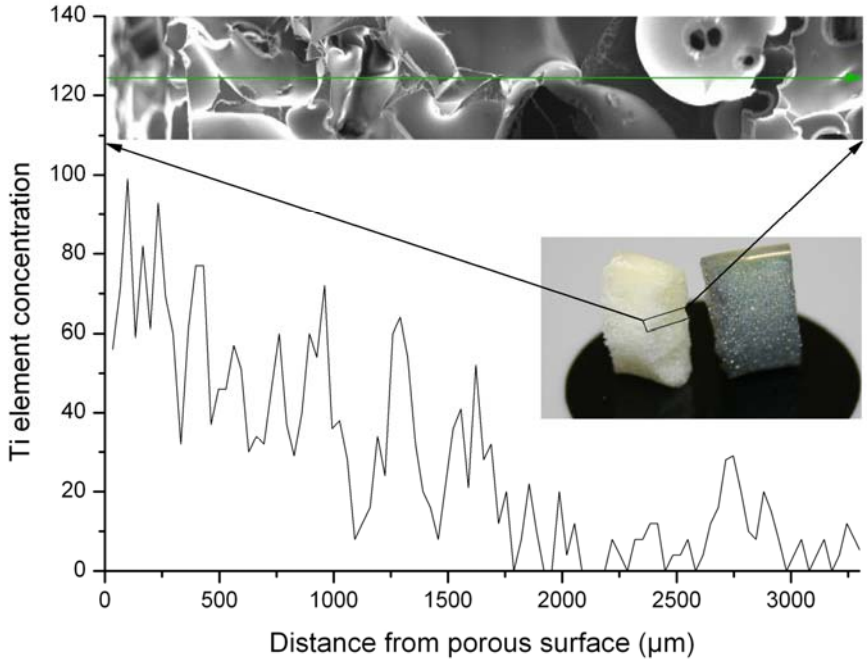

Fig. 6.4: The Ti-atom distribution on the fracture of the implant
The observed fracture of the implant is shown in the figure. The right half part was coated with gold. It is seen that from left to right the Ti-atom concentration has decreased continuously. The Ti-atom was found even in 3 mm deep inside the implant.

According to Fig. 6.4 titanium atoms could be found as deep as 3 mm inside the implant. The concentration of titanium atoms reduced with going deep into the implant. Therefore, the penetrability of the TiO_2-coating into the special porous structure of the implant was confirmed.

The thermal analysis was performed using DSC and shown in Fig. 6.5. It was observed that the injected and γ-sterilized samples had 3 peaks in curves. The first and second peak (ca. 70° C, 115° C) came from the disruption of short- and long-range order chains. The third peak (ca. 175° C) can be attributed to the melting of microcrystalline region in the hard segment microphase [167]. Unprocessed TPU granules had only 2 inconspicuous peaks at curve. The peak area has direct proportion to the crystallinity of polymers, so that the peak changes in this figure can also indicate the influences of the processing as well as the sterilization on the TPU sample structure.

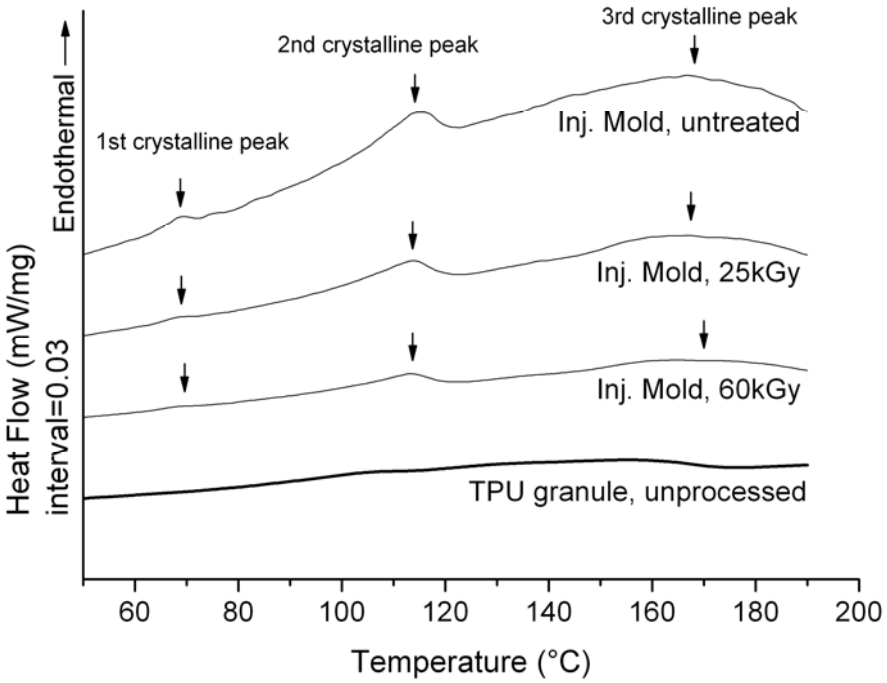

Fig. 6.5: DSC curves of TPU granules and samples with gamma ray sterilization

The crystallinity of the TPU sample had a significant increase after the injection molding, compared with the unprocessed TPU granule. This can be explained by the increased orientation degree of TPU long molecule chains due to the shearing and heat. As mentioned, the γ radiation could cause a cross linking of polymer long chains, so that the free motion of these chains were limited and hence the crystallite regions were prevented. As results the crystallinity of the implant by 25 kGray showed a reduction according to the smaller peak area, compared with unsterilized TPU sample, and the lowest value was by 60 kGray due to more cross linking of polymer long chains.

Finally the weight average molar mass of the TPU sample was tested in this study. The molar mass is a key characteristic of polymers in chemistry. Many physical properties of polymers has related to the molar mass, such as rheological properties of the polymer melt [66]. Some chemical structure changes of polymer can be observed by measuring the molar mass of polymer. Consequently, the degradation of polymers can be proved if the molar mass has changed due to the breaking of the long chain molecule. Fig. 6.6 shows the molar mass of TPU samples with or without surface treatments and sterilizations.

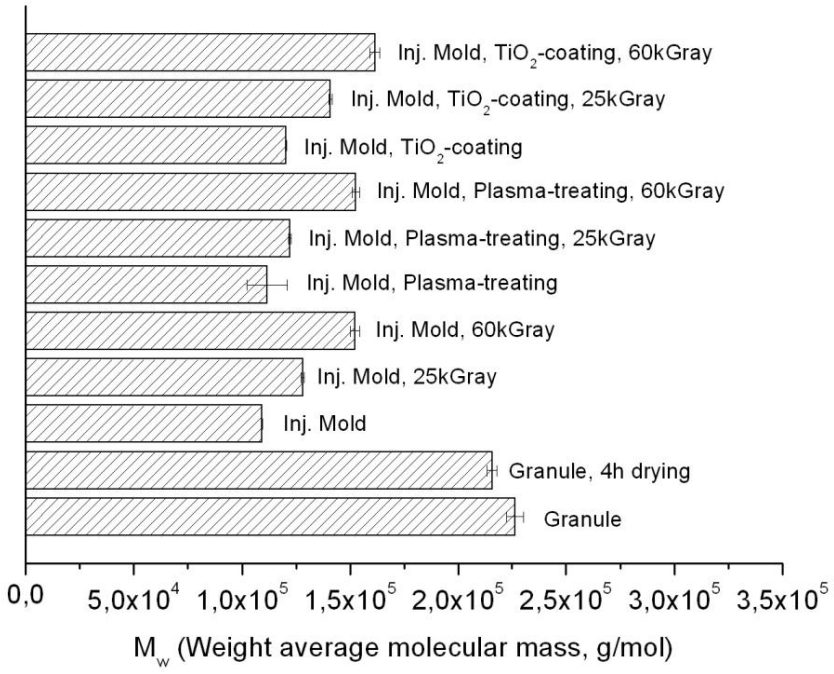

Fig. 6.6: Molar mass of TPU samples (n=6)

It is obvious that the unprocessed TPU granule has the largest molar mass, M_w of 226 kg/mol. After 4 hours of hot air drying a small loss of M_w (approx 5 %) was observed. After injection molding the M_w decreased quickly to the value of 109 kg/mol, almost half of the TPU granules unprocessed. The molar mass loss of polymers due to the processing was widely found in most polymers [173]. The molar mass loss of TPU due to injection molding was also found in different studies [77,109,204]. General agreement is that the polymer processing methods such as extrusion and injection molding have a stress on the polymer long chain due to the high temperature, high pressure in the cylinder as well as the shearing of screw. Those factors lead to a breaking of the molecule long chain of the polymers and the consequent molar mass loss.

The TPU samples that were irradiated by γ-ray behaved reversely and gained molar mass. The M_w of implant for 25 kGray and 60 kGray irradiation, was 128 kg/mol, 152 kg/mol, 17 % and 39 % improvement respectively. The γ-ray irradiation is widely used for inducing a cross linking between free monomers or short polymer chains to control the mechanical properties of polymers [45,208,220]. It could be assumed that the cross linking of the TPU molecule chain has taken place due to γ-ray irradiation. One of the results of γ-ray irradiation is the rise of molar mass. Similar observation were found for PU [178,218]; but reverse results were also reported [74,76]. It seemed that at a low dose range of radiation the molar mass increases with rises of the dose but acts on the contrary at a high dose range of radiation.

The plasma activation and TiO_2-coating had basically no influence on the molar mass of TPU samples. It is plausible because both plasma activation and TiO_2-coating had taken place in a low pressure and low temperature environment (s. chapter 4). No information was found about the influence of plasma activation or TiO_2-coating on the molar mass of polymers.

All tests mentioned above have indicated that the surface treatments and γ-ray sterilization have changed the surface properties of TPU foamed samples in micro-scale as well as the physical characters of TPU itself. These changes are expected for the change of biocompatibility of the implants. In the following sections the biological tests as well as the influence of surface treatments and sterilizations on the implants will be detailed described.

6.2 In-vitro test

Biocompatibility tests normally have three steps, *in vitro* test, *in vivo* test and clinical studies in humans. The *in vitro* test is basically performed always at the beginning of the biocompatibility test. The aim of the *in vitro* test is using cell and tissue cultures to evaluate the biological reaction of materials.

In this study the implants with different surface treatments and sterilizations were tested by WST-1 assay, LIVE/DEAD® assay and cell seeding.

6.2.1 The influence of surface treatments

As mentioned above the surface treatment such as plasma activation and TiO_2-coating have improved the surface wettability of the implants. Fig. 6.7 illustrates the cytotoxicity tests of extract (chapter 4.8.3) from implants after different surface treatments. The effects of surface treatments on the biocompatibility of the implant are shown clearly.

The implants after surface treatments showed a higher optical density at each test day compared to implants without treatment and all results were just consistent with the changes of the wettability of the implants after surface treatments (Fig. 6.3). The optical density was directly proportional to the number of viable cells. This rise of optical density indicated that the surface treatments such as plasma activation or TiO_2-coating could effectively improve the biocompatibility of the treated implant surface. The similar results were also found in other studies [115,210]. On days 1, 3 and 7 after cell seeding, the optical density of every sample type had a durative increase, which meant a good cell proliferation. All samples showed the optical density values over 70 % of the values of negative controls, which meant that the implants were well biocompatible.

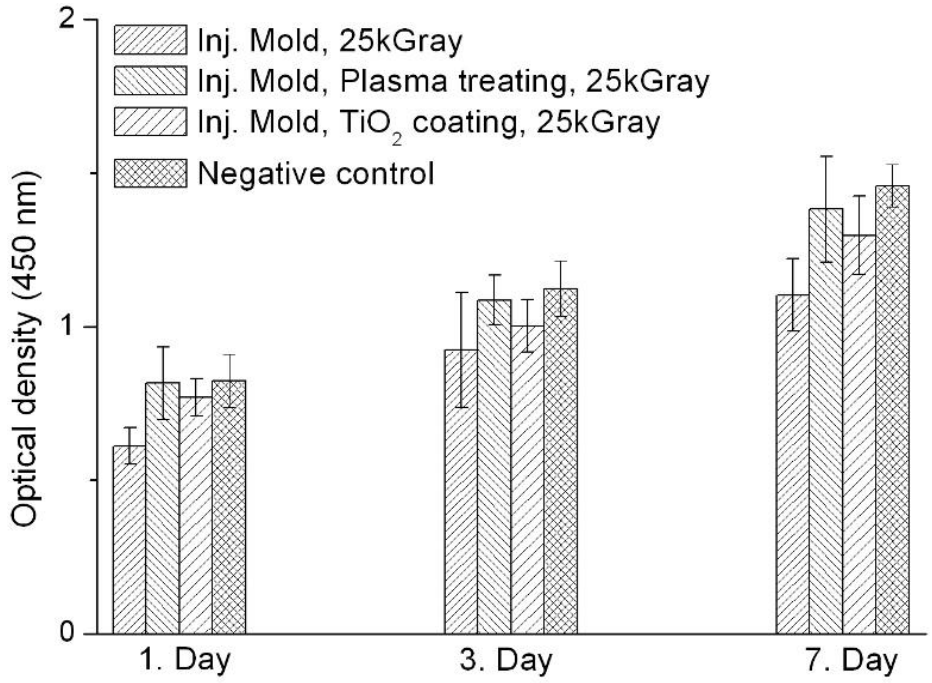

Fig. 6.7: WST-1 assays to compare the cytotoxicity of implant surface with different treatments
Implants with plasma activation, TiO_2-coating and no treatment were sterilized by γ-ray irradiation (25 kGray). The negative control was pure medium. The tests were performed at the 1st, 3rd and 7th day after cell seeding to indicate the proliferation of cells on the implant surface. The optical density is directly proportional to the amount of viable cells. (n=8)

Another cell vitality colouring test, LIVE/DEAD® colouring assay, was also performed as the qualitative test of the biocompatibility of implants and is shown in Fig. 6.8. The results from LIVE/DEAD® colouring assay agreed with those from the WST-1 assay. The untreated sample showed the worst cell vitality, relative fewer vital cells and more nuclei of non-vital cells, whereas higher cell vitality levels (more green vital cells) were found in samples after plasma activation and TiO_2-coating. A netlike morphology of cells was found in tests of implants after surface treatments, like negative control.

The increase of optical density in WST-1 assay and vitality of cells in LIVE/DEAD® colouring assay could primarily be attributed to the modified surface of implants induced by plasma activation or TiO_2-coating, which prevented efficiently the release of toxic degradation products. Methylenedianiline (MDA) was generally considered as the main toxic degradation product released from TPU [77,107]. So far the results indicated that there was only a slight cytotoxic effect of the extract of implants after surface treatment.

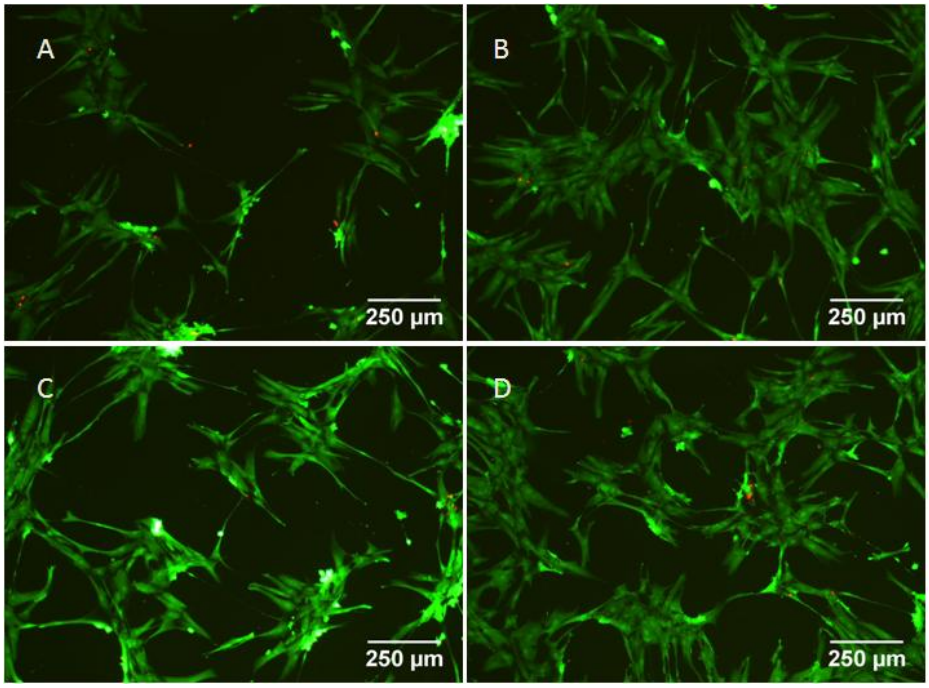

Fig. 6.8: Vitality colouring (LIVE/DEAD®) after cultivation of fibroblastic cell with extract medium
A) Untreated sample; B) Sample after plasma activation; C) Sample after TiO_2-coating; D) Negative control. All samples were sterilized with 25 kGray gamma ray. Green is vital cells and red is nuclei of non-vital cells. The images were taken after 3 days incubation.

The proliferation of cells on the implant surface was tested through cell seeding described in chapter 4.8 and is shown in Fig. 6.9. After 7 days incubation all samples were attached by seeded cells. The untreated implant surface was just slightly covered by cells. On the contrary the implant surface with treatments (plasma activation and TiO_2-coating) was completely covered by a cell layer. The cells attached themselves onto the implant surface and some even into the porous structure. This ingrowth of cells into the pore was desired because it could prevent the migration of implants along the oesophagus. A significant acceleration of the cell adhesion and proliferation was observed due to the surface treatment. The results of cell seeding suggested that the hydrophilic implant surface after the plasma treating and TiO_2-coating was more favourable for the cell spreading and growth than the hydrophobic surface of the untreated implant. Consequently, oxygen atoms or radicals played a very important role in enhancing the cell spreading, proliferation behaviours as well as the biocompatibility of the implant.

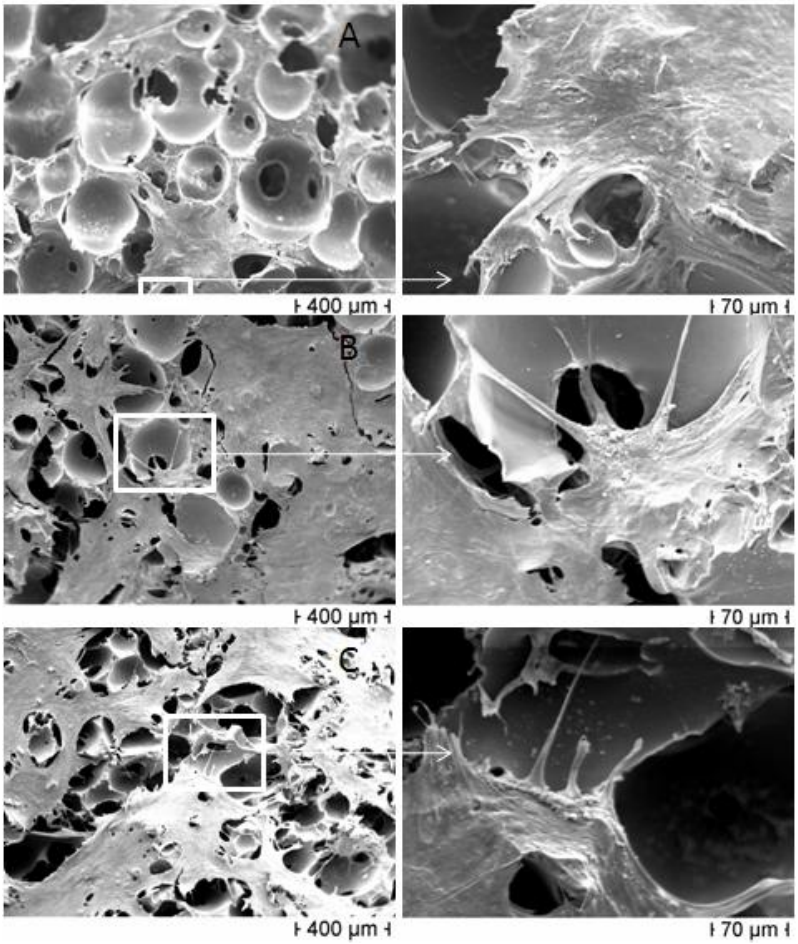

Fig. 6.9. SEM images of the surface of the implant with/without treatment after 7 day incubation
A) Untreated sample; B) Sample after plasma activation; C) Sample after TiO_2-coating. All samples were sterilized with a 25 kGray gamma ray.

6.2.2 Influence of γ-ray irradiation as sterilization method

All the samples were sterilized through γ-ray irradiation before cytotoxicity tests were performed. In this case two different doses of irradiation were test on the implant to understand potential effects of γ-ray irradiation on the surface properties after treatment as well as biological behaviors of implants.

The cytotoxicity tests of extract of untreated and TiO_2-coated implants with different γ-ray irradiation doses are illustrated in Fig. 6.10. The tests of plasma treated implants will be separately discussed.

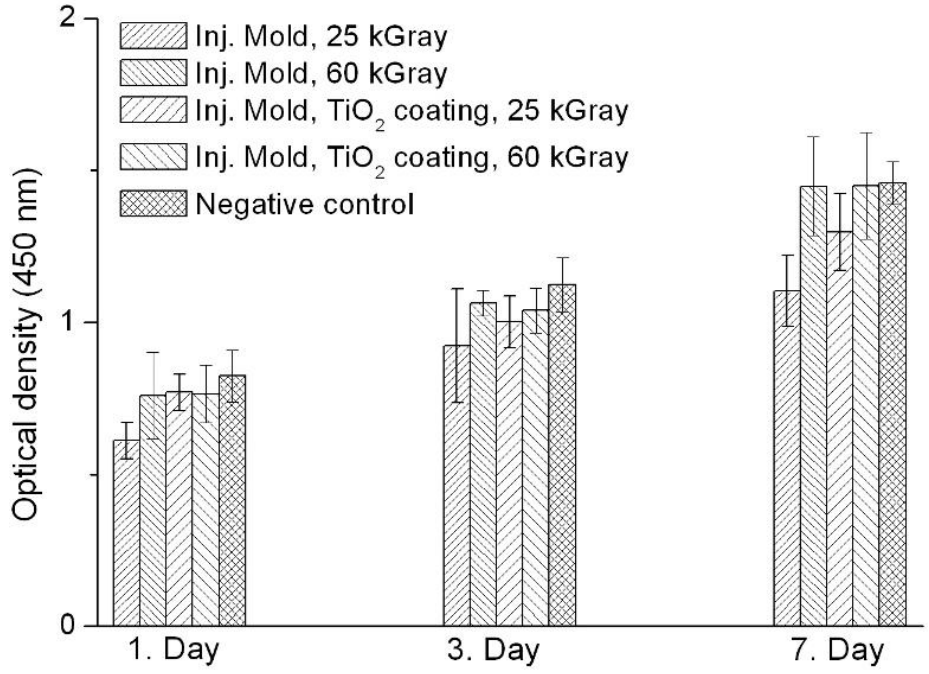

Fig. 6.10. WST-1 assays to compare the cytotoxicity of the implant surface with different γ-ray irradiation
The untreated and TiO_2-coated samples were sterilized through γ-ray with 25 and 60 kGray respectively. The negative control was pure medium. (n=8)

The optical density of the untreated implant increased significantly with an increasing dose of γ-ray irradiation, at every test day. The reason could be changes of chemical structure of TPU after the irradiation. It was assumed that the cross linking of the TPU molecule chain has taken place due to the γ-ray irradiation and the release of toxic degradation product from implants was consequently prevented. As result a rise of optical density with increase of the γ-ray dose was observed. The increase of optical density of TiO_2-coated implants from 25 to 60 kGray γ-ray irradiation could also be explained by the same reason. The TiO_2-layer coated on the implant surface acted as a protection layer to prevent the release of toxic degradation product, so that the TiO_2-coated implant at 25 kGray of γ-ray had always higher optical density than those without treatment. All implants showed the optical density over 70 % of negative control and indicated a good biocompatibility.

The LIVE/DEAD® assay tests (Fig. 6.11) proved the results from WST-1 assays qualitatively. The untreated sample with 25 kGray of γ-ray irradiation showed the worst cell vitality. With rise of the γ-ray dose more viable cells was found; this effect was not obvious by TiO_2-coated implants.

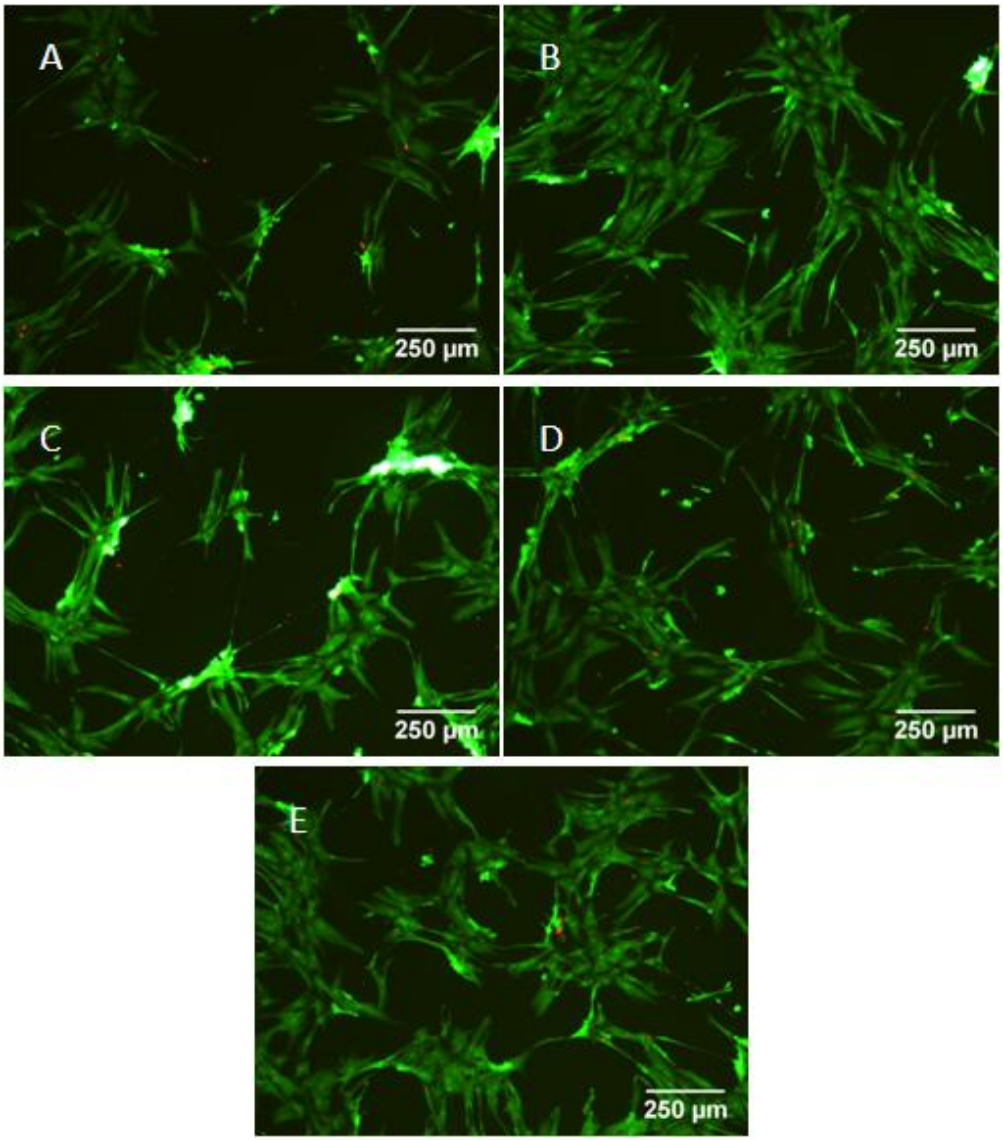

Fig. 6.11: Vitality colouring (LIVE/DEAD®) of the extract of untreated and TiO_2-coated implants
A) Untreated sample, 25 kGray; B) Untreated sample, 60 kGray; C) TiO_2-coated sample, 25 kGray; D) TiO_2-coated sample, 60 kGray; E) Negative control of pure medium. The images were taken after 3 days incubation.

The cell seeding tests are shown in Fig. 6.12. After 7 days incubation the cells have well proliferated on the TiO_2-coated surface of implants. A homogeneous cell layer was found by both γ-ray doses and no apparent difference on cell proliferation was seen. Untreated implants showed few cells on their surface. The cells spread heterogenously and just covered partially the surface of implants. But all implants showed ingrowth of cells into the porous structure, especially in the TiO_2-coated implants.

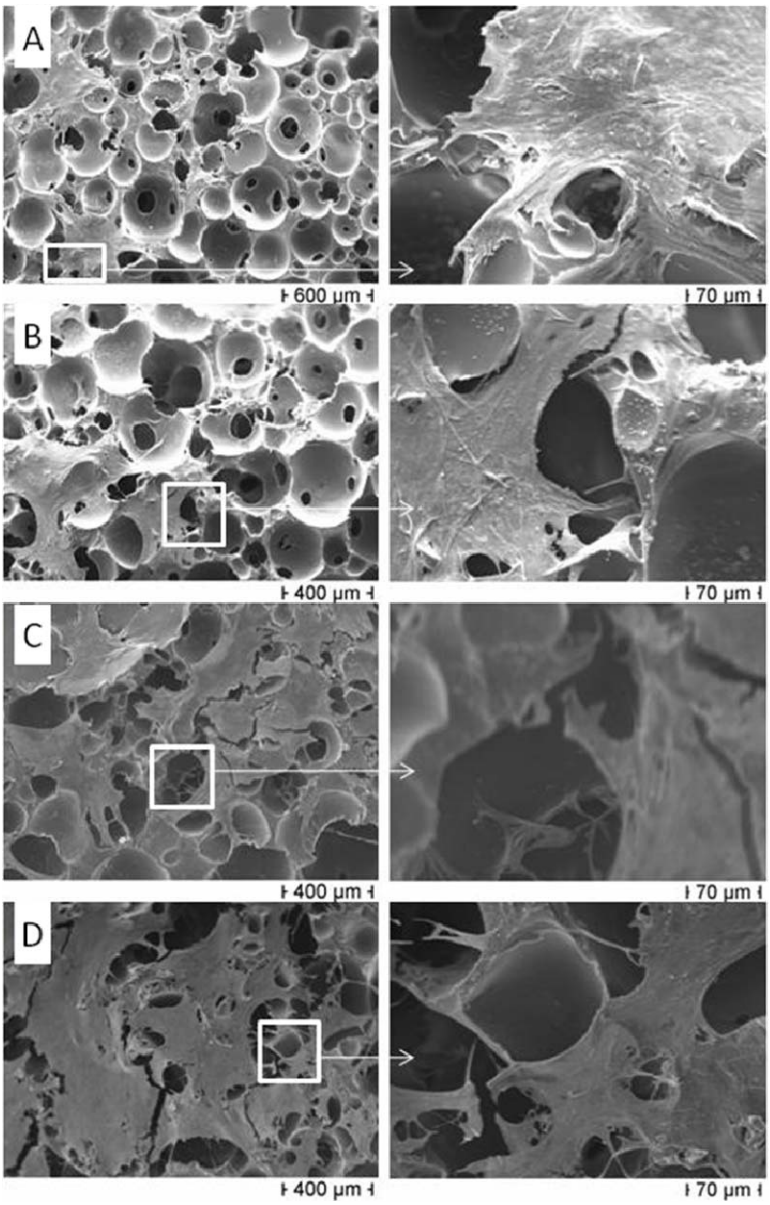

Fig. 6.12: SEM images of the surface of the implant with different γ-ray dose after 7 days of incubation
A and B are untreated samples with 25 and 60 kGray γ-ray, C and D are TiO_2-coated samples with 25 and 60 kGray γ-ray.

The following contents will focus on the interaction between plasma activation and γ-ray irradiation after discussing the effect of γ-ray irradiation on the biocompatibility of implants untreated and TiO_2-coated.

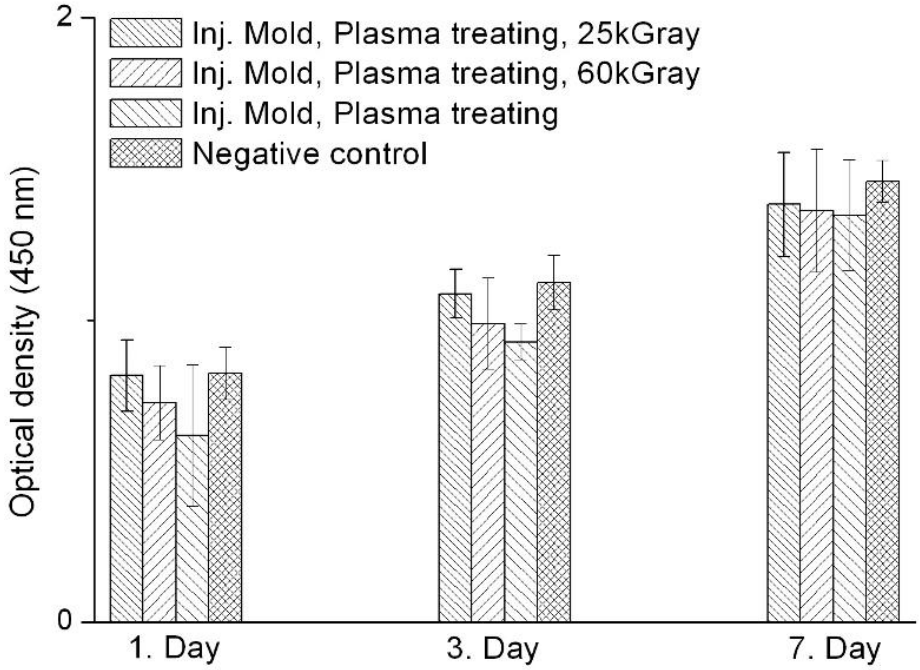

Fig. 6.13: WST-1 assays (extract) to indicate the effects of γ-ray irradiation on the plasma treated implant
The implants after plasma activation were sterilized through γ-ray irradiation, the same implant without sterilization was simultaneously performed. The negative control was the pure medium. (n=8)

Fig. 6.13 demonstrates the cytotoxicity tests of implants treated by plasma activation with and without the sterilization. The optical density of unsterilized implants had the lowest value. The reason can be attributed to the unsterilized state of the implant. The implants after sterilization showed the higher optical density at every test day, because the irradiation prevented the release of the toxic degradation product of TPU. The rise of irradiation doses from 25 to 60 kGray leaded to a reduction of optical density. This change was clear on the 1st and 3rd test day but not significant on the 7th test day. The reduction of optical density with the increased irradiation dose was due to the changes in the chemical structure of the modified implant surface [178]. This change could possibly destroy the formed layer induced by plasma activation on the surface of implants and reduce the positive effect of the plasma activation on the biological behavior of implant. Fig. 6.14 indicates that the percentage of the oxygen element of the implant surface was changed after γ-ray irradiation. The content of oxygen has increased from 29.7 ± 0.2 % to 36.6 ± 7.11 % after 25 kGray irradiation. More irradiation leaded to a slight drop of this content. The significant deviation change at 25 kGray irradiation indicated a less homogeneous oxygen distribution on the implant surface, which could partly prove the present chemical structure changes on the modified implant surface. The exact reaction induced by irradiation was not clear, however changes of chemical structure of the implant was verified. This change, maybe damage, of formed layer induced by

plasma activation could lead to more release of toxic degradation product and lower optical density with the rise of irradiation dose.

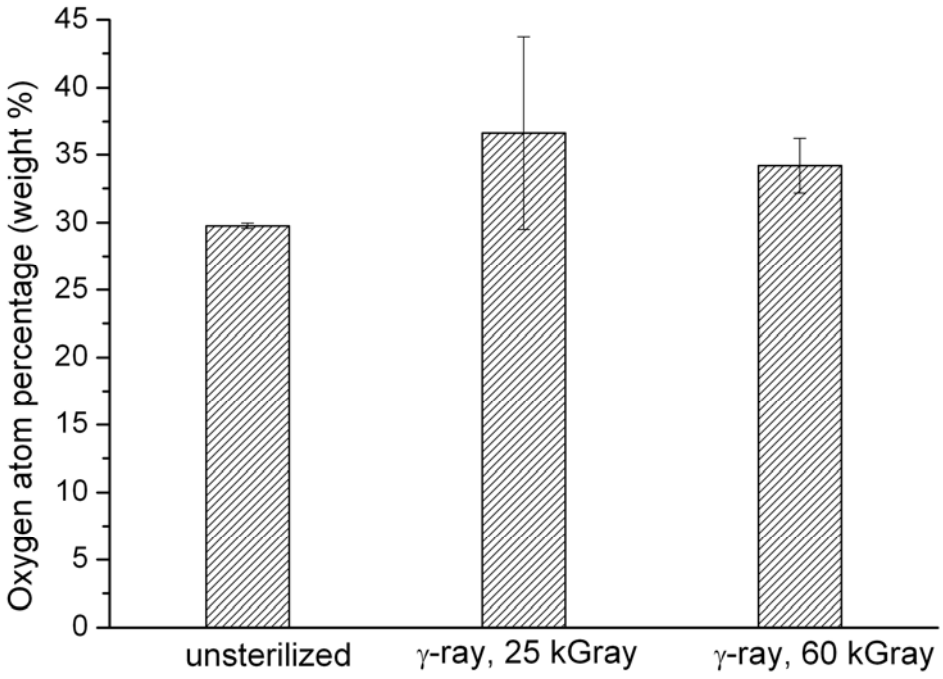

Fig. 6.14: Oxygen atom weight percentage of plasma treated implant surface with/without γ-ray irradiation
The percentage of O atom on the implant surface was measured through EDX (Energy-dispersive X-ray spectroscopy) coupled with SEM. (n=3)

The LIVE/DEAD® assay tests were consistent with the results of the WST-1 assays (Fig. 6.15). The unsterilized implant showed the worst case of vitality of cells due to its unsterilized state. The implants after sterilization have shown a better cell vitality. But the effect of the γ-ray irradiation on the cell vitality was not so apparent.

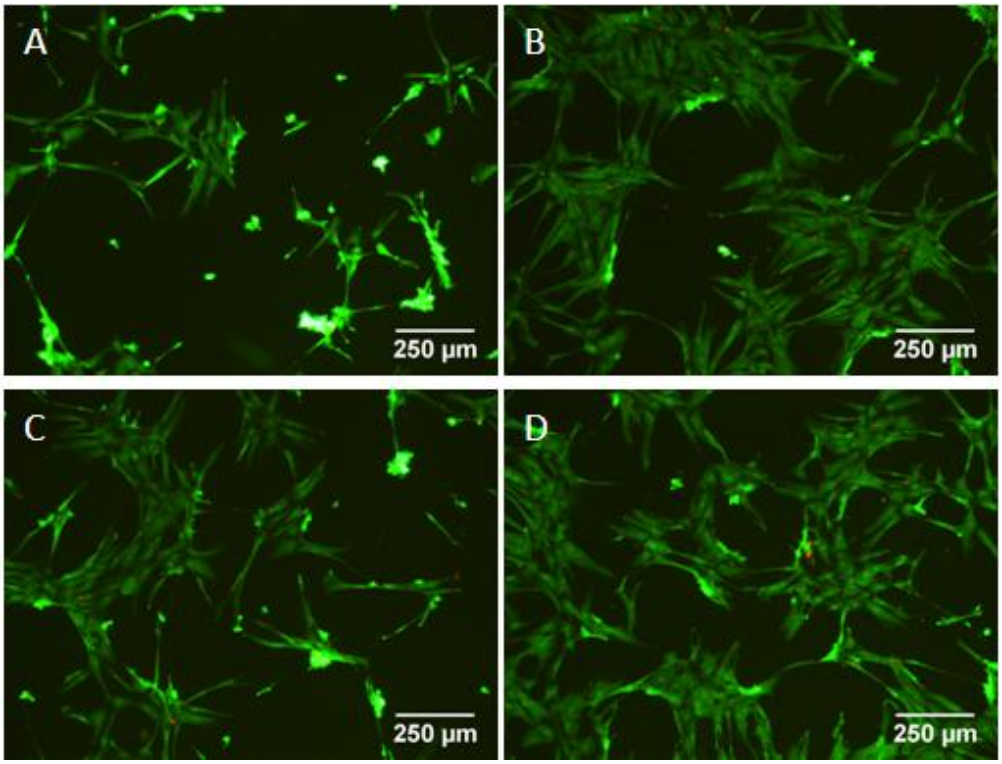

Fig. 6.15: Vitality colouring (LIVE/DEAD®) to indicate the effects of γ-ray irradiation on the plasma treated implant
A) Sample unsterilized; B) Sample with 25 kGray γ-ray irradiation; C) Sample with 60 kGray γ-ray irradiation; D) Negative control of pure medium. All samples were treated by plasma activation. The green is vital cells and red is cell nuclei of non-vital cells. The images were taken after 3 days incubation.

If the cells were directly seeded onto the implant surface, the protective function of formed layer induced from the plasma activation could not be the premier factor which affected the biological behavior of implants. In this situation the positive effect of formed polar species or radicals should play the most important role for improving the biocompatibility of implants.

Fig. 6.16 shows the cytotoxicity tests based on direct cells seeding process (chapter 4.8.3). In this experiment the unsterilized implant had the highest optical density, i.e. best biocompatibility, despite the unsterilized state. The γ-ray irradiation has changed, maybe destroyed, the formed layer induced from plasma activation and consequently the optical density has significantly decreased from 0.45 by unsterilized implant to 0.18 by implants with 25 kGray irradiation, after 7 days incubation. The lowest value of optical density was found at the 60 kGray irradiation by every test day. The results have proved that the interaction between implant surface and cells has dominated the cell growth and proliferation by the contact of cells with the surface of the implant.

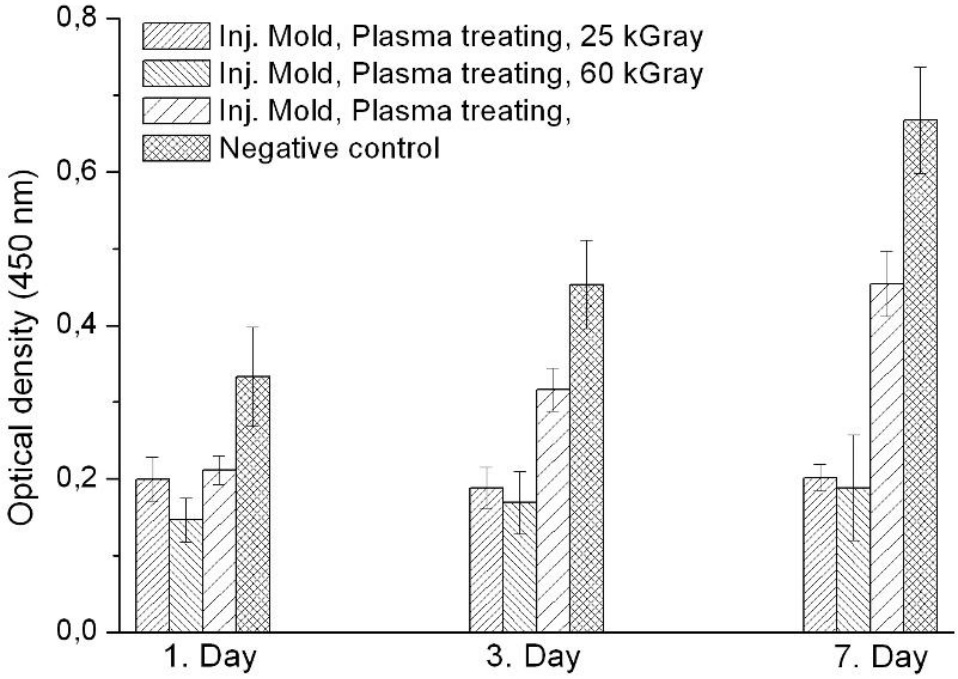

Fig. 6.16: WST-1 assays (direct cell seeding) to indicate the effects of γ-ray irradiation on the plasma treated implant
The WST-1 assays were performed as described in chapter 4.8.3. The cells were first seeded onto the implant surface and covered with medium. After a defined culture time the WST-1 reagent was added into the medium and the optical density was measured.

Direct cell seeding tests onto the implant surfaces were performed to testify the results from WST-1 assays. The results from SEM image (Fig. 6.17) after certain cultivation time were consistent with the results from WST-1 assays. The unsterilized implant had a homogeneous cell covering like carpet, whereas the implant after γ-ray irradiation of 60 kGray showed the surface just partly covered by cells. The cell ingrowth into the porous structure of the implant was found by all three variants.

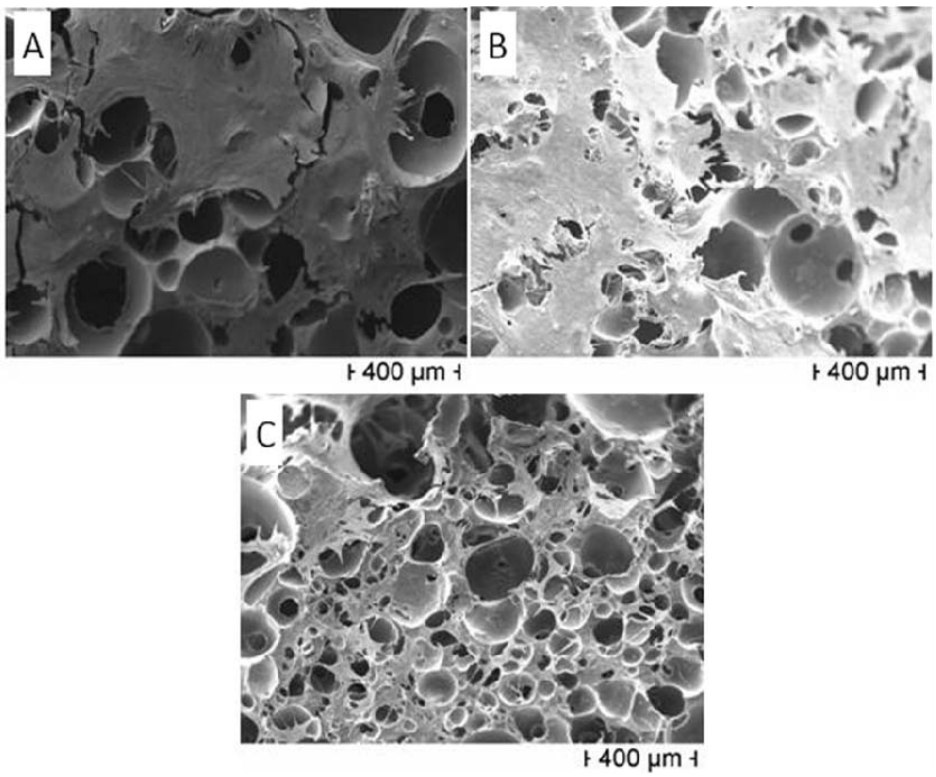

Fig. 6.17. SEM images of plasma treated implant with/without γ-ray irradiation
A) Implant unsterilized; B) Implant sterilized of 25 kGray γ-ray irradiation; C) Implant sterilized of 60 kGray γ-ray irradiation. All samples were treated by plasma activation.

6.3 In vivo test

After *in vitro* tests the implant should be tested *in vivo* to indicate its functionality and biocompatibility. In this study the implant was first tested on rabbits to prove the cell ingrowth and biocompatibility of implants. Then the anti-reflux function of the implant was tested on pigs. All animal tests were performed at clinical center (Klinikum rechts der Isar, TU München, Munich, Germany) and the biological behaviour of implants was evaluated at MedTech (Lehrstuhl für Medizintechnik, TU München, Munich, Germany).

The experimental process was described in chapter 4.9. The *in vivo* tests on rabbit severed as preliminary test of cells ingrowth into the porous structure considering the high cost and complexity of tests on pigs. The implant was cut into pieces and subcutaneously implanted in the dorsal region of rabbits for 2, 6, 12 and 26 weeks. Three rabbits for each implantation period were operated, i.e. 12 pieces of each implant type for every implantation time were available. At the conclusion of each implantation period, all pieces of implants were explanted for the further histological analysis.

All operated rabbits were healthy in the entire implantation period, no remarkable signs of inflammation or infection in any of surviving animals were found. The histological micrographs of implants after 2 weeks embedding time are shown in Fig. 6.18. All implants were fully encapsulated by a fibrous connective tissue induced due to the cellular response. The thickness of a capsule varied from 200 µm to 800 µm. The untreated implant showed no ingrowth of tissues and cells into the porous structure of implants, whereas the plasma activated implant induced an obvious ingrowth of tissue and cells. The TiO_2-coated implant showed just some ingrowth of tissues but less than in plasma activated implants.

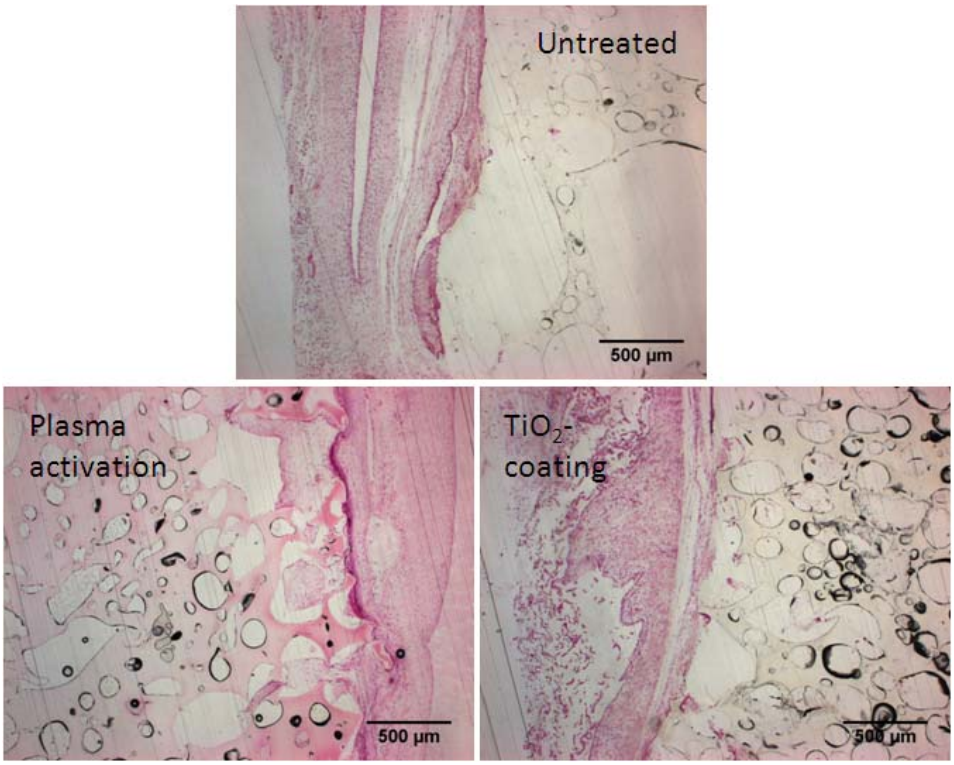

Fig. 6.18: Histological micrographs of implants after 2 weeks embedding time
The red region represents the fibrous tissue outside the implants. The black arrow marked the tissue and cells which have grown into the porous structure of implants. The black areas were the contamination during the sample preparation.

After 24 weeks the thickness of capsule around the implants decreased by all three implant types, maximal 200 µm. The ingrowth of tissues and cells has strongly increased by untreated and plasma activated implants, but the TiO_2-coated implants showed the worst results, unlike the results at two weeks implantation (Fig. 6.19). In the case of plasma activated and untreated implants the tissue has grown almost 1 mm deep into the implant, some cells were even found in the middle of the implant. Considering the fibrous capsule and cells ingrowth, the aim of fixing implant around the sphincter of the esophagus through cell ingrowth could be achieved.

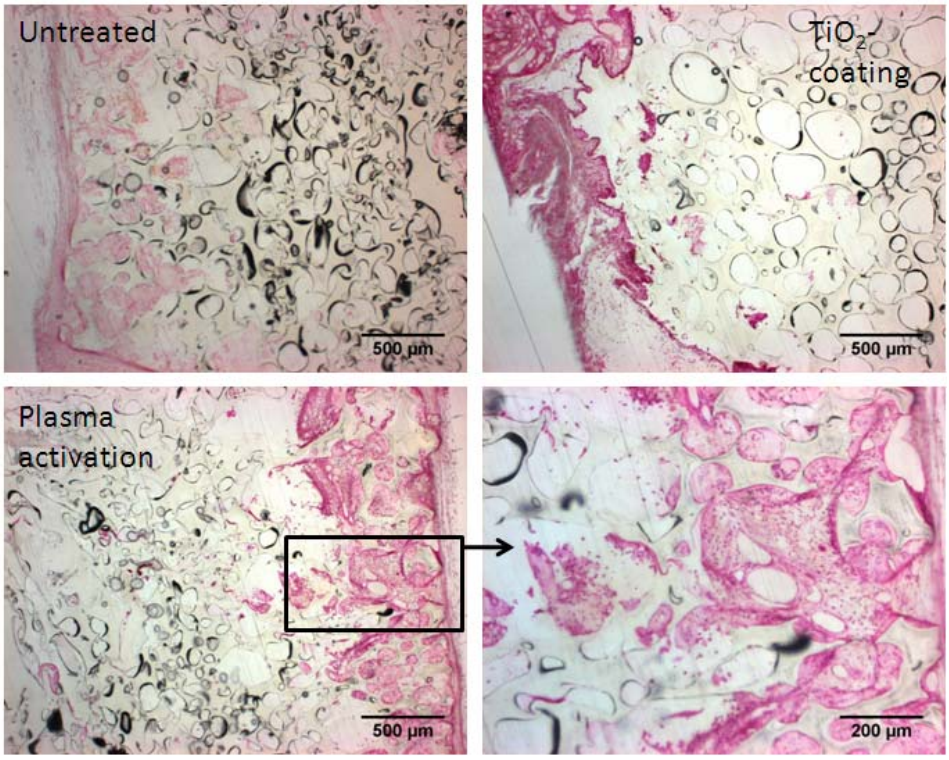

Fig. 6.19: Histological micrographs of implants after 24 weeks embedding time
Untreated and plasma activated implants showed an increase of ingrowth of tissues and cells.

The reduction of thickness of the capsule after a long time implantation was also found in the other study. Lehle et al found that after 4 weeks the implants made of PET and PP, uncoated and TiO_2-coated respectively, showed a thinner capsule compared with results from 1 week implantation in rats [113]. It was to notice that the TiO_2-coated implant *in vivo* did not show the comparable behavior like *in vitro*. The histocompatibility of TiO_2-coated implants was worse than plasma treated, even untreated, whereas in earlier study of *in vitro* tests with human fibroblast the TiO_2-coated implants had always a comparable biocompatibility to plasma treated implants and better than untreated implants. It was reported that an increased foreign body giant cell density and thick collagen bundles around TiO_2-coated implant compared with uncoated controls was observed in tests on rabbit [217]. This may be the reason of less histocompatibility of TiO_2-coated implants. On the other side the tissue reactions depend on many aspects such as surface properties, dimension and nature of the implant which is in this case relevant [176]. So the proved increase in hydrophilic properties of TiO_2-coated implant and consequent increase of biocompatibility *in vitro* test were not consistent with biological tissue reactions from tests *in vivo*.

7 Conclusions

7.1 Processing

One of the main aims in this study was to produce a porous implant through MuCell® process and to determine the relationship between the resulting porous morphology and the processing parameters. This aim was fully achieved and is described in detail in chapter 5.

With help of foaming theory and literatures six key parameters were targeted and further investigated. It was found that gas content, weight reduction of implant compared with compact injection molding and plasticizing temperature were the prime influence factors of pore morphology and porosity in MuCell® process. An increase of gas content lead to pore size reduction and rise of porosity, is one example. Injection speed, plasticizing pressure and mold temperature were the second prime influence factors of pore morphology. The pore size of foamed implants during the whole study ranged from 130 µm to 870 µm. The maximal porosity and interconnective pore size were 77 % and 135 µm. It was proved that a large scale of pore morphology of foamed implant could be arrived through varying the parameters of MuCell® process. Even though the foaming theory could be applied to describe the pore development, interaction of different parameters must be taken into account to fit the experimental data into the theory. Empirical data were found to be more valid than just the theory at itself. It is apparent that in order to reach the intended porous structure, experimental data is essential.

It was found in this study that the mold design could improve the pore morphology. A higher porosity, large mean pore size and smaller deviation were found by the foamed samples from the mold which was more foam suitable constructed.

Another advantage of MuCell® process was verified in this study. It could effectively reduce the mold inner pressure, which gave the possibility to prolong the life of mold and decrease the holding pressure during the cooling phase. On the other side the mixing of gas into polymer melt increased the fluidity of the mixture with consequent reduction of plasticizing pressure in cylinder. This could also reduce the degradation of the polymer during the production. At last the foaming ability of polymer melt eliminated the incomplete filling of the cavity and surface shrinkage of molded part by some product with thick wall.

7.2 Biological analysis

The *in vitro* tests proved that the biocompatibility of implants after surface treatment was significantly increased. The surface treatments such as plasma activation and TiO_2-coating had changed the properties of implants in micro-scale. The surface hydrophilicity of implants was improved after treatments and the biocompatibility of implants as well as the adhesion

properties of cells were consequently increased. Only a slight decrease in cell cytotoxicity was present. All samples showed more than 70 % optical density of control. Cell seeding studies also showed that fibroblasts adhered to the surface and proliferated carpet-like after 7 days of incubation. The cell ingrowth in porous structure was also found by all implant types.

The γ-ray sterilization was proved to improve the biocompatibility of implants, untreated and TiO_2-coated, because it led to a cross linking of TPU molecule chain and consequent prevention of release of toxic degradation product from implant. But γ-ray could damage the formed layer induced by plasma activation and reduce the positive effect of plasma treatment on the biocompatibility of implants. The tests *in vitro* proved that with rise of γ-ray dose the optical density decreased and this finding was consistent with LIVE/DEAD® tests. A change of percentage of oxygen on the implant surface after surface treatment was found, which corresponded to the results from *in vitro* tests.

The cell and tissue ingrowth in porous structure of implants were testified through *in vivo* tests on rabbits. After long term implantation the tissue was found about 1 mm deep within the implants. At the same time the implants were completely encapsulated in fibrous tissue. The capsule thickness decreased with implantation time. It was to notice that the TiO_2-coated implants showed the worst histocompatibility. Similar results were also reported [176,217], that the *in vitro* findings could not be confirmed in the *in vivo* implantation due to the complexity of tissue responses.

7.3 Summary

The main goal of the project has been reached: It has been shown that a biocompatible implant with porous structure could be produced with MuCell® process, an established microcellular injection molding technology. The desired porous structure was achieved and the pore morphologies such as pore size, porosity as well as interconnectivity were adjustable by altering the processing parameters.

Biocompatibility tests have proven that the surface treatments such as plasma activation and TiO_2-coating could improve the hydrophilicity of implants surface and by consequence the biocompatibility of implants. The *in vitro* tests demonstrated a good cell adhesion and proliferation on the implant surface. Cell ingrowth into porous structure of implants was found both *in vitro* and *in vivo* tests, but *in vivo* tests showed that the TiO_2-coated implant was less biocompatible than the others. So the recommended surface treatment in this study is plasma activation.

As summary the implant for treating GORD was successfully produced by using TPU as raw material and MuCell® technology as manufacturing process.

8 Outlook

The MuCell® process is an effective manufacturing method for foamed polymers. But there is still a limitation of porosity in this process in comparison with other laboratory methods of foamed polymers. For example, using phase separation, the porosity of a foamed polymer could be easily above 90 % [79], but in this study the maximal porosity of foamed TPU is 75 %. As porosity plays a very important role in biomedical implants the porosity of implants made by MuCell® need to be further enhanced, which means, some modifications of machine or mold needs to be done.

According to the foaming theory and practice one condition of the polymer foaming is enough space in a mold cavity. In this study a reduced volume of polymer melt was filled into the mold cavity to give space for the formation of foam structure. In market there is an alternative of mold design to realize the same function. The mold can “breathe”, which means the mold will open for a preset distance after injection of the polymer melt, so that the cavity of mold increases for providing extra space for the polymer foam. In this way the mold cavity is firstly full filled by polymer-gas-solution like compact injection molding, then the mold breathes, mold cavity increases and the foaming of polymer takes place during the mold breathing. According to the reports from industrial companies this mold design can produce more homogenous pore morphology and higher porosity. In this study the breath function of the mold was partially simulated without any modification of mold. The mold was opened just at the beginning of the cooling phase. In this phase the polymer melt was still in half-fluidic state and not completely foamed; therefore, the process of mold opening was similar to the standard process of mold breathing. The produced porous structure is shown in Fig. 8.1. A super porous structure of TPU was observed with a high porosity of about 92 %. This structure looked more like tissue and should be more functional for the cell ingrowth. So this mold with breath could be a solution to increase the porosity.

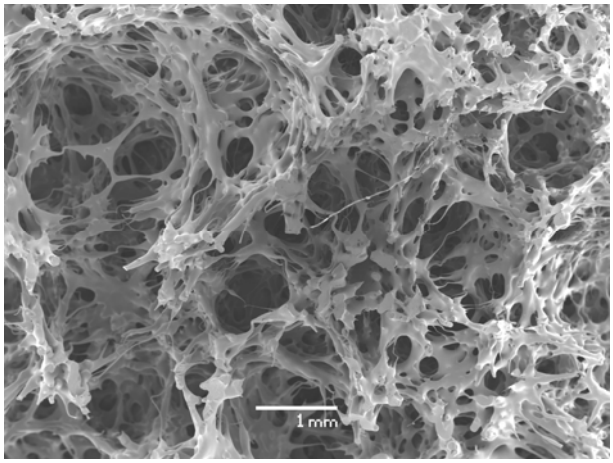

Fig. 8.1: The porous structure produced by simulation of breathing mold

Another possibility to improve the pore morphology in microcellular injection molding is a combination of MuCell® process and salt or sugar leaching process. Salt or sugar leaching process has been used in injection molding to generate a porous structure of polymer for a long time. The salt or sugar is mixed with the polymer granules in a preparatory process; then the polymer granules with mixed particles were processed through injection molding machine. The mixed particles could absorb the moisture from air and release the moisture during the processing due to heat; the polymer is consequently foamed. After production the molded parts are dipped into the water to dissolve the particles and an open porous structure is arrived. H.J. Haugen [77] has used this leaching methods combined with injection molding process to produce a porous implant with maximal porosity of 60 %. If MuCell® process is combined with a particle leaching method, some advantages could be expected. Firstly the mixed particles like salts and sugar could function as foaming agent and induce a more homogenous pore structure. Secondly the dissolution of particles out from foamed samples could improve the porosity as well as interconnectivity of porous structure.

As shown in biological analysis the implant after surface treatment showed a higher biocompatibility and cell adhesion. But the γ-ray sterilization has reduced the positive effect of plasma activation. In fact the plasma treatment has been widely used as a sterilization method in medical and food industries [132,133]. So the combination of plasma activation and TiO_2 but without γ-ray sterilization is possible. The TiO_2 particles could be mixed in polymers before the foaming process; then the polymer with TiO_2 particles is processed by MuCell® technology. After production the foamed samples will be activated by plasma treatment. So the positive effect of plasma activation and antibacterial properties of Ti nano-particle could be best combined, without damage by γ-ray sterilization.

Nomenclature

A	Surface of the gas bubble
C	Saturation concentration of gas
D_{diff}	Diffusion coefficient
$D_{diff,0}$	Maximum diffusion coefficient at infinite temperature
D_{Corr}	Corrected median pore diameter
$D_{Measured}$	Measured median pore diameter
DSC	Differential scanning calorimeter
DIN	Deutsches Institut für Normung
DMSO	Dimethylsulfoxid
ΔE_s	Activation energy
E_D	Activation energy for diffusion
EDX	Energy dispersive X-ray analysis
f_0	Factor the frequency of gas accumulation on the nucleus by homogeneous nucleation
GORD	Gastro Oesophageal Reflux Disease
ΔG_{hom}	Free energy of homogenous nucleation
ΔG^*_{hom}	Nucleation energy
GPC	Gel Permeation Chromatography
h	Thickness of the mold cavity
HDI	Hexamethylen-1, 6-diisocyanat
H_2RA	H_2 receptor antagonists
LOS	Lower oesophageal sphincter
m_{gas}	Gas mass
$m_{polymer}$	Polymer mass
MDA	Methylene dianiline diamino-diphenylmethane
MDI	Methylene-diphenyldiisocyanate
N_{hom}	Nucleation rate
N_w	Reciprocal of the unit mass of the shell
N_f	Pore density in two-dimension
p	Partial pressure
Δp	Pressure difference between the inside of gas bubble and polymer-gas-solution
P	Porosity
PE	Polyethylene
PET	Polyethylene terephthalate
PP	Polypropylene
PPI	Proton pump inhibitors
PS	Polystyrene
PVC	Polyvinylchloride
R	Gas constant
r	Radius of gas bubble
r^*	Critical radius

S	Solubility coefficient
S_0	pre-exponential factor
SEM	Scanning electron microscopy
TPU	Thermoplastic polyurethane
T	Temperature
T_g	Glass transition temperature
T_m	Crystallization temperature
TDI	Toluol-2, 4-diisocyanat
V	Volum of gas bubble
V_f	Volume fraction of gas in foamed polymer
V_{cell}	Volume of the polymer melt shell
V_{pore}	Pore volume
WST-1	4-[3-(4-jodopheny1)-2-(4-nitropheny1)-2H-5-tertazolio]-1,3-benzene disulfonate
z	Local thickness coordinate

Greek letters

ρ	Density	η	Viscosity
ρ_{cell}	Cell density	η_0	Zero-shear viscosity
ρ_f	Density of foamed polymer	τ^*	Model parameter
ρ_0	Density of unfoamed polymer	ϕ	Volum fraction of the gas
γ	interface tension or gamma rays		

References

[1] Abraham, F.F., Homogeneous Nucleation, Academic Press, New York/London, 1974

[2] Agreus, L., Borgquist, L., The cost of gastro-oesophageal reflux disease, dyspepsia and peptic ulcer disease in Sweden. PharmacoEconomics, 20 (5), 2002, S. 347-355

[3] Aho, A.J., Tirri, T., Kukkonen, J., Injectable bioactive glass/biodegradable polymer composite for bone and cartilage reconstruction: Concept and experimental outcome with thermoplastic composites of poly(epsilon-caprolactone-co-d,l-lactide) and bioactive glass. Journal of Materials Science: Materials in Medicine, 15 (10), 2004, S. 1165-1173

[4] Allgöwer, M., Harder, F., Hollender, L.F., et al., eds. Chirurgische Gastroenterologie. Refluxkrankheit, ed. Siewert J.R., Blum A.L. Springer Verlag, Berlin, 1981, S. 291-305

[5] Amon, M., Denson, C.D., A study of the dynamics of foam growth: analysis of the growth of closely spaced spherical bubbles. Polym Eng Sci, 24, 1984, S. 1026-1034

[6] Anderson, S.H.C., Yadegarfar, G., Arastu, M.H., et al., The relationship between gastro-oesophageal reflux symptoms and achalasia. European Journal of Gastroenterology and Hepatology, 18 (4), 2006, S. 369-374

[7] Anvari, M., Allen, C., Borm, A., Laparoscopic Nissen fundoplication is a satisfactory alternative to long-term omeprazole therapy. British Journal of Surgery, 82 (7), 1995, S. 938-42

[8] Arefmanesh, A., Advani, S.G., Michaelides, E.E., A numerical study of bubble growth during low pressure structural foam molding process. Polym Eng Sci, 30, 1990, S. 1330-1337

[9] Armbrecht, U., Abucar, A., et al, Treatment of reflux oesophagitis of moderate and severe grade with ranitidine or pantoprazole—comparison of 24-hour intragastric and oesophageal pH. Alimentary Pharmacology & Therapeutics, 11 (5), 1997, S. 959–965

[10] Armstrong, D., Chir, B., et al, Symptom relief in gastroesophageal reflux disease: a randomized, controlled comparison of pantoprazole and nizatidine in a mixed patient population with erosive esophagitis or endoscopy-negative reflux disease. The American Journal of Gastroenterology, 96 (10), 2001, S. 2849-2857

[11] Bae, J.-S., Seo, E.-J., Kang, I.-K., Synthesis and characterization of heparinized polyurethanes using plasma glow discharge. Biomaterials, 20 (6), 1999, S. 529-537

[12] Barlow, E.J., Langlois, W.E., Diffusion of gas from a liquid into an expanding bubble. IBM J. Res. Dev., 6, 1962, S. 329-337

[13] Baryer Corporation, Texin 985 thermoplastic polyurethane, Pittsburgh, PA, USA, 2002

[14] Baue, J., Belsey, R.H.R., The treatment of sliding hiatus hernia and reflux esophagitis by the Mark IV technique. Surgery, 62, 1967, S. 396–406

[15] Beckmann, I.A., Speiseröhrenkrebs - ein Ratgeber für Betroffene, Angehörige und Interessierte, Deutsche Krebshilfe und Deutsche Krebsgesellschaft, 2002

[16] Ben-Menachem, T., Goel, S., Zonca, M., et al., Endoscopic surveillance of plication after endoluminal gastroplication (ELGP) for GERD. Gasrointest Endosc, 57, 2003, S. 128

[17] Blander, M., Katz, J.L., Bubble nucleation in liquids. A.I.Ch.E. J., 21, 1975, S. 830-848

[18] Boeckxstaens, G.E., The lower oesophageal sphincter. Neurogastroenterology and Motility, 17 (1), 2005,

[19] Bonavina, L., Fontebasso, V., et al, Surgical treatment of reflux stricture of the oesophagus. Br J Surg, 80 (3), 1993, S. 317-20

[20] Brandrup, J., Immergut, E.H., Polymer Handbook, Wiley, New York, 1989

[21] Brunette, D.M., Tengvall, P., Textor, M., et al., Titanium in medicine, Springer Verlag, Berlin, 2001, S. 4-10

[22] Bytzer, P., Christensen, P.B., Damkier, P., et al., Adenocarcinoma of the esophagus and Barrett's esophagus: a population-based study. The American Journal of Gastroenterology, 94 (1), 1999, S. 86-91

[23] Caro, J.J., Salas, M., Ward, A., Healing and relapse rates in gastroesophageal reflux disease treated with the newer proton-pump inhibitors lansoprazole, rabeprazole, and pantoprazole compared with omeprazole, ranitidine, and placebo: evidence from randomized clinical trials. Clinical Therapeutics, 23 (7), 2001, S. 998-1017

[24] Chapmann, W.G., Gubbins, K.E., Jackson, G., et al., New feference equation of state of association liquids. Industral and Engineering Chemistry Research, 29, 1990, S. 1709-1721

[25] Charles, J., et al, Transoral, flexible endoscopic suturing for treatment of GERD: A multicenter trial. Gastrointestinal Endoscopy, 53 (4), 2001, S. 416-422

[26] Chiou, J.S., Barlow, J.W., Paul, D.R., Plasticization of glassy polymers by CO_2. Journal of applied polymer science, 30, 1985, S. 2633-2642

[27] Chow, T.S., Molecular interpretation of the glass transition temperature of polymer diluent systems. Macromolecules, 13, 1980, S. 362-364

[28] Chu, P.K., J.Y., C., Wang, L.P., et al., Plasma-surface modification of biomaterials. Materials Science and Engineereing, 36, 2002, S. 143-206

[29] Cloud, M.L., Enas, N., Humphries, T.J., et al., The Rabeprazole study group. Rabeprazole in the treatment of acid peptic diseases: results of three placebo-controlled dose-response clinical trials in duodenal ulcer, gastric ulcer and GERD. Digestive Diseases and Sciences, 43, 1998, S. 933-1000

[30] Cohen, L.B., Johnson, D.A., Ganz, R.A., et al., Enteryx implantation for GERD: expanded multicenter trial results and interim postapproval follow-up to 24 months. Gastrointestinal Endoscopy, 61 (6), 2005, S. 650-658

[31] Cohen, S., Parkman, H., Heartburn -- A Serious Symptom. The New England Journal of Medicine, 340 (11), 1999, S. 878-879

[32] Colton, J.S., The nucleation of micricellular foams in semi-crystalline thermoplastics. Materials & Manufacturing Processes, 4, 1989, S. 253-262

[33] Colton, J.S., Suh, N.P., The nucleation of microcellular thermoplastic foam;process model and experimental data. Advanced Manufacturing Processes, 1 (3/4), 1986, S. 341-364

[34] Colton, J.S., Suh, N.P., The nucleation of microcellular thermoplastic foam with additives. Part 1: Theoretical considerations. Polymer Engineering & Science, 27 (7), 1987, S. 485-492

[35] Dai, X., Liu, Z., Wang, Y., et al., High damping property of microcellular polymer prepared by friendly environmental approach. The Journal of supercritical fluids, 33, 2005, S. 259-267

[36] Daltona, P.D., Grafahrend, D., Klinkhammer, K., et al., Electrospinning of polymernext term melts: Phenomenological observations. Polymer, 48 (23), 2007, S. 6823-6833

[37] Daniel F. Baldwin, Amicrocellular processing study of poly(ethylene terephthalate) in the amorphous and semicrystalline states. Part 2: cell growth and process design. Polymer Engineering & Science, 36 (11), 1996, S. 1446-1453

[38] De Angelis, C., Repici, A., Dughera, L., et al., 38 P EUS-assisted radiofrequency energy delivery (stretta procedure) for the treatment of gastro-oesophageal reflux disease. Digestive and Liver Disease, 34 (1), 2002, S. ab 10

[39] Delale, C.F., Hruby, J., Marsik, F., Homogeneous bubble nucleation in liquids: The classical theory revisited. Journal of Chemical Physics, 118 (2), 2003, S. 792-806

[40] Demeester, T.R., Bonavina, L., Albertucci, M., Nissen fundoplication for gastroesophageal reflux disease. Evaluation of primary repair in 100 consecutive patients. annals of surgery, 201 (1), 1986, S. 9-20

[41] Demeester, T.R., Bonavina, L., Albertucci, M., Nissen fundoplication for gastroesophageal reflux disease. Evaluation of primary repair in 100 consecutive patients. Ann Surg, 204, 1986, S. 9–20

[42] Dent, J., Holloway, R.H., Toouli, J., et al., Mechanisms of lower oesophageal sphincter incompetence in patients with symptomatic gastrooesophageal reflx. Gut., 29, 1988, S. 1020-1028

[43] Dettmer, A., Vogt, R., Sielaff, F., et al., Pantoprazole 20mg is effective for relief of symptoms and healing of lesions in mild oesophagitis. Alimentary Pharmacology & Therapeutics, 12 (9), 1998, S. 865-872

[44] Devesa, S.S., Blot, W.J., Fraumeni, J.F., Changing patterns in the incidence of esophageal and gastric carcinoma in the United States. Cancer, 83 (10), 1998, S. 2049-53.

[45] Djafar, G., Abbas, B., Radiation crosslinking of LDPE and HDPE with 5 and 10 MeV electron beams. European Polymer Journal, 37 (10), 2001, S. 2011-2016

[46] Dodds, W.J., Dent, J., Hogan, W.J., et al., Mechanisms of gastroesophageal reflux in patients with reflux esophagitis. New England Journal of Medicine, 307 (25), 1982, S. 1547-1552

[47] Donahue, P.E., Bombeck, P.T., The modified Nissen fundoplication—reflux prevention without gas bloat. Review of Surgery, 11, 1977, S. 15–27

[48] Donnellan, C., Sharma, N., Preston, C., et al., Medical treatments for the maintenance therapy of reflux oesophagitis and endoscopic negative reflux disease. Cochrane Database of Systematic Reviews, (4), 2004,

[49] Durril, P., Griskey, R., Diffusion and solution of gases in thermally softened or molten polymers: Part 1. Development of technique and tetermination of data. A.I.Ch.E. Jouranl, 12, 1966, S. 1147-1151

[50] Durril, P., Griskey, R., Diffusion and solution of gases in thermally softened or molten polymers: Part 2. Relation of diffusivities and solubilities with temperature pressure and structureal characteristics. A.I.Ch.E. Journal, 15, 1969, S. 106-110

[51] Earnest, D.L., Dorsch, E., Jones, J., et al., A placebo-controlled dose-ranging study of lansoprazole in the management of reflux esophagitis. The American Journal of Gastroenterology, 93 (2), 1998, S. 238-243

[52] El-Serag, H.B., Satia, J.A.C., Rabeneck, L., Dietary intake and the risk of gastro-oesophageal reflux disease: A cross sectional study in volunteers. Gut, 54 (1), 2005, S. 11-17

[53] Emerenziani, S., Gabbrielli, A., Cicala, M., et al., Effect of the gatekeeper reflux repair system on intra-esophageal distribution of acid reflux in gastroesophageal reflux disease patients: Relation with typical symptoms. Gastroenterology, 124 (4), 2003, S. 418

[54] Farley, A., et al, Rabeprazole versus ranitidine for the treatment of erosive gastroesophageal reflux disease: A double-blind, randomized clinical trial. The American Journal of Gastroenterology, 95 (8), 2000, S. 1894-1899

[55] Fass, R., Ofman, J.J., Gastroesophageal reflux disease - Should we adopt a new conceptual framework? American Journal of Gastroenterology, 97 (8), 2002, S. 1901-1909

[56] Feder, J., Russel, K.C., Lothe, J., et al., Homogeneous nucleation and growth of droplets in vapors. Adv. Phys., 15, 1966, S. 111-178

[57] Feng, G., Swain, P., Kadirkamanathan, S., et al., Cutting thread at flexible endoscopy. Gastrointestinal Endoscopy, 44 (6), 1996, S. 667-674

[58] Fennerty, M.B., Sampliner, R.E., Johnsson, F., et al., Gastroesophageal Reflux Disease. Hospital Medicine, 29 (4), 1988, S. 28-40

[59] Feretis, C., Benakis, P., Dimopoulos, C., et al., Endoscopic implantation of Plexiglas (PMMA) microspheres for the treatment of GERD. Gastrointestinal Endoscopy, 53 (4), 2001, S. 423-426

[60] Ferry, J.D., Viscoelastic properties of polymers, Wiley, New York, 1970

[61] Fleischer, D.E., The Stretta procedure: technique optimization and complication rates. Gastrointest endosc, 55, 2002, S. ab 256

[62] Fock, K.-M., Talley, N., et al, Report of the Asia-Pacific consensus on the management of gastroesophageal reflux disease. Journal of Gastroenterology and Hepatology, 19, 2004, S. 357–367

[63] Fockens, P., Boeckxstaens, G., Gabbrielli, A., et al., Endoscopic Augmentation of the Lower Esophageal Sphincter for GERD: Final Results of a European Multicenter Study of the Gatekeeper SystemTM. Gastrointestinal Endoscopy, 59 (5), 2004, S. 242

[64] Fraser-Moodie, C.A., Norton, B., Gornall, C., et al., Weight loss has an independent beneficial effect on symptoms of gastro-oesophageal reflux in patients who are overweight. Scandinavian journal of gastroenterology, 34 (4), 1999, S. 337-40

[65] Gabbrielli, A., Cipolloni, L., Pandolfi, M., et al., Gatekeeper TM Reflux Repair System: Results of Two Years Follow-up. Gastrointestinal Endoscopy, 59 (5), 2004, S. 244

[66] Gahleitner, M., Melt rheology of polyolefins. Progress in polymer science, 26, 2001, S. 895-944

[67] Gear, M.W.L., Gillison, E.W., Dowling, B.L., Angelchik antirefluxprosthesis. The Lancet, 327 (8471), 1986, S. 42

[68] Gendorn, R., Daigneault, L., Caron, L., Rheological behavior of polystyrene/blowing agent mixtures. Proceedings of the 54th. Annual Technical Conference (ANTEC) of the Society of Plastic Engineering (SPE), Indianapolis, 1996

[69] Gendron, R., Daigneault, L., Rheological behavior of various polymer melts with CO_2. Proceedings of the 55th Annual Technical Conference (ANTEC) of the Society of Plastic Engineering (SPE), Toronto, 1997

[70] Gendron, R., Daigneault, L., Rheology of thermoplastic foam extrusion process. In: Foam extrusion, (Hrsg.), Technomic Publishing company, Lancaster, Pennsylvania, 2000, S.

[71] Gerechta, S., Townsend, S.A., Pressler, H., et al., A porousnext term photocurable elastomer for cell encapsulation and culture. Biomaterials, 28 (32), 2007, S. 4826-4835

[72] Go, M.R., Dundon, J.M., Karlowicz, D.J., et al., Endoluminal delivery of radiofrequency energynext term to the gastroesophageal junction in uncomplicated GERD: Efficacy and potential mechanism of action. Surgery, 136 (4), 2004, S. 786-794

[73] Goh, K.L., Chang, C.S., Fock, K.M., et al., Gastro-oesophageal reflux disease in Asia. Journal of Gastroenterology and Hepatology, 15 (3), 2000, S. 230-238

[74] Gorna, K., Gogolewski, S., The effect of gamma radiation on molecular stability and mechanical properties of biodegradable polyurethanes for medical applications. Polymer degradation and stability, 79, 2003, S. 465-474

[75] Greassley, W., The entanglement concept in polymer rheology. Advances in polymer science, 16, 1974, S. 1-179

[76] Guignot, C., Betz, N., Legendre, B., et al., Degradation of segmented poly(etherurethane) Tecoflex induced by electron beam irradiation: Characterization and evaluation. Nuclear instruments and methods in physics research B, 185, 2001, S. 100-107

[77] Haugen, H.J., Development of an implant to treat gastro-oesophageal reflux disease, Lehrstuhl für Medizintechnik, TU München, Munich, 2004

[78] Helen, H., Lu, et al, Three-dimensional, bioactive, biodegradable, polymer-bioactive glass composite scaffolds with improved mechanical properties support collagen synthesis and mineralization of human osteoblast-like cells in vitro. Journal of Biomedical Materials Research Part A, 64A (3), 2003, S. 465 - 474

[79] Hentze, H.-P., Antonietti, M., Porous polymers and resins for biotechnological and biomedical applications. Reviews in Molecular Biotechnology, 90, 2002, S. 27-53

[80] Hill, L.D., An effective operation for hiatal hernia: an 8 year appraisal. annals of surgery, 166, 1967, S. 681-692

[81] Hobbs, J.K., Humphris, A.D.L., Miles, M.J., In situ atomic force microscopy of polyethylene crystallization. 1. Crystalliziation from an oriented backbone. Macromolecules, 34, 2001, S. 5508-5519

[82] Huang, Q., Lösemittelfreie Herstellung von porösen polymeren Membranen durch Schaumextrusion, Universität Hamburg, 2000

[83] Isolauri, J., Luostarinen, M., Isolauri, E., et al., Natural course of gastroesophageal reflux disease: 17-22 year follow-up of 60 patients. Am J Gastroenterol, 92 (1), 1997, S. 37-41

[84] Jacobs, M.A., Kennere, M.F., Keurenties, J.T.F., Foam processing of poly(ethylene-co-vinyl acetate) rubber using supercritical carbon dioxied. Polymer, 45, 2004, S. 7539-7547

[85] John, K., DiBaise, Brand, R.E., et al., Endoluminal delivery of radiofrequencynext term energy to the gastroesophageal junction in uncomplicated GERD: previous termEfficacynext term and potential mechanism of action. The American Journal of Gastroenterology, 97 (4), 2002, S. 833-842

[86] John K. DiBaise, R.E.B.a.E.M.M.Q., Endoluminal delivery of radiofrequency energy to the gastroesophageal junction in uncomplicated GERD: Efficacy and potential mechanism of action. The American Journal of Gastroenterology,, 97 (4), 2002, S. 833-842

[87] Johnson, D.A., Ganz, R., et al, Endoscopic deep mural implantation of Enteryx for the treatment of GERD: 6 month follow-up of a multicenter trial. Am J Gastroenterol, 98, 2003, S. 250

[88] Johnston, B.T., The significance of heartburn. The Quarterly Journal of Medicine, 93 (6), 2000, S. 321-322

[89] Joshi, K., et al, Prediction of cellular structure in free expansion of viscoelastic media. Journal of applied polymer science, 67, 1988, S. 1353-1368

[90] Kadirkamanathan, S.S., Evans, D.F., Gong, F., et al., Antireflux operations at flexible endoscopy using endoluminal stitching techniques: an experimental study. Gastrointestinal Endoscopy, 44 (2), 1996, S. 133-143

[91] Kagan, Y., The kinetics of boiling of a pure liquid. Russ. J. Phys. Chem., 34, 1960, S. 42-46

[92] Kahrilas, P.J., The role of hiatus hernia in GERD. Yale Journal of Biology and Medicine, 72 (2-3), 1999, S. 101-111

[93] Kahrilas, P.J., Lin, S., Chen, J., et al., The effect of hiatus hernia on gastro-oesophageal junction pressure. Gut, 44 (4), 1999, S. 476-482

[94] Kang, J.Y., Systematic review: Geographical and ethnic differences in gastro-oesophageal reflux disease. Alimentary Pharmacology and Therapeutics, Supplement, 28 (7), 2004, S. 705-717

[95] Katz, J.L., Blander, M., Condensation and boiling: Corrections to homogeneous nucleation theory for nonideal gases. Journal of Colloid and Interface Science, 42, 1973, S. 496-502

[96] Kawashima, H., Shimbo, M., Effect of key process variables on microstructure of injection molded microcellular polystyrene foams. Cellular Polymers, 22 (3), 2003,

[97] Kawashima, H., Shimbo, M., Effect of key process varibles on microstructure of injection molded microcellular polystyrene foams. Cellular Polymers, 22 (3), 2003, S. 175-190

[98] Kelly, J.J., Watson, D.I., Devitt, P.G., et al., Laparoscopicnext term Nissen Fundoplication: Clinical previous termOutcomesnext term at 10 Years. Journal of the American College of Surgeons, 205 (4), 2007, S. 570-575

[99] Kennedy, P., Flow analysis of injection molds, Hanser Publishers, Munich, 1995

[100] Kim, M.S., Holloway, R.H., Dent, J., et al., Radiofrequency energy delivery to the gastric cardia inhibits triggering of transient lower esophageal sphincter relaxation and gastroesophageal reflux in dogs. Gastrointestinal Endoscopy, 57 (1), 2003, S. 17-22

[101] Klauser, A.G., Schindlbeck, N.E., Muller-Lissner, S.A., Symptoms in gastro-oesophageal reflux disease. Lancet, 335 (8683), 1990, S. 205-208

[102] Koopmanns, R.J., et al, Modeling foam growth in thermoplastics. Advanced Materials, 12 (1873-1800), 2000,

[103] Kropp, D., Extrusion thermoplastischer schäume mit alternativen Treibmitteln, RWTH Aachen, Aachen, 1999

[104] Kühnel, W., Taschenatlas der Zytologie, Histologie und mikroskopischen Anatomie, Georg Thieme Verlag, Stuttgart, New York, 1999, S. 96

[105] Kumar, V., Suh, N.P., A process of making microcellular thermoplastic parts. Polymer Engineering & Science, 30, 1990, S. 1323-1329

[106] Kwag, C., Manke, C.W., Gulari, E., Part B: Polymer Physics. Jornal Polymer Science, 1999, S. 2771-2781

[107] Labow, R.S., Meek, E., Santerre, J.P., Hydrolytic degradation of poly(carbonate)-urethanes by monocyte-derived macrophages. Biomaterials, 22, 2001, S. 3025-3033

[108] Lagergren, J., Bergström, R., Lindgren, A., et al., Symptomatic Gastroesophageal Reflux as a Risk Factor for Esophageal Adenocarcinoma. The New England Journal of Medicine, 340 (11), 1999, S. 825-831

[109] Lamba, N.M.K., Woodhouse, K.A., Cooper, S.L., Polyurethanes in Biomedical Applications, CRC Press LCC, 1997

[110] Landis, S.H., Murray, T., Bolden, S., et al., Cancer statistics, 1999. Cancer Journal for Clinicians, 49, 1999, S. 8-31

[111] Lauren, B., A little weightnext term gain, how much gastroesophageal previous termrefluxnext term disease. Gastroenterology, 131 (5), 2006,

[112] Lee, S.-H., Hasch, B.M., McHugh, M.A., Calculation copolymer solution behavior with statistical associating fluid theory. Fluid Phase Equilibria, 117, 1996, S. 61-68

[113] Lehle, K., Lohn, S., Reinerth, G., et al., Cytological evaluation of the tissue-implant reaction associated with subcutaneous implantation of polymers coated with titaniumcarboxonitride in vivo. Biomaterials, 25, 2004, S. 5457-5466

[114] Leicher, S., Wlter, A., Schneebauer, M., Key processing parameters for microcellular molded polystyrene material. Cellular Polymers, 25 (2), 2006, S. 99-108

[115] Lim, H.R., Baek, H.S., Lee, M.H., et al., Surface modification for enhancing behaviors of vascular endothelial cells onto polyurethane films by microwave-induced argon plasma. Surface & Coating Technology, 202, 2008, S. 5768-5772

[116] Lindl, T., Zell- und Gewebekultur. 4 ed, Spektrum - Akademischer Verlag, München, 2000, S. 110

[117] Lodeg, A.S., Meissner, J., Comparison of network theory predictions with stress/time data in shear and elongation for a low density polyethylene melt. Rheologica Acta, 21, 1973, S. 41-47

[118] Lothe, J., Pound, G.M., Reconsiderations of Nucleation Theory. J. Chem. Phys., 36, 1962, S. 2080-2085

[119] Mahmood, Z., Byrne, P.J., Barry, P., et al., Comparison of Transesophageal Endoscopic Plication (TEP) with Laparoscopic Nissen Fundoplication (LNF) in the Treatment of Uncomplicated Reflux Disease. The American Journal of Gastroenterology, 101 (3), 2006, S. 431-436

[120] Maquet, V., Boccaccini, A.R., Pravata, L., et al., Preparation, characterization, and in vitro degradation of bioresorbable and bioactive composites based on Bioglass®-filled polylactide foams. Journal of Biomedical Materials Research Part A, 66A (2), 2003, S. 335 - 346

[121] Martini, G.A., Wienbeck, M., Does alcohol favour the development of Barret's syndrome (endobrachy-oesophagus)? Deutsche medizinische Wochenschrift, 99 (10), 1974, S. 434-439

[122] Mason, J., Hungin, A.P.S., Review article: Gastro-oesophageal reflux disease - The health economic implications. Alimentary Pharmacology and Therapeutics, Supplement, 22 (1), 2005, S. 20-31

[123] Mason, R.J., DeMeester, T.R., et al, Per oral endoscopic Nissen fundoplication: the introduction of a new era. Gastrointest endosc, 53, 2001, S. ab 73

[124] Meier, P.N., Efficacy of endoscopic antireflux procedures: at least durability for radiofrequency energy delivery. Gastrointestinal Endoscopy, 65 (3), 2007, S. 375-376

[125] Michael, L., Larson, B.T., Treatment of lower urinary tract symptoms in benign prostatic hyperplasianext term and its impact on sexual function. Urology, 58 (6), 2001, S. ab40

[126] Michaeli, W., Pfannschmidt, O., Habibi-Naini, S., Spritzgießen mikrozellulärer Schäume. Kunststoffe, 92, 2002, S. 56-60

[127] Miner, M., Rosenberg, M.T., Perelman, M.A., Treatment of lower urinary tract symptoms in benign prostatic hyperplasia and its impact on sexual function. Clinical Therapeutics, 28 (1), 2006, S. 13-25

[128] Mitsuishi, K., Ueno, S., Kodama, S., et al., Crystallization behavior of polypropylene. Polymer International, 50, 1991, S. 515-523

[129] Mittal, R.K., Balaban, D.H., The esophagogastric junction. New England Journal of Medicine, 336 (13), 1997, S. 924-932

[130] Moayyedi, P., Delaney, B., Forman, D., Gastro-oesophageal reflux disease. Clinical Evidence, 11, 2004, S. 583-600

[131] Moayyedi, P., Talley, N.J., Gastro-oesophageal reflux disease. The Lancet, 367 (9528), 2006, S. 2086-2100

[132] Moisan, M., Barbeau, J., Crevier, M.-C., et al., Plasma sterilization. Methods and mechanisms. Pure & Applied Chemisty, 74 (3), 2002, S. 349-358

[133] Moreira, A.J., Mansano, R.D., de Jesus Andreoli Pinto, T., et al., Sterilization by oxygen plasma. Applied surface science, 235, 2004, S. 151-155

[134] N.N., Gebrauchsanleitung Casy 1 Model TT. In: Schärfe-System, (Hrsg.), Schärfe System GmbH, Reutlingen, 2000, S. 4

[135] N.N., Dyspepsia: management of dyspepsia in adults in primary care, National institute of clinical excellence,, 2004

[136] N.N., Engel Foammelt: Light prats for heavy duty, 2005

[137] Naguib, H.E., et al, Fundamental foaming mechanisms governing the volume expansion of extruded polyporpylene foams. Journal of applied polymer science, 91, 2004, S. 2661-2668

[138] Naguib, H.E., Song, S.-W., Park, C.B., et al., Effect of supercritical CO_2 and N_2 on crystallization of linear and branched propylene resins filled with foaming additives. Industral and Engineering Chemistry Research, 44 (17), 2005, S. 6685-6691

[139] Narsimhan, G., Ruckenstein, E., A new approach for the prediction of the rate of nucleation in liquids. Journal of Colloid and Interface Science, 128, 1989, S. 549-565

[140] Neuhaus, H., Benson, M., et al, Enteryx solution, a minimally invasive injectable treatment for GERD: update on European multicenter human trial results. Gut, 51, 2002, S. 228 ff.

[141] Nissen, R., Rossetti, M., Modern operations for hiatal hernia and reflux esophagitis: gastropexy and fundoplication. Archivio Chir Torace, 13, 1959, S. 375-87

[142] Niu, Z.Q., Gao, F., Jia, X.Y., et al., Synthesis studies of sputtering TiO2 films on poly(dimethylsiloxane) for surface modification. Colloids and Surfaces A: Physicochemical and Engineering Aspects, 272 (3), 2006, S. 170-175

[143] Niu, Z.Q., Jia, X.Y., Zhang, W.P., et al., Reactive spuutering TiO_2 films for surface coating of poly(dimethylsiloxane). Applied surface science, 252, 2006, S. 2259-2264

[144] Okamoto, K.T., Microcellular Processing, Carl Hanser Verlag, Munich, 2003

[145] Ozawa, S., Yoshida, M., Kumai, K., et al., New Endoscopic Treatments for Gastroesophageal Reflux Disease. Ann Thorac Cardiovasc Surg, 11, 2005, S. 146-153

[146] Ozdemir, Y., Hasirdi, N., Serbetci, K., Oxygen plasma modification of polyurethane membranes. Journal of Materials Science: Materials in Medicine, 13 (12), 2002, S. 1147-1152

[147] Park, C.B., The role of polymer/gas solution formation in continuous processing of microcellular polymers, Massachusetts Institute of Technology, Cambridge, 1993

[148] Park, C.B., Suh, N.P., Filamentary extrusion of microcellular polymers using a rapid decompressive element. Polymer Engineering & Science, 36, 1996, S. 34-38

[149] Park, C.B., Suh, N.P., Rapid polymer/gas solution formation for continuous production of microcellular plastics. Journal Manufacturing Science and Engineering, 118, 1996, S. 639-645

[150] Patel, R.D., Bubble growth in viscous Newtonian liquid. Chem. Eng. Sci., 35, 1980, S. 2352-2356

[151] Perdikis, G., Hinder, R.A., Wetscher, G.J., Nissen fundoplication for gastroesophageal reflux disease: laparoscopic Nissen fundoplication—technique and results. Diseases of the Esophagus, 9, 1996, S. 272–277

[152] Pohler, O.E.M., Unalloyed titanium for implants in bone surgery. Injury, Int. J. Care Injured, 31, 2000, S. D7-D13

[153] Polk, H.C., Zeppa, R., Hiatal hernia and esophagitis. A survey of indications for operation and technique and results of fundoplication. Ann Surg, 173, 1971, S. 775–781

[154] Powell, J., McConkey, C.C., The rising trend in oesophageal adenocarcinoma and gastric cardia. European journal of cancer prevention : the official journal of the European Cancer Prevention Organisation (ECP), 1 (3), 1992, S. 265-269

[155] Ramesh, N.S., et al, Numerical and experimental studies of bubble growth during the microcellular foaming process. Polymer Engineering and Science, 31 (1657-1664), 1991,

[156] Reiss, H., The kinetics of phase transition in binary systems. J. Chem. Phys., 18, 1950, S. 840-848

[157] Reymunde, A., Santiago, N., Long-term results of radiofrequency energy delivery for the treatment of GERD: sustained improvements in symptoms, quality of life, and drug use at 4-year follow-up. Gastrointestinal Endoscopy, 65 (3), 2006, S. 361-366

[158] Richter, J.E., Bochenek, W., Oral pantoprazole for erosive esophagitis: a placebo-controlled, randomized clinical trial. The American Journal of Gastroenterology, 9 (11), 2000, S. 3071-3080

[159] Richter, J.E., Castell, D.O., Gastroesophageal reflux. Pathogenesis, diagnosis, and therapy. Annals of Internal Medicine, 97 (1), 1982, S. 93-103.

[160] Roether, J.A., Boccaccin, A.R., Hench, L.L., et al., Development and in vitro characterisation of novel bioresorbable and bioactive composite materials based on polylactide foams and Bioglass® for tissue engineering applications. Biomaterials, 23 (18), 2002, S. 3871-3878

[161] Rossetti, M., Heill, K., Fundoplication for the treatment of gastroesophageal reflux in hiatal hernia. World J Surg, 1, 1977, S. 439-443

[162] Roth, S., Mantey, A., Kunz, D., et al., Thermoplast-Schaumspritzgießen (TSG) von Formteilen hoher Dichtereduktion. Intensiv-Workshop Spritzgieß-Sondertechnologie, Bayreuth, 2005

[163] Rothstein, R.I., Filipi, C.J., Endoscopic therapy for gastroesophageal reflux disease. Gastrointest Endosc Clin N Am, 13 (1), 2003, S. 7-14

[164] Roy-Shapira, A., Schwartz, D., al., e., Ex vivo efficacy of stapled anterior partial fundoplication vs Nissen fundoplication. A prelude to endoscopic antireflux procedure. Journal of Clinical Gastroenterology, 2003,

[165] Roy-Shapira, A., Stein, H.J., Scwartz, D., et al., Endoluminal methods of treating gastroesophageal reflux disease. Diseases of the Esophagus, 15 (2), 2002, S. 132-136

[166] Ruckenstein, E., Nowakowski, B., A kinetic theory of nucleation in liquids. J. Colloid Interface Sci., 137, 1990, S. 583-592

[167] Rudnik, E., Resiak, I., Wojciechowski, C., Thermoanalytical investigations of polyurethanes for medical purpose. Thermochimica Acta, 320, 1998, S. 285-289

[168] Sanchis, M.R., Calve, O., Fenollar, O., et al., Surface modification of a polyurethane film by low pressure glow discharge oxygen plasma treatment. Journal of applied polymer science, 105 (3), 2007, S. 1077-1085

[169] Sandler, R.S., Everhart, J.E., The burden of selected digestive diseasesnext term in the United States. Gastroenterology, 122 (5), 2002, S. 1500-1511

[170] Sato, Y., et al, Solubilities and diffusion coefficients of carbon dioxide and nitrogen in polypropylene, high density polyethylene, and polystyrene under high pressures and tempetraures. Fluid Phase Equilibria, 162 (261-279), 1999,

[171] Sato, Y., Fujiwara, K., Takikawa, T., et al., Solubilities and diffusion coefficients of carbon dioxide and nitrogen in polypropylene, high-density polyethylene, and polystyrene under high pressures and temperatures. Fluid Phase Equilibria, 162 (1-2), 1993,

[172] Schmitz-Moormann, P., Thomas, C., Gebert, G., et al., Verdauungsapparat. 1 ed, Schattauer Verlagsgesellschaft mbH, Stuttgart, New York, 1989, S. 187

[173] Schwarzl, F.R., Polymermechanik, Springer Verlag, Berlin, 1990

[174] Shackelford, A., CRC Practical Handbook of Materials Selection, CRC Press, Boca Raton, 1995

[175] Shafi, M.A., Joshi, K., Flumerfelt, R.W., Bubble size distributions in freely expanded polymer foams. Chemical Engineering Science, 52 (4), 1997, S. 635-644

[176] Shannon, C., Thull, R., Von Recum, A., Types I und III collagen in the tissue capsules of titanium and stainless-steel implants. Journal of Biomedical Materials Research, 34, 1997, S. 401-408

[177] Shih, J.-T., Lee, H.-M., Monopolar Radiofrequencynext term Electrothermal Shrinkage of the Scapholunate Ligament. Arthroscopy: The Journal of Arthroscopic & Related Surgery, 22 (5), 2006, S. 553-557

[178] Simmons, A., Hyvarinen, J., Poole-Warren, L., The effect of sterilisation on a poly(dimethylsiloxane)/poly(hexamethylene oxide) mixed macrodiol-based polyurethane elastomer. Biomaterials, 27, 2006, S. 4484-4497

[179] Skripov, V.P., Metastable Liquids, Wiley, New York/London, 1974

[180] Sloan, S., Kahrilas, P.J., Impairment of esophageal emptying with hiatal hernia. Gastroenterology, 100 (3), 1991, S. 596-605

[181] Smith, R.S., Chang, F.C., Hayes, K.A., et al., Complications of the Angelchik antireflux prosthesis. The American Journal of Surgery, 150 (6), 1985, S. 735-738

[182] Spoerke, E.D., Murray, N.G., Li, H., et al., A bioactive titanium foam scaffoldnext term for previous termbone repairnext term. Acta Biomaterialia, 1 (5), 2005, S. 523-533

[183] Stein, H.J., Ambulante 24-h--Manometrie der tubulären Speiseröhre. In: Gastric Cancer, Siewert J.R., Kelsen D., Maruyama K. (Hrsg.), Springer-Verlag, Heidelberg, Germany, 2001, S. 47-60

[184] Steward, D.L., Methods and outcomes of radiofrequencynext term ablation for obstructive previous termsleep apneanext term. Operative Techniques in Otolaryngology-Head and Neck Surgery, 17 (4), 2006, S. 233-237

[185] Street, J.R., Arthur, L.F., Reiss, L.P., Dynamics of phase growth in viscous, non-Newtonian liquids. Industrial and Engineering Chemistry Fundamentals, 10, 1971, S. 54-64

[186] Sud, R., Puri, R., Chung, S., et al., The His-Wiz Antireflux Procedure Results in Symptomatic and pH Improvement At 1 Year of Follow-Up. Gastrointestinal Endoscopy, 63 (5), 2006, S. ab131

[187] Sugarman, B.J., Aggarwal, B.B., Hass, P.E., et al., Recombinant human tumor necrosis factor-alpha: effects on proliferation of normal and transformed cells in vitro. Science, 230 (4728), 1985, S. 943-5

[188] Swain, P., P.O., P., Kjellin, T., et al., Endoscopic gastroplasty for gastro-esophageal reflux disease. Gastroenterology, Gastrointest Endosc (51), 2000, S. ab 144

[189] Taboas, J.M., Maddox, R.D., Krebsbach, P.H., et al., Indirect solid free form fabrication of local and global porous, biomimetic and composite 3D polymer-ceramic scaffolds. Biomaterials, 24, 2003, S. 181-194

[190] Tam, W.C.E., Schoeman, M.N., Zhang, Q., et al., Delivery of radiofrequency energy (RFe) to the lower esophageal sphincter (LES) and gastric cardia inhibits transient LES relaxations and gastroesophageal reflux in patients with reflux disease. Gastroenterology, 120 (5), 2001, S. ab 16

[191] Tauber S., Gross M., Issing W. J., Association of laryngopharyngeal symptoms with gastroesophageal reflux disease. Laryngoscope, 112 (5), 2002, S. 879-86

[192] Throne, J.L., Thermoplastic Foams, Sherwood Publishers, Hinckley, Ohio, 1996

[193] Triadafilopoulos, G., DiBaise, J.K., Nostrant, T.T., et al., Radiofrequency energynext term delivery to the gastroesophageal junction for the treatment of GERD. Gastrointestinal Endoscopy, 53 (4), 2001, S. 407-415

[194] Utley, D.S., Kim, M., Vierra, M.A., et al., Augmentation of lower esophageal sphincter pressure and gastric yield pressure after radiofrequency energy delivery to the gastroesophageal junction: A porcine model. Gastrointestinal Endoscopy, 52 (1), 2000, S. 81-86

[195] Vakil, N., Sharma, P., Rewiew article: endoscopic treatments for gastro-oesophageal reflux disease. Aliment pharmacol ther, 17, 2003, S. 1427-1434

[196] Van Den Boom, G., Go, P.M., Hameeteman, W., et al., Cost effectiveness of medical versus surgical treatment in patients with severe or refractory gastroesophageal reflux disease in the Netherlands. Scand J Gastroenterol, 31 (1), 1996, S. 1-9

[197] van der Linden, E., Kroft, L.J.M., Dijkstra, P.D.S., Treatment of Vertebral Tumornext term with Posterior Wall Defect Using Image-guided previous termRadiofrequencynext term Ablation Combined with Vertebroplasty: Preliminary Results in 12 Patients. Journal of Vascular and Interventional Radiology, 18 (6), 2007, S. 741-747

[198] van Krevelen, D.W., Properties of polymers, Elsevier, Amsterdam, 1990

[199] van Meerveld, J., Peters, G.W.M., Hütter, M., Towards a rheological classification of flow induced crystallization experiments of polymer melts. Rheologica Acta, 4 (119-134), 2004,

[200] van Pinxteren, B., Numans, M.E., Bonis, P.A., et al., Short-term treatment with proton pump inhibitors, H2-receptor antagonists and prokinetics for gastro-oesophageal reflux disease-like symptoms and endoscopy negative reflux disease. Cochrane Database of Systematic Reviews, (1), 2007,

[201] van Tienen, T.G., Heijkants, R.G., Buma, P., et al., Tissue ingrowth and degradation of two biodegradable porous polymers with different porosities and pore sizes. Biomaterials, 23 (8), 2002, S. 1731-8

[202] Velasco, J., De Saja, J.A., Martinez, A.B., Crystallization behavior of polypropylene filled with surface-modified talc. Journal of applied polymer science, 61, 1996, S. 125-132

[203] Veldhuyzen van Zanten, S.J.O., Bardette, M., Chiba, N., et al., Evidence-based recommendations for short- and long-term management of uninvestigated dyspepsia in primary care: An update of the Canadian Dyspepsia Working Group (CanDys) clinical management tool. Canadian Journal of Gastroenterology, 19 (5), 2005, S. 285-303

[204] Vermette, P., Griesser, H.J., Biomedical applications of polyurethanes, Eurekah, Georgetown, Texas, 2001

[205] Vieth, W., Diffusion in and throuth polymers: principles and applications, Hanser, Munich, Vienna, New York, Barcelona, 1991

[206] Wagner, M.H., Rubio, P., Bastian, H., The molecular stress function model for polydispers and polymer melts with dissipative convective strain release. Journal of Rheology, 45, 2001, S. 1387-1412

[207] Walther, C., Zilling, T., et al, Increasing prevalence of adenocarcinoma of the oesophagus and gastro-oesophageal junction: A study of the Swedish population between 1970 and 1997. European Journal of Surgery, 167 (10), 2001, S. 748-757

[208] Wang, M., Xu, L., Zhai, M., et al., γ-ray radiation-induced synthesis and Fe(III) ion adsorption of carbosymethylated chitosan hydrogels. Carbohydrate polymers, 74, 2008, S. 498-503

[209] Wedler, G., Lehrbuch der physikalischen Chemie, VCH Weinheim, 1987

[210] Wei, J., Chen, O.Z., Stevens, M.M., et al., Biocompatibility and bioactivity of PDLLA/TiO_2 and PDLLA/TiO_2/Bioglass® nanocomposites. Materials Science and Engineereing, C 28, 2008,

[211] Wilt, P.M., Nucleation rates and bubble stability in water-carbon dioxide solutions. Journal of Colloid and Interface Science, 112, 1986, S. 530-538

[212] Wintermantel, E., Ha, S.-W., Medizintechnik. 4th ed, Springer Verlag, Berlin, 2008, S. 62

[213] Wintermantel, E., Ha, S.-W., Medizintechnik. 4th ed, Springer Verlag, Berlin, 2008, S. 121-141

[214] Wintermantel, E., Ha, S.-W., Medizintechnik. 4th ed, Springer Verlag, Berlin, 2008, S. 78

[215] Wintermantel, E., Ha, S.-W., Medizintechnik. 4th ed, Springer Verlag, Berlin, 2008, S. 556

[216] Yamada, T., Reflux oesophagitis. In: Textbook of Gastroenterology, Orlando R.C. (Hrsg.), JB Lippincott Co, Philadelphia, Pa., 1991, S. 1123-1147

[217] Yan, J.Y.J., Cooke, F.W., Vaskelis, P.S., et al., Titaniumcoated Dacron velour: a study of interfacial connective tissue formation. Journal of Biomedical Materials Research, 23 (2), 1989, S. 171-189

[218] Zahraoui, C., Sharrock, P., Influence of sterilization on injectable bone biomaterials. Bone, 25 (1), 1999, S. 63S-65S

[219] Zeltinger, J., Sherwood, J.K., Graham, D.A., et al., Effect of pore size and void fraction on cellular adhesion, proliferation, and matrix deposition. Tissue Engineering, 7 (5), 2001, S. 557-72.

[220] Zhang, Y., Zhao, S.F., Li, Y., et al., Radiation effects on styrene-butadiene-styrene copolymer. Nuclear instruments and methods in physics research B, 266, 2008, S. 3431-3436

[221] Zhang, Z., Handa, Y.P., An in situ study of plasticization of polymers by high pressure gases. Journal of applied polymer science, Part B: Polymer physics, 36, 1998, S. 977-982

[222] Zurek, W.H., Schiever, W.C., Molecular dynamics study of clustering. J. Chem. Phys., 68, 1978, S. 840-846

Appendix A, Culture medium additives

Medium for cultivation of Detroit 551 fibroblasts

Minimum essential medium (Eagle) 1 ×	Biochrom AG, Cat.no. FG0325
+ 0.1 mM Non-essential amino acids	Biochrom AG, Cat.no. K0293
+ 1.0 mM Sodium Pyruvat (100mM)	Biochrom AG, Cat.no. L0473
+10 % Fetale bovine serum (heat inactivated)	Biochrom AG, Cat.no. S0115
+1 % Penicillin/Streptavidin (10000U/10000ug/ml)	Biochrom AG, Cat.no. A2213
+1 % Partricin (Fungicide, 50ug/ml)	Biochrom AG, Cat.no. A2812

Trypsination

Trypsin/EDTA-Solution (0.05 %/0.02 %)	Biochrom AG, Cat.no. L2143

Culture dishes

Well-Plates (6,12,24,48,96)	TPP, Trasadingen, Switzerland
Cell culture dishes (T25, T75)	TPP, Trasadingen, Switzerland
Certrifuge tubes (15 ml, 50ml)	TPP, Trasadingen, Switzerland

Appendix B, Histological preparation

As mentioned in chapter 4, the histological preparation of the implant with tissues based on the paraffin wax embedding is not possible because of the flexibility and porous structure of TPU samples. As an alternative method the cold polymerasation of PMMA (poly-methylmethacrylate) was used for the production of the histological preparation.

1 Ascending alcohol series

First of all the implant with tissues must be dehydrated before the PMMA-polymerization begins. The dehydration was performed through an ascending alcohol series. The implants were immerged in 70 %, 80 % und 90 % ethanol with room temperature for two days, separately; then in 100 % methanol for two days, twice.

2 Embedding in methylmethacrylate (MMA)

2.1 Preparation of the MMA-embedding

The benzoyl peroxide must be dehumidified before it is used, because the benzoyl peroxide contains ca. 25 % water in the delivery condition. After the dehumidification the benzoyl peroxide is potentially explosive, so that it should be as freshly as possible prepared. The dehumidification takes place in a hot cabinet. The benzoyl peroxide was laid in the hot cabinet for two hours by 60° C and then by 37° C overnight, at last by 60° C for two hours. Subsequently the benzoyl peroxide can be temporarily conserved in a glass placed in a dark condition.

2.2 Production of the embedding mixture

The mixture consists of 50 ml methylmethacrylate, 10 ml nonylphenyl - polyethylene glycol – acetate and 1.5 g benzoyl peroxide (dehumidified). The mixture was agitated by the magnetic stirrer for ca. 30 minutes and can be conserved in the fridge for a few weeks.

2.3 Embedding and polymerization

The implant and MMA-embedding mixture were filled in a snap-cap vial and the vial was laid in the exsiccator under vacuum condition for two hours, then the vial was laid in the fridge by 4° C for a day.

After the soakage of samples in the MMA-mixture the vial was filled with new MMA-mixture and laid again in the exsiccator for two hours in vacuum condition. At last the

implants in vials were laid in a water bath by 37° C in the drying chamber for three days to ensure an slow, stable and homogeneous polymerization of MMA-mixture.

3 Histological preparation

After the polymerization the block of the implant and PMMA was taken out from the vial (the vial was broken) and glued to a sample holder of the inside hole saw for cutting. The block was cut into slices with ca. 100 um thickness, then the slices were further ground to 50 um thick to ensure the transparence for the transmitted light microscope.

After the grinding of sample slices the Paragon coloring was used to distinguish the tissue and cytoblast from polymer. The paragon solution was produced by 0.73g Toluidin Blue (Sigma, C.I. 52040 Basic Blue 17) and 0.27g bas. Fuchsin (Sigma 1A 308, C.I. 42510 Chroma 780) in 100ml 30 % ethanol. The sample slices were washed through the Paragon solution under 60° C for two minutes and carefully washed by water to remove the Paragon solution for the further microscopic observation.